Reference PICC for Extended Modulation and LMA Measurement Principles

MASTER'S THESIS

MA722

Christoph Egger

Institute for Electronics
Graz University of Technology
Head: Univ.-Prof. Dipl.-Ing. Dr.techn. Wolfgang Bösch

in Cooperation with

Infineon Technologies Austria AG

Assessor: Univ.-Prof. Dipl.-Ing. Dr.techn. Peter Söser
Advisor: Dipl.-Ing. Stephan Rampetzreiter, Dipl.-Ing. Andreas Wörle

Graz, March 2013

Contents

List of Figures

List of Tables

Abstract

One of the numerous fields of application for RFID systems is the contactless payment sector. This market is predicted a tremendous growth in the coming years. To ensure the global interoperability of contactless payment cards (PICC) with their reader devices (PCD), members of EMVCo - originally Europay, MasterCard and Visa - have developed the EMV™ Contactless Specifications for Payment Systems including the definition of reference test setup called EMV Contactless Level 1 Test Equipment. Due to constant development of chips intended for usage in payment cards and therewith changed behavior and new fields of applications like mobile payment, parts of the EMV Contactless Level 1 Test Equipment, are no longer a good representation for real-world systems.

In the course of this thesis the EMV Contactless Level 1 Test Equipment's limitations regarding evaluation of a PICC's load modulation parameters are shown, and in order to overcome these limitations, a novel method is introduced. Furthermore, it is demonstrated that the current EMV-TEST PICC, which is used for reader testing, is not capable of fully emulating the behavior of nowadays' real-world PICCs. For this reason, a new test PICC based on the EMV-TEST PICC V2.1 and able to load-modulate a reader's magnetic field actively is developed, simulated and verified. The new reference PICC allows to arbitrarily set amplitude modulation, phase modulation and influence on the field within the range of modern real-world systems.

Zusammenfassung

Kontaktlose Zahlung ist eine der zahlreichen Anwendungen von RFID Systemen, welchen in den kommenden Jahren ein enormes Wachstum prognostiziert wird. Um die globale Interoperabilität von kontaktlosen Karten (PICC) mit ihren Lesegeräten (PCD) zu gewährleisten, haben Mitglieder von EMVCo - ursprünglich Europay, MasterCard und Visa - die EMV™ Contactless Specifications for Payment System entwickelt, welche die Definition eines Referenzaufbaus mit speziellen Komponenten, genannt "EMV Contactless Level 1 Test Equipment", inkludiert. Aufgrund der konstanten Entwicklung und das dadurch veränderte Verhalten von Chips für die Verwendung in Karten zur kontaktlosen Zahlung, sowie neue Anwendungen, wie mobile Zahlung, stellen Teile des EMV Contactless Level 1 Test Equipment nicht länger eine gute Repräsentation realer System dar.

Im Rahmen dieser Arbeit werden die Beschränkungen des EMV Contactless Level 1 Test Equipments zur Evaluierung der Parameter der Lastmodulation einer PICC gezeigt. Eine neue Methode wird eingeführt, um diese Beschränkungen zu überwinden. Weiters wird demonstriert, dass die aktuelle EMV-TEST PICC, welche zum Testen von Lesegeräten verwendet wird, nicht vollständig in der Lage ist, das Verhalten heutiger realer PICCs nachzubilden. Aus diesem Grund wird eine neue Test PICC auf Grundlage der EMV-TEST PICC V2.1 entwickelt, simuliert und verifierziert. Sie erlaubt es, Amplitudenmodulation, Phasenmodulation und die Rückwirkung auf das Feld des Lesegerätes innerhalb des Bereichs moderner realer Systeme beliebig einzustellen.

Chapter 1

Introduction

RFID (Radio Frequency Identification) is an omnipresent technology in our industrialized community. The product portfolio is rising constantly and has extended far beyond mere identification solutions. While earlier systems did not incorporate writable memories or information processing capabilities, a lot of todays RFID transponders have both. This opens a number of new markets. One of these new branches is the contactless payment sector. Numbers from the UK impressively show that contactless payment is rapidly growing: While at the end of July 2010 the number of debit and credit cards with contactless functionality was approximately 9.6 million. This number has grown to 24.6 million until the end of March 2012 [17]. The business consulting firm Frost & Sullivan predicts a compound annual growth rate for contactless cards in Europe of 28.7% in 2011-2017 [1]. A closely related application is mobile payment based on Near Field Communication. The research and advisory firm Forrester anticipates a 48% compound annual growth rate for the U.S. market from 2013 to 2017 when 90 billion US Dollars will be spent per mobile payment [21].

For the international standardization of contactless payment systems, the responsible regulation authority, EMVCo, has released the standard "EMV™ Contactless Specification for Payment Systems". EMV stands for Europay, MasterCard and Visa which are the companies that started to develop the specifications. Manufacturers of contactless readers and transponders can check the compliance of their products with test equipment that includes reference hardware provided by EMVCo. Unfortunately, the setup is incapable of testing certain modern transponders: While the cards can communicate with modern as well as legacy readers without problems, they will fail the EMVCo test. It is the aim of this thesis to work out new measurement procedures and reference hardware to enable the check of modern proximity coupling chipcards as well as actively modulating proximity devices. This includes the calculation of the load modulation amplitude without the EMV-TEST CMR Circuit Board - a part of the provided test hardware - and the development of an EMV-TEST PICC with advanced load modulation capabilities.

Chapter 2

Technical Background - Proximity Coupling RFID Systems

All RFID systems consist of two basic components: a reader device and a transponder. In case of proximity coupling RFID systems as defined in ISO/IEC 14443, these devices are coupled by a time varying electromagnetic field produced by the reader with a carrier frequency of 13.56 MHz. Contactless smart cards, in ISO/IEC 14443 referred to as Proximity Integrated Circuit Cards (PICC), can communicate with the reader device over distances of up to $7 - 15$ cm [18]. This range is well inside the near field of the reader's electromagnetic field and can therefore be considered as a time varying magnetic field. Proximity coupling RFID systems belong to the class of systems that employ inductive coupling, not only for communication, but also to supply the mostly passive transponders with the energy necessary for the device to operate. Figure 2.1 shows the basic configuration of a proximity coupling RFID system. The fundamental

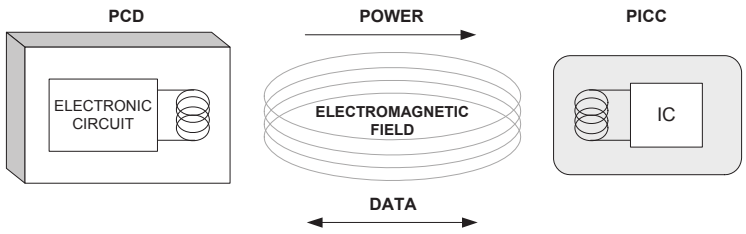

Figure 2.1: PCD and PICC configuration [6]

components of such a system will be explained in terms of their electrical representation in the following sections.

2.1 PICC - Proximity Integrated Circuit Card

In its simplest description the PICC consists of an antenna coil and a chip. The antenna coil provides the interface to the magnetic field of the reader whereas the chip comprises a number of analog and digital functions that are necessary for device operation. Figure 2.2 shows a simplified equivalent circuit of a PICC. The antenna of the PICC - sometimes

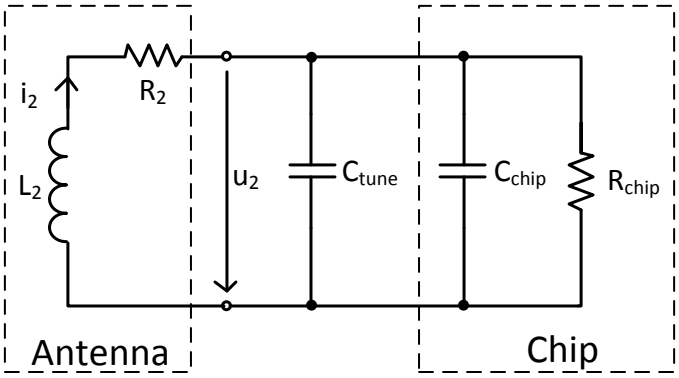

Figure 2.2: Simple equivalent circuit of a PICC [8]

also referred to as coil in the course of this thesis - is represented as an inductor L_2 with a series resistor R_2. To induce sufficiently high voltages in the PICC's antenna, its resonance frequency is tuned to a value close to the carrier frequency of the magnetic field. This is accomplished by the tuning capacitor C_{tune}. The chip connected to the antenna can be represented as a capacitor C_{chip} - which can incorporate C_{tune} - in parallel to a resistor R_{chip}. It is important to say that most of these components are either frequency dependent or nonlinear or both.

2.2 PCD - Proximity Coupling Device

A simple electrical representation of a PCD is depicted in figure 2.3. It consists of an antenna, in this case represented by an inductor L_1 in series to a resistor R_1, a signal source with an internal resistance R_i, and a matching network to match the antenna to the source. The depicted matching network comprises the capacitors C_{ms} and C_{mp}. If the matching condition is fulfilled, the load impedance and the internal impedance of the signal source are equal. In this case, the maximum power is transferred from the source

to the load. Note that with the matching circuit shown in figure 2.3 only matching at a

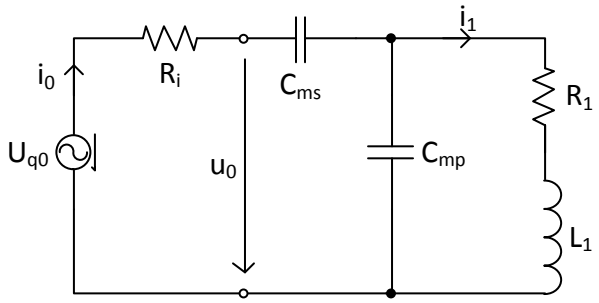

Figure 2.3: Simple equivalent circuit of a PCD [8]

specific frequency is possible. In case of systems according to ISO/IEC 14443, this will be the carrier frequency of 13.56 MHz.

2.3 System Interaction

2.3.1 Power Supply of the PICC

If a PICC is inserted into the magnetic field of a PCD, a voltage $\underline{V}_{Q1}$ will be induced in its antenna. Figure 2.4 shows the equivalent circuit of this setup: The induced voltage

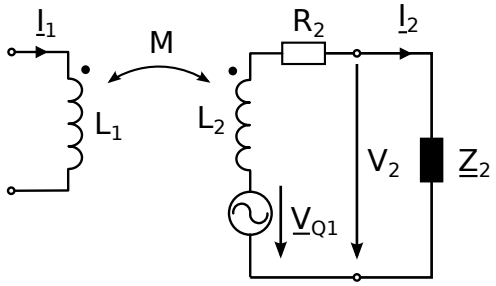

Figure 2.4: Induction of a voltage in the antenna of the PICC

.

can be calculated by:

$$\underline{V}_{Q1} = j\omega M \underline{I}_1 \tag{2.1}$$

In equation 2.1 j stands for the complex unit, ω is the angular frequency of the magnetic field and $\underline{I}_1$ is the current through the PCD's antenna. The mutual, M, describes the magnetic coupling between the antennas. In practice, the coupling is mostly quantified

by the coupling factor k, which is defined by:

$$k = \frac{M}{\sqrt{L_1 L_2}} \tag{2.2}$$

The impedance $\underline{Z}_2$ incorporates the tuning capacitance C_{tune} as well as the impedance of the chip which is C_{chip} in parallel to R_{chip}. From these quantities, the voltage at the input of the chip can be calculated as follows:

$$\underline{V}_2 = \underline{V}_{Q1} \frac{\underline{Z}_2}{R_2 + j\omega L_2 + \underline{Z}_2} = \underline{V}_{Q1} \frac{\dfrac{R_{chip}}{1 + j\omega R_{chip}(C_{tune} + C_{chip})}}{R_2 + j\omega L_2 + \dfrac{R_{chip}}{1 + j\omega R_{chip}(C_{tune} + C_{chip})}} \tag{2.3}$$

After defining C_2 as the sum of C_{tune} and C_{chip}, equation 2.3 can be transformed to:

$$\underline{V}_2 = \underline{V}_{Q1} \frac{1}{1 + \dfrac{R_2}{R_{chip}} - \omega^2 L_2 C_2 + j\omega \left(R_2 C_2 + \dfrac{L_2}{R_{chip}} \right)} \tag{2.4}$$

As one can see from equation 2.4, the voltage $\underline{V}_2$ can be much higher than $\underline{V}_{Q1}$ under certain conditions. The magnitude of the denominator has its minimum value at the parallel resonance frequency, when the real part of the denominator becomes zero. To quantifiy the voltage and current step up at the resonance frequency, the Q-factor is introduced [18]:

$$Q = \frac{1}{\dfrac{R_2}{\omega_{res} L_2} + \dfrac{\omega L_2}{R_{chip}}} \tag{2.5}$$

According to equation 2.5, the Q-factor tends toward zero when R_2 takes very large values or R_{chip} is made very small. The dependence on the voltage step up on R_{chip} is exploited to regulate the voltage at the chip. Keeping in mind that the supply voltage of the chip - which is a DC voltage of a certain level - is derived from the voltage $\underline{V}_2$, it is obvious that some kind of voltage regulation is needed. A simple approach of limiting the input voltage of the chip is shown in figure 2.5. It should be quite clear at this

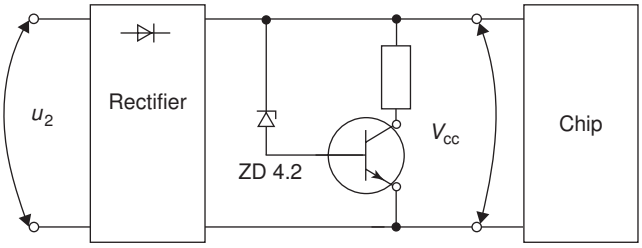

Figure 2.5: Example circuit for a simple shunt regulator [18]

point that $\underline{Z}_2$, the load impedance of the PICC's antenna, is highly nonlinear and varies significantly, even over the time of half a carrier period.

2.3.2 Transformed Transponder Impedance

So far it has been omitted that a PICC that is supplied by the magnetic field of the PCD will itself produce an effect in the PCD antenna. In the end, the communication concept of load modulation - which will be explained later on - is based on this behavior. For the sake of convenience, the PCD antenna is in this section represented as a series resonance circuit comprising the elements C_1, R_1 and L_1. As depicted in figure 2.6, the current that flows through the PICC's antenna as a result of the voltage induced by the magnetic field of the reader, induces a voltage in the PCD antenna. The direction of

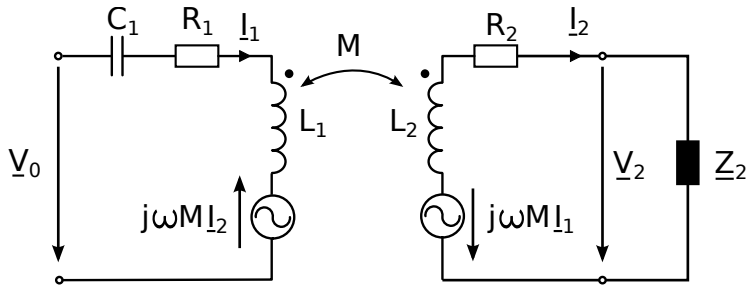

Figure 2.6: The voltage induced in the PICC's antenna leads to a current that induces a voltage in the PCD's antenna.

this voltage is given by Lenz' law, which states that an induced current always produces a flux that counteracts the flux that generated it.

It is assumed that a current $\underline{I}_1$ flows through the PCD antenna and that the voltages at C_1 and L_1 cancel each other out due to series resonance. The voltage $\underline{V}_0$ at the pins of the PCD antenna can be calculated with the following equation:

$$\underline{V}_0 = \underline{I}_1 R_1 - j\omega M \underline{I}_2 \tag{2.6}$$

From the relations derived in the previous section, the current $\underline{I}_2$ can be calculated as follows:

$$\underline{I}_2 = \frac{\underline{V}_2}{\underline{Z}_2} = \frac{j\omega M \underline{I}_1}{R_2 + j\omega L_2 + \dfrac{R_{chip}}{1 + j\omega R_{chip} C_2}} \tag{2.7}$$

If $\underline{I}_2$ in equation 2.6 is substituted with this expression, one obtains:

$$\underline{V}_0 = \underline{I}_1 \left(R_1 - j\omega M \frac{j\omega M}{R_2 + j\omega L_2 + \dfrac{R_{chip}}{1 + j\omega R_{chip} C_2}} \right) \tag{2.8}$$

Note that the second term inside the braces appears as an impedance, which is called the *transformed transponder impedance* or $\underline{Z}'_T$. After some rearrangement and the sub-

stitution of M with $k\sqrt{L_1 L_2}$, $\underline{Z}'_T$ finally takes the following shape:

$$\underline{Z}'_T = \frac{\omega^2 k^2 L_1 L_2}{R_2 + j\omega L_2 + \dfrac{R_{chip}}{1 + j\omega R_{chip} C_2}} \tag{2.9}$$

The relations derived so far show that it is possible to express the influence of the PICC on the PCD with a single element, as can be seen in figure 2.7. The transformed

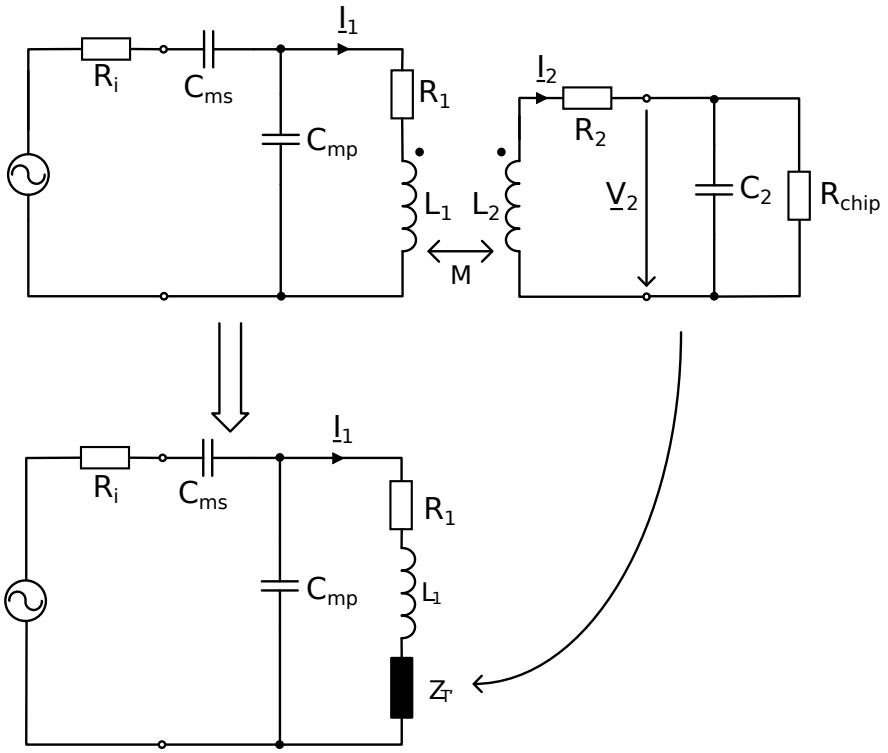

Figure 2.7: Simple equivalent circuit of an inductively coupled RFID-system (adapted from [8])

transponder impedance can be considered as damped parallel resonant circuit. Its circular resonance frequency is:

$$\omega_{res,ZT} = \sqrt{\frac{1}{L_2 C_2} - \frac{1}{R_{chip}^2 C_2^2}} \tag{2.10}$$

R_{chip} is usually in the range of some kΩ, which means that the term $\frac{1}{R_{chip}^2 C_2^2}$ is very small compared to $\frac{1}{L_2 C_2}$ and thus the resonance frequency of $\underline{Z}'_T$ equals the resonance frequency of the transponder.

2.3.3 Load modulation

In proximity coupling RFID systems, load modulation is the most common approach of data transmission from the PICC to the PCD. As it was shown in the previous section, a PICC that is introduced into the magnetic field of the PCD has a measurable effect on the voltage across its antenna, which can be modeled by the transformed transponder impedance $\underline{Z}'_T$. It is therefore nearby to transmit data from the transponder to the reader by varying $\underline{Z}'_T$ in time according to the data stream. Taking a glance at equation 2.9, one realizes that there are two possible parameters in the PICC that lead to modulation when varied: the first is the resistance of the chip R_{chip}, the second is the capacitance C_2 in parallel to the antenna. A modulation of R_{chip} is referred to as *ohmic load modulation*, whereas the other is called *capacitive load modulation*.

Ohmic Load Modulation

The concept of ohmic load modulation is shown in figure 2.8. The resistor R_{chip} is changed between the values R_L and $R_L||R_{mod}$. Contrary to intuition, the magnitude of the current through the PICC's antenna is lowered, when the switch is closed and therefore the resistance R_{chip} is reduced. A glance at equation 2.5 shows that this is due to the reduction of Q, which corresponds to a reduction of the voltage step up due to resonance. At the PCD, the modulation of R_{chip} appears as a change of magnitude and

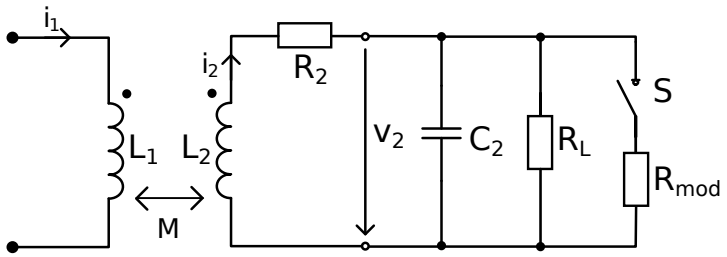

Figure 2.8: Ohmic load modulation (adapted from [8])

phase of the transformed transponder impedance $\underline{Z}'_T$. This leads in the final analysis to a change of the voltage between the terminals of the PCD's antenna, in magnitude as well as in phase. The modulation of the magnitude of the field in order to transmit data is called amplitude modulation or AM. If data is transmitted by variation of the phase of the carrier signal the techniqe is referred to as phase modulation of PM. In the practice of load modulation, the result is always a combination of both. However, under the assumption that the PICC's resonance frequency is close to the carrier frequency of the PCD, the modulation of amplitude will dominate.

2.3.4 Capacitive Load Modulation

Contrary to ohmic load modulation, capacitive load modulation doesn't change the Q-factor of the PICC, but rather its resonance frequency. This is accomplished by switching a capacitance C_{mod} in parallel to the antenna as shown in figure 2.9. Under the

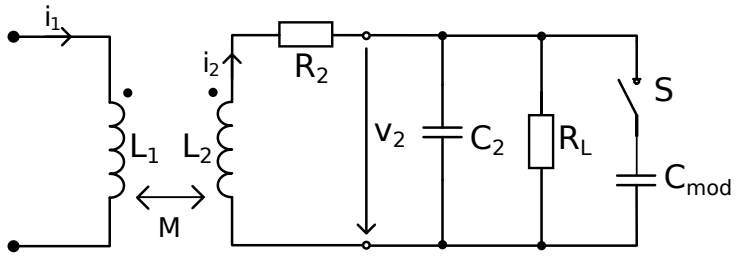

Figure 2.9: Capacitive load modulation (adapted from [8])

assumption that the carrier frequency of the magnetic field and the resonance frequency of the PICC are equal, $\underline{Z}'_T$ acts as a purely ohmic load in the unmodulated case. As soon as C_{mod} is added to the capacitance in parallel to the PICC's antenna, the resonance frequency will drop and $\underline{Z}'_T$ will take the appearance of a complex load which goes hand in hand with amplitude as well as phase modulation of the voltage at the terminals of the PCD's antenna. Figure 2.10 shows the dependence of $\underline{Z}'_T$ on the parallel capacitance C_2 and how it is changed by a modulation of the load resistance R_L.

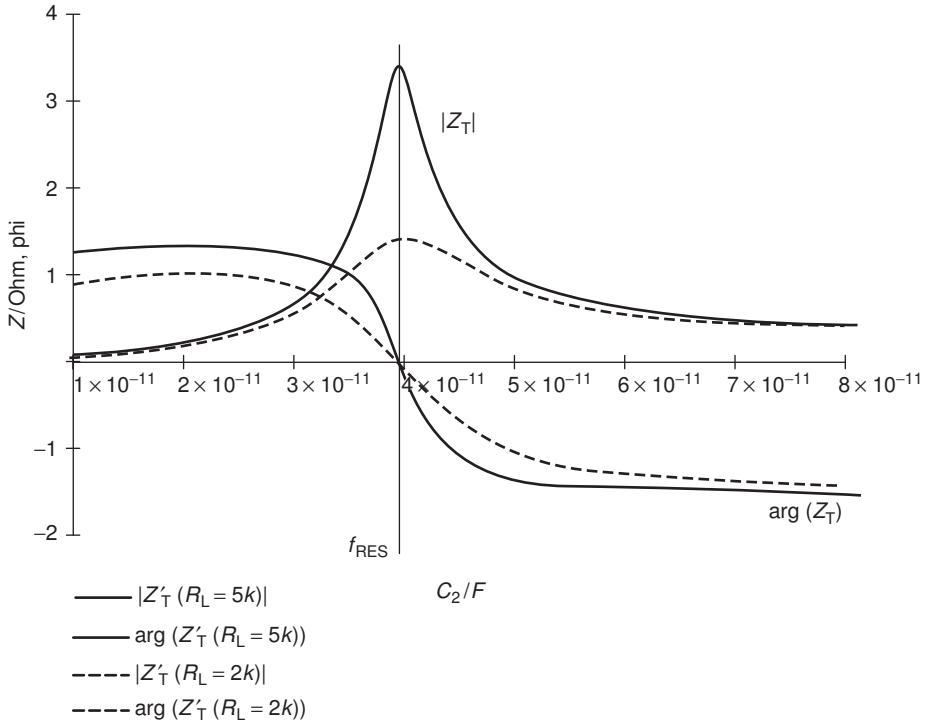

Figure 2.10: Value and phase of the transformed transponder impedance $\underline{Z}'_T$ as a function of C_2 . The maximum value of $\underline{Z}'_T$ is reached when the transponder resonant frequency matches the transmission frequency of the reader. The polarity of the phase angle of $\underline{Z}'_T$ varies [18]

Chapter 3

Normative Background

3.1 ISO/IEC and EMVCo

When working in the field of proximity coupling chipcards for payment applications one will soon discover that there are two institutions defining specifications and testing procedures: ISO/IEC and EMVCo.

The ISO (International Organization for Standardization) is the world's largest developer of voluntary international standards. It is a network of national standard bodies, which represent ISO in their countries [11]. The IEC (International Electrotechnical Commission) is the world's leading organization that prepares and publishes International Standards for all electrical, electronic and related technologies and a global sister organization of the ISO. When appropriate, IEC cooperates with ISO to ensure that international standards fit together seamlessly and complement each other [10].

EMVCo LLC (Limited Liability Company) is a company owned by American Express, JCB, MasterCard and Visa. It manages, maintains and enhances the EMV™ Integrated Circuit Specifications to ensure global interoperability of chip-based payment cards with acceptance devices [4].

3.2 ISO/IEC 14443 - Proximity Coupling Chipcards

The standard ISO/IEC 14443 describes the operating principles and parameters of PICCs and PCDs. The first edition was published in the year 2001 [19]. Proximity coupling systems have a range of up to 10 cm and work with a carrier frequency of 13.56 MHz. They are commonly used in payment- and ID-applications as well as for ticketing. The ISO/IEC 14443 consists of four parts:

1. Physical characteristics

2. Radio frequency power and signal interface
3. Initialization and anticollision
4. Transmission protocol

The corresponding testing methods are defined in ISO/IEC 10373-6.

3.3 EMV Contactless Specifications for Payment Systems

In 2007, the EMV™ Contactless Communication Protocol Specification was published so that the hardware and firmware specifications would be common for all contactless payment applications [5]. Up to this time, organisations of the payment industry were developing contactless technology competitively. The first edition of the EMV Contactless Specification for Payment Systems was published in 2008, today's current version is 2.2. It consists of the following documents:

Book A: Architecture and General Requirements

Book B: Entry Point

Books C [C-1, C-2, C-3, C-4 :] Kernel Specifications

Book D: Contactless Communication Protocol

The EMV Contactless Communication Protocol is based on the ISO/IEC 14443 1-4. In the scope of this thesis, only parameters of the section **Radio Frequency Power and Signal Interface**, which is based on ISO/IEC 14443-2, are used. The major difference to parameters defined in the ISO standard is that all of the EMV requirements of the RF power and signal interface for the PCD and PICC are specified with respect to the EMV Contactless Level 1 Test Equipment [6]. In other words: while tests performed according to ISO/IEC 10373-6 measure certain parameters of a device under test (for example PCD field strength) the EMV procedure measures a parameters that results of the overall system interaction (i.e. DUT (device under test) and EMV Contactless Level 1 Test Equipment) to conclude a DUT's parameter (for example DC voltage at the EMV-TEST PICC as a result of PCD field strength). Though the limits in the standard are defined in a way that compatibility with the limits defined in ISO/IEC 14443-2 should follow, a direct conversion of measured values is hardly possible.

Chapter 4

EMV Contactless Level 1 Test Equipment

The EMV standards define a set of test cases that need to be passed by a vendor's device for full accreditation. These tests are performed by certified test houses with reference hardware that is offered by EMVCo. The purpose of this hardware is to provide a defined framework that is representative for real-world applications. This chapter describes the components as well as the problems of the EMV Contactless Level 1 Test Equipment.

4.1 EMV-TEST PICC

The EMV-TEST PICC - the current version is V2.1 - shown in Figure 4.1 is used for a number of purposes [7]:

- Measurement of the field strength of a PCD.
- Sensing the PCD signal through the PICC's pickup coil.
- Sending PICC emulated data to the PCD being tested.

To provide these functionalities the EMV-TEST PICC comprises the following components:

- **EMV-TEST PICC Antenna:** It represents the antenna, real-world PICCs use to draw power from the reader's field and to communicate with it. Concerning communication, the EMV-TEST PICC Antenna is only used to transmit data to the PCD. The reception of data from the PCD is accomplished by the next component:

- **Pickup Coil:** As the name suggests, this antenna is used to pick up the signal of the PCD while being decoupled from the EMV-TEST PICC Antenna. The output signal of the Pickup Coil can be acquired at the connector **J9**. In the course of this thesis, the pickup coil will be referred to as *Leti Coil* to differentiate it from other pickup coil topologies.
- **Calibration Connector:** The SMA-jack **J6** is used to connect the EMV-TEST PICC to a VNA (vector network analyzer) in the process of tuning its resonance frequency. Note that the GND of **J6** is not connected to local GND on the PCB!
- **Varible Capacitor VC1:** It is used to tune the resonance frequency of the EMV-TEST PICC.
- **Rectifier, Load and Modulation Circuitry:** These components are connected to the EMV-TEST PICC Antenna. The user can set the load with the jumpers **J7** and **J8** to different values. In the default settings a nonlinear load is used. For the sake of data transmission, the load can be varied by applying a modulation signal at **J2**. This voltage signal is called V_{mod} in the course of this thesis. At the SMA connector **J1** the PCD field strength V_{OV} can be measured.

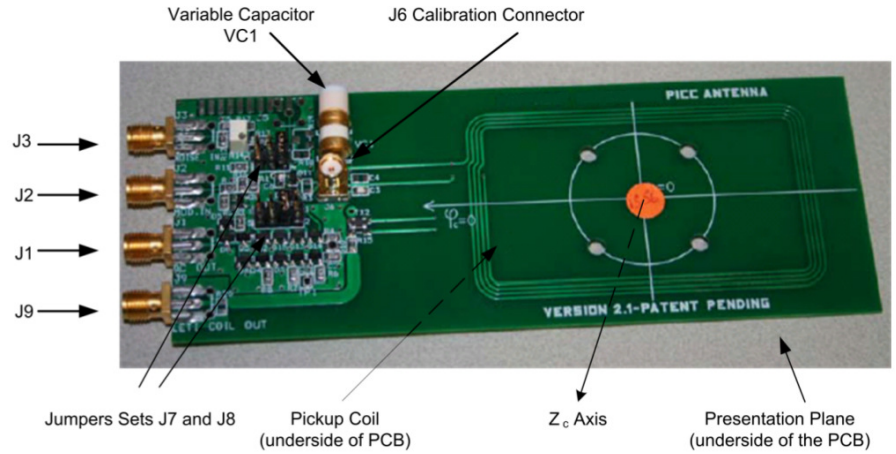

Figure 4.1: EMV-TEST PICC V2.1 [7]

4.2 EMV-TEST PCD

The EMV-TEST PCD is used to transform a carrier voltage of a signal source at the input connector **J1** into a magnetic field used to power and communicate with PICC's. It is matched to an input impedance of 50Ω at 13.56 MHz.

At the output connector **J2** it delivers a voltage that is representative for the antenna current. In the course of this thesis this voltage is referred to as V_{pp} or *shunt voltage*.

Note that in the EMV-documents the term V_{pp} is only used for the parameter "Load Modulation", which is derived from that very voltage. Instead the term *Unprocessed PCD Analogue Sensing* is used in these documents for the output signal of the EMV-TEST PCD.

To simulate different coupling factors between EMV-TEST PCD and a PICC, the actual placement of the PICC relative to the EMV-TEST PCD is varied within a defined operation volume. This can be accomplished by placing a multi-slot construction of acrylic glass on top of the EMV-TEST PCD (see Figure 4.2). The construction is not part of the specification, only the positioning of the PICC in the operation volume, described by three parameters, z, r and φ. In the current standard a position is specified in the form (z, r, φ), e.g. $(2, 0, 0)$ as the position in which the EMV-TEST PICC is placed to measure the EMV-TEST PCD's field strength while setting its value. In this thesis an older convention is used, where a position is described as $x - y - z$, e.g. $0 - 0 - 2$ instead of $(2, 0, 0)$. For all of the measurements executed in this thesis the parameters r and φ are zero (and so are x and y).

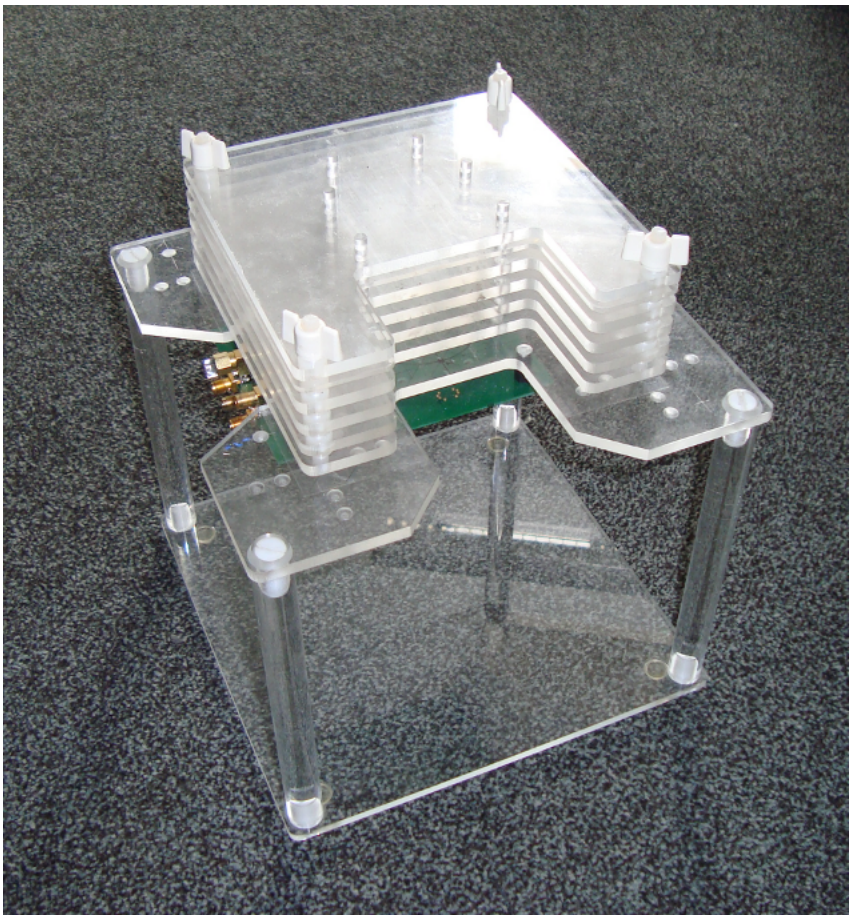

Figure 4.2: EMV-TEST PCD V1.2 with positioning construction on top.

4.3 EMV-TEST CMR Circuit Board

The EMV-TEST CMR Circuit Board is used for signal conditioning and switching between it's inputs and outputs. In it's basic configuration as used during the project at Infineon, the output of the EMV-TEST PCD is connected to **J2** of the EMV-TEST CMR Circuit Board. The term CMR (common mode rejection) is misleading in a way, Signal Conditioning Board would be more appropriate. One of its main functions is the derivation of a sampling clock from one of the input signals by detecting its zero transitions. This clock signal is used as an external trigger for a sampling device that is used to acquired signals from the EMV-TEST PCD or the EMV-TEST PICC. With a number of delay lines the derived clock can be shifted until the sampling device acquires exactly the peak values of the modulated carrier signal. In this approach it is assumed that the time difference between a zero transition and a peak value is constant, or in other words that no phase modulation takes place. Otherwise the sampling device would not sample the exact peak value of a carrier period but a voltage smaller than this.

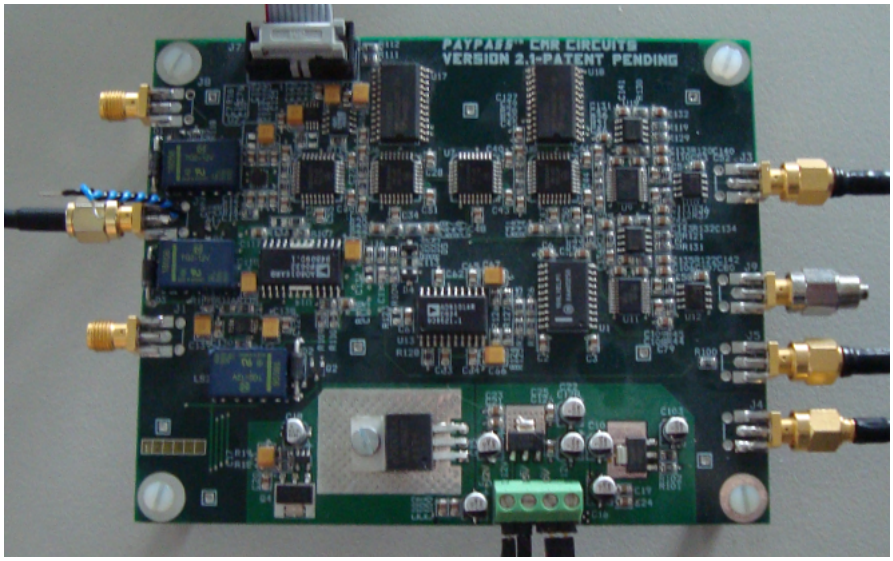

Figure 4.3: EMV-TEST CMR

4.4 Problems with the EMV Contactless Level 1 Test Equipment

The whole EMV Contactless Level 1 Test Equipment was designed with the special focus on a realistic representation of real-world equipment. The functional principle of the EMV-TEST CMR Circuit Board reveals that it should emulate a reader that uses peak sampling for signal demodulation. It is obvious that such an approach as described

above is incapable to correctly demodulate a phase modulated signal. Pure AM only occurs when the PICC appears as an ohmic load to the reader, which is actually rarely the case in reality. In most of the cases amplitude and phase of the magnetic field of the reader will be modulated during the load modulation process. An analysis with the mentioned peak sampling approach will underestimate the true AM in such a case. This error is directly proportional to the PM of the signal.

What exactly is the problem about this? The problem is that virtually all reader devices in today's use utilize IQ demodulation, a procedure that is capable of amplitude- as well as phase-demodulation. So it is possible that a PICC that strongly modulates the phase of the magnetic field fails the EMV tests although all real-world PCDs can properly communicate with it. In other words, the EMV Contactless Level 1 Test Equipment is no longer a proper representation of reality. This issue is becoming more and more important as the mobile payment sector is growing rapidly. These systems often implement active modulation where the PM content can be much higher than in load modulation systems. It is therefore necessary that representative test equipment is at hand to test these new applications.

Chapter 5

Limitations of the EMV-TEST PICC, Version 2.1

5.1 Motivation

The scope of this chapter is to evaluate if it is possible with the EMV-TEST PICC to set AM, PM and the influence on the field to any combination that can be encountered in existing applications. For this purpose the resonance frequency and load resistance of the EMV-TEST PICC will be varied and the influence on the EMV-TEST PCD during load modulation will be measured. The same measurement will be executed with a number of real-world applications. After this it will be analyzed if the particularly measured PICCs can be emulated with the EMV-TEST PICC.

A further question is the effort that needs to be spent to operate in a certain point in the AM-PM-influence on the field space. Is such an operating point simple to find without the necessity to iteratively tune a number of parameters? Is this process easy to repeat? If each of these questions can be answered with YES, then there is obviously no need for a new reference PICC.

5.2 Measurements

5.2.1 Equipment

All measurements were executed using the EMV Contactless Level 1 Test Equipment explained in the previous chapter. Fig. 5.1 shows the basic configuration for load modulation measurement.

AWG1 (Arbitrary Waveform Generator) is used to control the reader field and sends a

sequence including a REQA command at 106 kbit/s to the PICC via the RF amplifier and the EMV-TEST PCD. With its synchronisation output it triggers AWG2 and the sampling device ADQ214 (Signal Processing Devices Sweden AB, Linköping, Sweden) that is connected to the PC and controlled by a MATLAB (Mathworks Inc., Natick, USA) program.

The arbitrary waveform generator AWG2 sends a square-wave burst for load modulation to the EMV-TEST PICC. The maximum value of this signal will be referred to as V_{mod} in the course of this thesis. The modulation burst of AWG2 has the following parameters:

Frequency	Vmin	Vmax	Duty Cycle	Number of Pulses
847.5 kHz	0 V	$1 - 5$ V	50 %	8

Table 5.1: Parameters of the square-wave burst of AWG2

The sampling device that was used for data acquisitions is the ADQ214. It has a sampling rate of up to 400 MSPs, a vertical resolution of 14 bit and an input voltage range of 2.2 V_{pp}. The measured signal is the voltage at the connector **J2** of the EMV-TEST PCD which represents the antenna current. As already explained, this current is varied by the load modulation of the PICC.

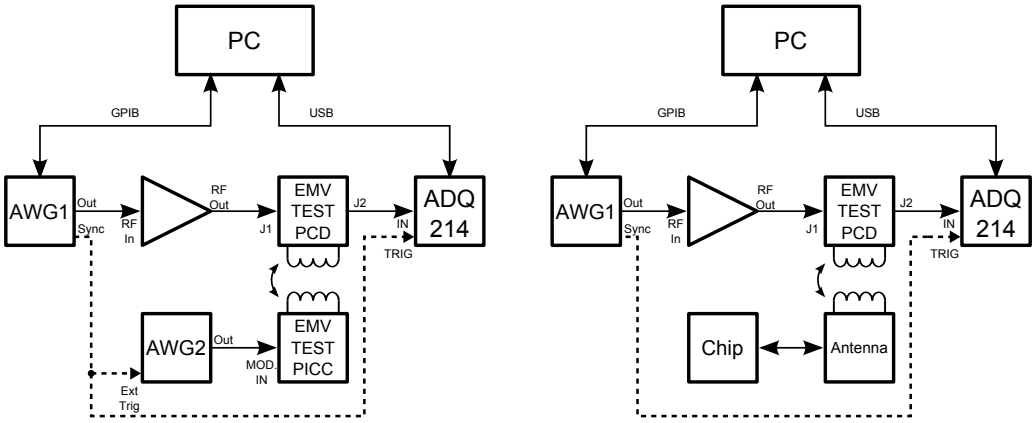

Figure 5.1: Block diagrams of the measurement procedures: The left picture shows the setup for measuring the EMV-TEST PICC, the right picture shows the setup for measuring real-world PICCs.

5.2.2 Measurement Procedure

First of all, the field strength is set according to the procedure described in [7]:

1. Ensure that the EMV-TEST PICC is tuned to its nominal resonance frequency of 16.1 MHz and set to its nominal load setting i.e. nonlinear load with two additional diode pairs.
2. Place the EMV-TEST PICC at the position 0-0-2 in the operation volume of the EMV-TEST PCD.
3. Measure the average voltage at **J1** of the EMV-TEST PICC.
4. Change the voltage at **J1** of the EMV-TEST PCD until the voltage at **J1** of the EMV-TEST PICC equals 5.53 V.

The values above refer to the nominal settings, min- and max-measurements were not performed.

A first analysis performed with different nonlinear loads revealed a nonmonotonic AM vs. modulation voltage characteristic. This makes it very difficult to derive general conclusions. It was therefore decided to replace the nominal nonlinear load with a linear load in the form of a $10k\Omega$ potentiometer, a value that was found by considering the nonlinear load circuit. By using a linear load it was expected to obtain a monotonic AM vs. modulation voltage characteristic. The setting up of the EMV-TEST PICC was performed in the following way:

1. Tune the EMV-TEST PICC to the desired resonance frequency with an impedance analyzer
2. Set the load jumper in the default positions, i.e. nonlinear load with four additional diodes
3. Place the EMV-TEST PICC at the desired position in the operation volume of the EMV-TEST PCD
4. Measure and note the peak-peak value of the unmodulated shunt voltage at **J2** of the EMV-TEST PCD as representation of the influence on the field
5. Set the load jumper to the variable linear load of $0 - 10\,\mathrm{k}\Omega$
6. Tune the load potentiometer until the influence on the field is the same as in 4.

After the EMV-TEST PICC had been tuned to the operation point of interest, the data acquisition was started. This was accomplished in the following way:

1. Place the PICC in the desired slot of the EMV-TEST PCD
2. In case of measuring with the EMV-TEST PICC: set $Vmax$ of AWG2 to the desired value
3. Start the MATLAB program used for signal acquisition with the ADQ214 described in the following subsection

4. After a trigger event has occured and data have been acquired they are stored on the hard disk

5.2.3 Software for Data Acquisition and Analysis

Figure 5.2 shows the data acquisition and analysis in detail. The ADQ214 can be controlled by MATLAB software. The program used in the course of this thesis was the self programmed *ADQ214_single_shot.m*. This program uses functions defined in *interface_ADQ.m*, *define_command_codes.m* and *mex_ADQ.dll* which are provided from the vendor of the device. The sampled data are stored as **.mat*-file after converting the sample codes into voltage values. Not shown in figure 5.2 is the trigger signal from AWG1 that starts the acquisition of data. Figure 5.3 gives an impression of the appearance of the unprocessed sampled signal. The data analysis is performed with another MATLAB program that was also developed in the context of this thesis, the **LMA calculator**. Following steps are performed to extract a value for AM and PM from the sampled signal:

1. The sampled data are imported from a **.mat*-file
2. Bandpass filtering is applied to remove noise and offset
3. Magnitude (see Figure 5.4) and phase information of the signal are calculated using the Hilbert-transform, the phase is normalized to 13.56 MHz. This means that the constant slope of the phase that is a result of the carrier frequency and the sampling rate is subtracted from the phase curve. The normalized phase (see Figure 5.5) is zero as long as no PM occurs.
4. Lowpass filtering is applied to the magnitude and phase data
5. The user has to select a time interval that contains seven cycles of the subcarrier signal
6. Min and max values of the magnitude and phase data within the selected interval are detected (see Figure 5.6)
7. The difference between the average max and min value is calculated. In case of magnitude data, the result is called AM, in case of phase data PM
8. AM and PM are displayed

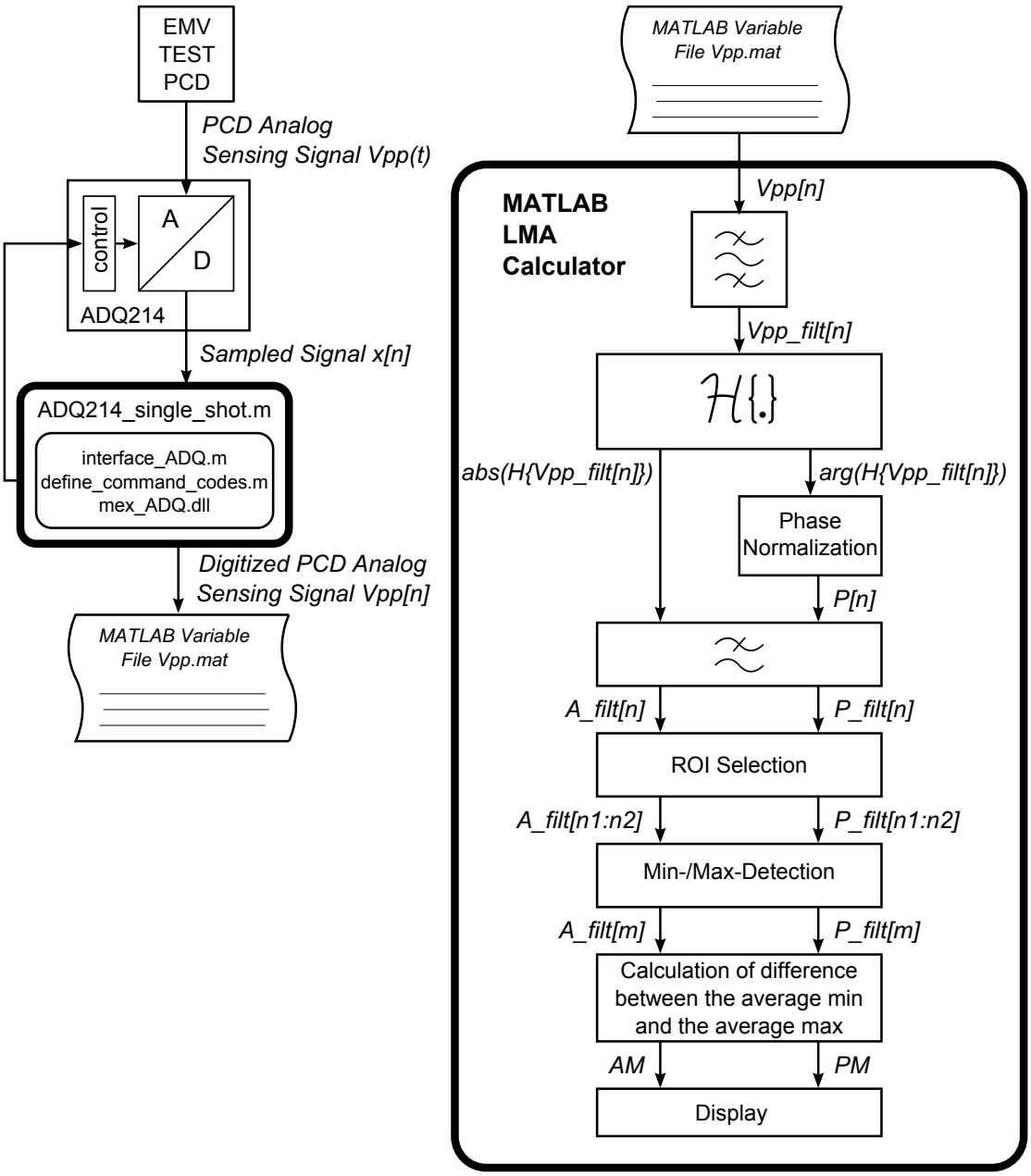

Figure 5.2: Diagram of the acquisition and demodulation procedure: the left picture shows how data are acquired with the ADQ214, the right picture shows how the signal is demodulated with MATLAB.

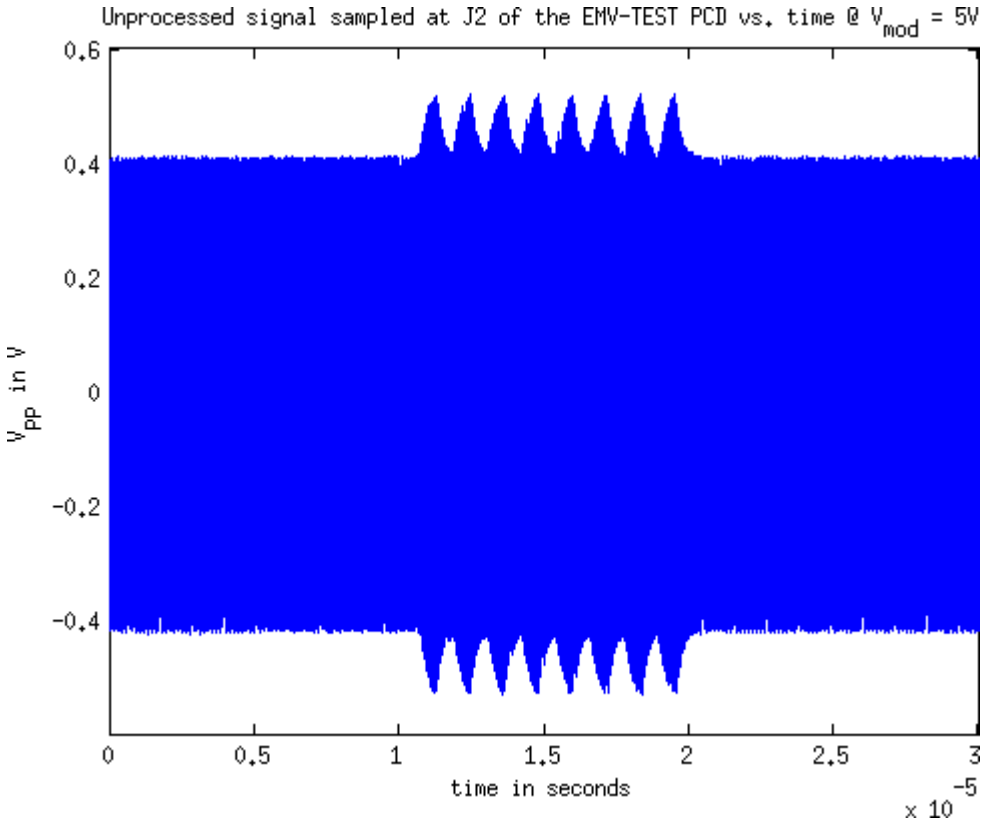

Figure 5.3: Unprocessed sampled signal as returned by the MATLAB program *ADQ214_single_shot.m* and processed by the MATLAB program **LMA calculator**.

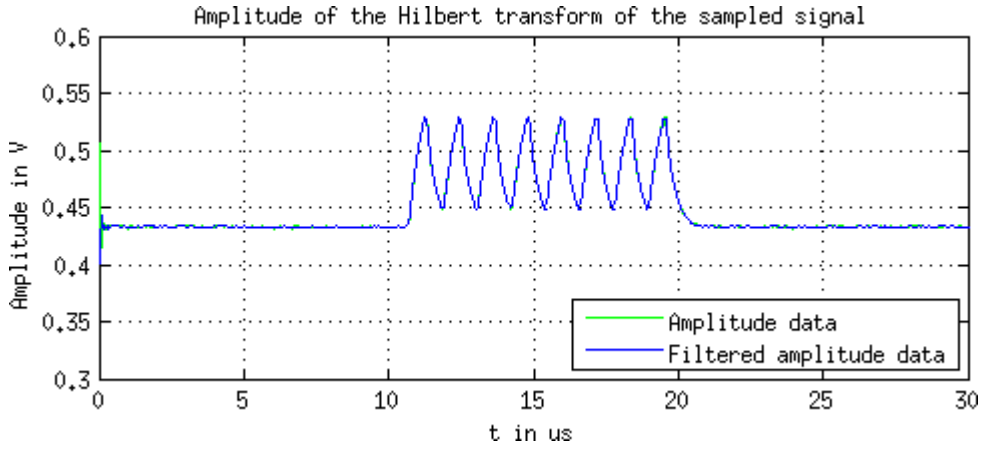

Figure 5.4: Amplitude of the Hilbert transformed filtered input signal.

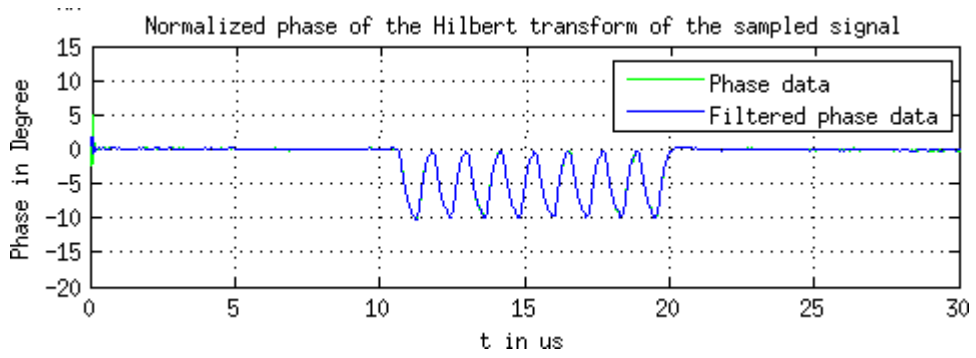

Figure 5.5: Normalized phase of the Hilbert transformed filtered input signal.

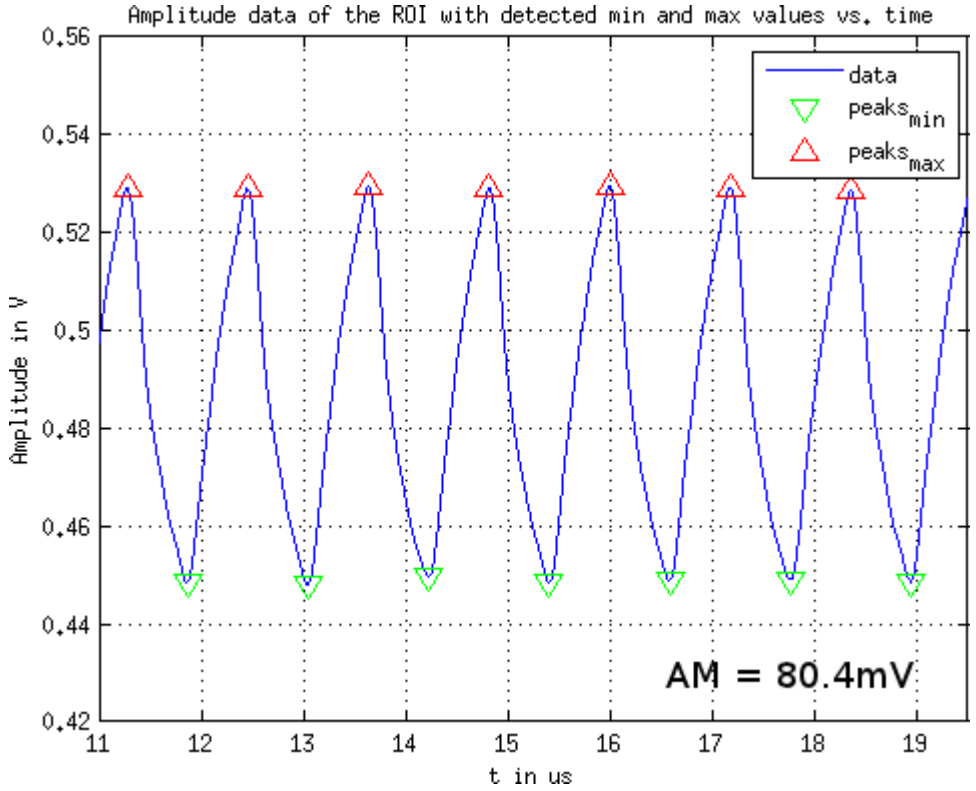

Figure 5.6: Amplitude of the Hilbert transformed filtered input signal within the interval selected by the user. The min and max values have been detected by the program, the resulting AM is noted in the plotting area.

5.3 Measurement Results

5.3.1 Measuring the EMV-TEST PICC V2.1

As already explained, the measurements with the EMV-TEST PICC are performed to evaluate the AM-PM-influence on the field space that can be covered by it. Figure 5.7 shows the AM values vs. f_{res} of the EMV-TEST PICC V2.1 for different V_{mod} at the position 0-0-0. It shows a clear maximum at around 15 MHz that is independent of V_{mod}. At this position AM values larger than 120 mV can be achieved. Around this peak the curve shows an almost symmetric behavior. A minimum can be found between 10 MHz and 11 MHz.

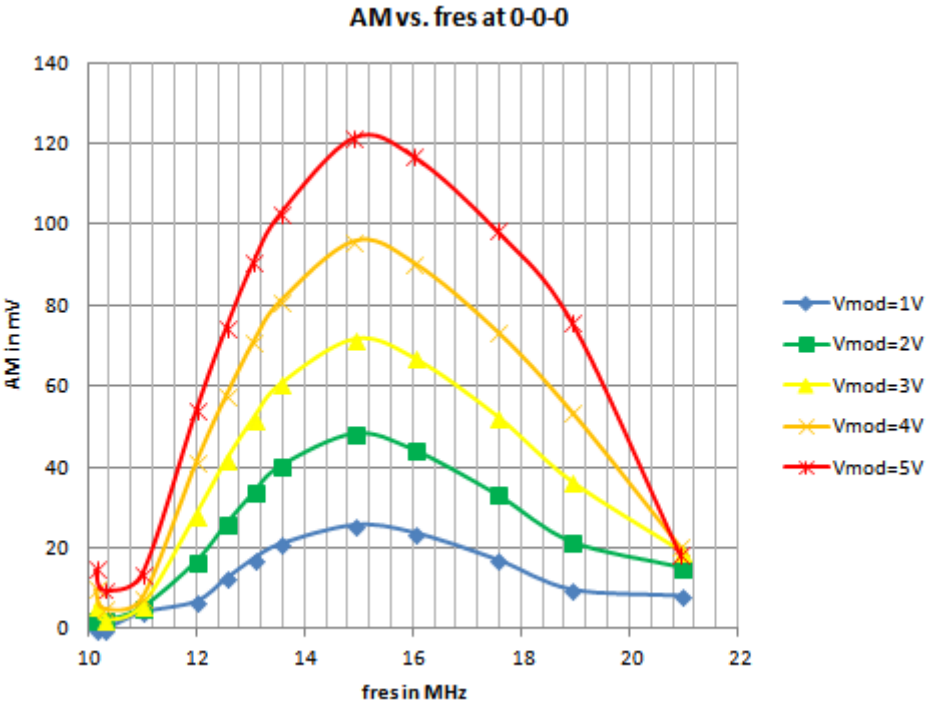

Figure 5.7: AM of the EMV-TEST PICC V2.1 for different f_{res} and modulation voltages with an ohmic load.

Figure 5.8 shows the PM-values over vs. f_{res} of the EMV-TEST PICC V2.1 for different V_{mod} at the position 0-0-0 in the operation volume. It is almost zero around 15 MHz, a result that is independent of V_{mod}. The curve is non-monotonic with a local extremum at around 13 MHz. At around 21 MHz the highest PM value is obtained. Note that for smaller V_{mod} the PM at around 19 MHz is higher.

Figure 5.9 shows the peak-peak value of the unmodulated shunt voltage at the output of

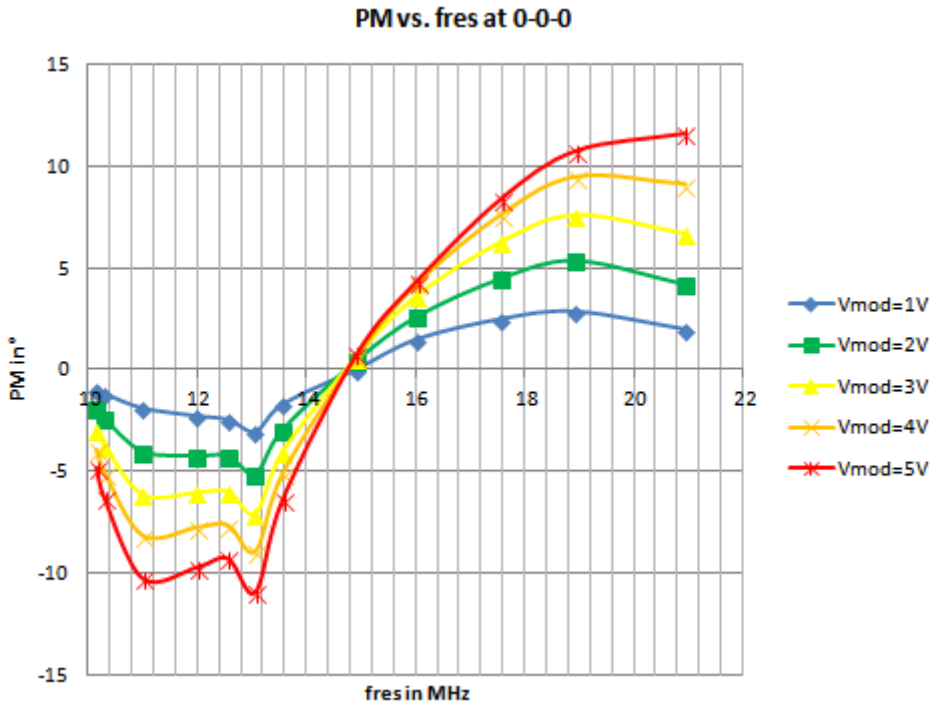

Figure 5.8: PM of the EMV-TEST PICC V2.1 for different resonance frequencies and modulation voltages with an ohmic load.

the EMV-TEST PCD. The lower $Vpp0$ is, the higher is the PICC's influence on the field. The highest influence on the field is found at around 13 MHz. Note that the influence on the field is lower at 13.56 MHz. The curve is not symmetric but steeper at lower resonance frequencies than at higher ones.

The results from the measurements above have been rearranged in Figure 5.10. The upper diagram shows the limits within those the AM value can be set for certain resonance frequencies and in dependence of V_{mod}, the lower diagram shows the same for the PM value. The given frequencies of 14.91 MHz - highest AM and lowest PM - and 20.94 MHz have been chosen due to the fact that the AM as well as PM-curve, are monotonic between these values and therefore it can be assumed that in every point in the yellow areas operation is possible by properly setting f_{res} and V_{mod}. However, it is also clear that not every arbitrary combination of AM and PM in the yellow areas can be obtained. Nevertheless, the plots can be used to justify whether a certain combination can be obtained or not as it will be shown later on.

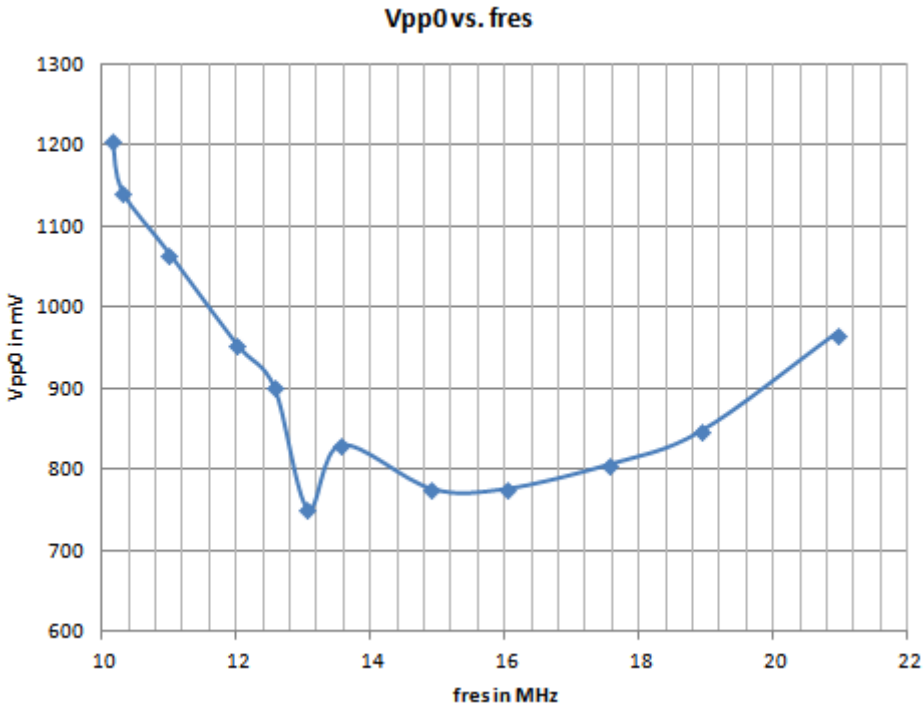

Figure 5.9: Influence on the field of the EMV-TEST PICC V2.1 for different resonance frequencies with an ohmic load.

5.3.2 Measuring Common PICCs

To justify whether the EMV-TEST PICC is capable of emulating all kinds of real-world PICCs, some of such PICCs were measured with the measurement procedure described above. Figure 5.11 shows AM and PM of an Infineon smartcard IC in combination with a Class 1 antenna at different resonance frequencies versus the position in the operation volume of the EMV-TEST PCD. With this chip-antenna combination the highest AM values were expected to occur, which gives a first estimate of the requirements on a future reference PICC. AM and PM both decrease with increasing distance to the PCD coil. At 0-0-0 the maximum AM value is 47 mV, the highest PM value is 3.5 °. While the AM is quite independent of f_{res} at this position the PM is influenced by the resonance frequency a lot. At a resonance frequency of 12.18 MHz the PM is almost independent of the position in the EMV-TEST PCD.

The following Figure 5.12 shows the results of the same measurement executed with an Infineon smartcard IC in combination with various inductively coupled antennas. In todays typical PICC, the module has a galvanic connection to the antenna. In inductively coupled antennas the card as well as the module have their own antennas, which are coupled by a common magnetic field. The different combinations have different resonance

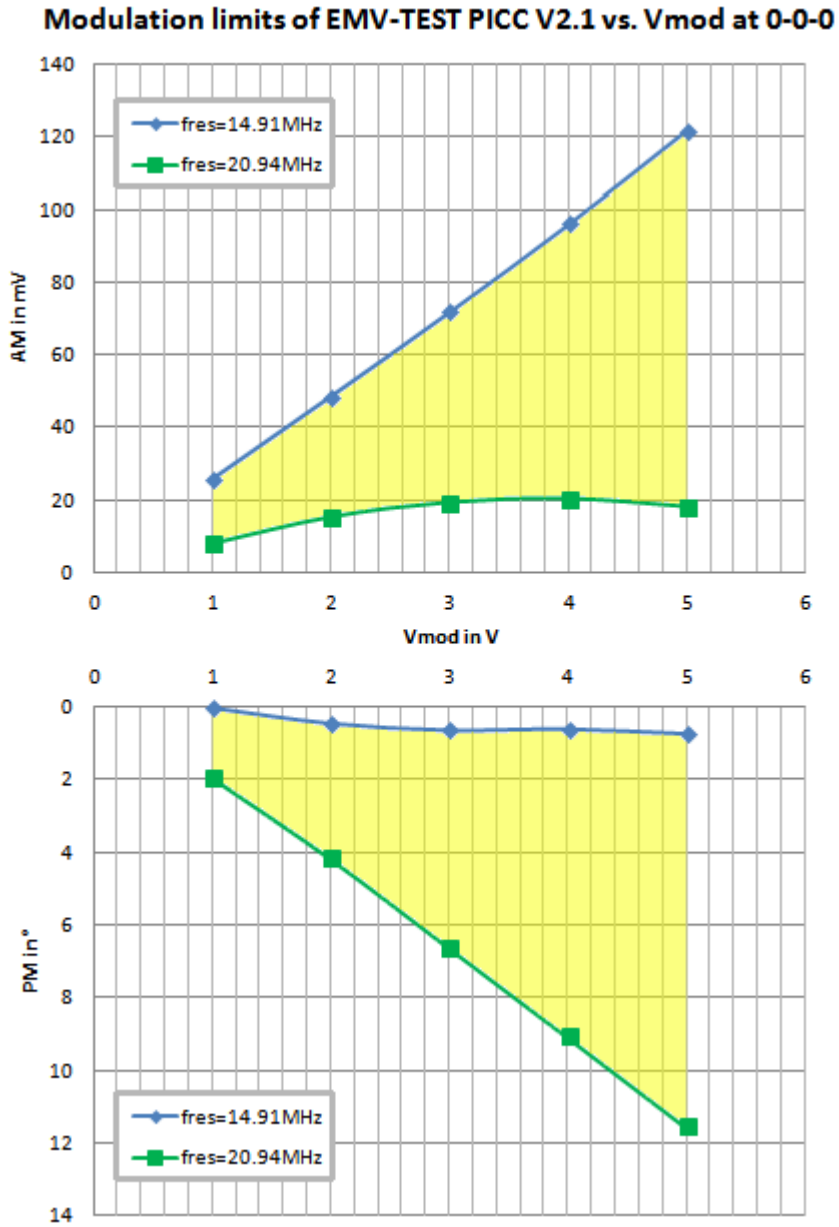

Figure 5.10: Modulation limits of the EMV-TEST PICC V2.1 over the modulation voltage with an ohmic load.

frequencies in the range of 13.86 MHz up to 15.99 MHz. The maximum AM that can be achieved with such a configuration at position 0-0-0 of the EMV-TEST PICC is around 17 mV, which is only about a third of the maximum AM of the measured Infineon smartcard IC connected to a Class 1 antenna. With about 6.5 ° the PM is almost

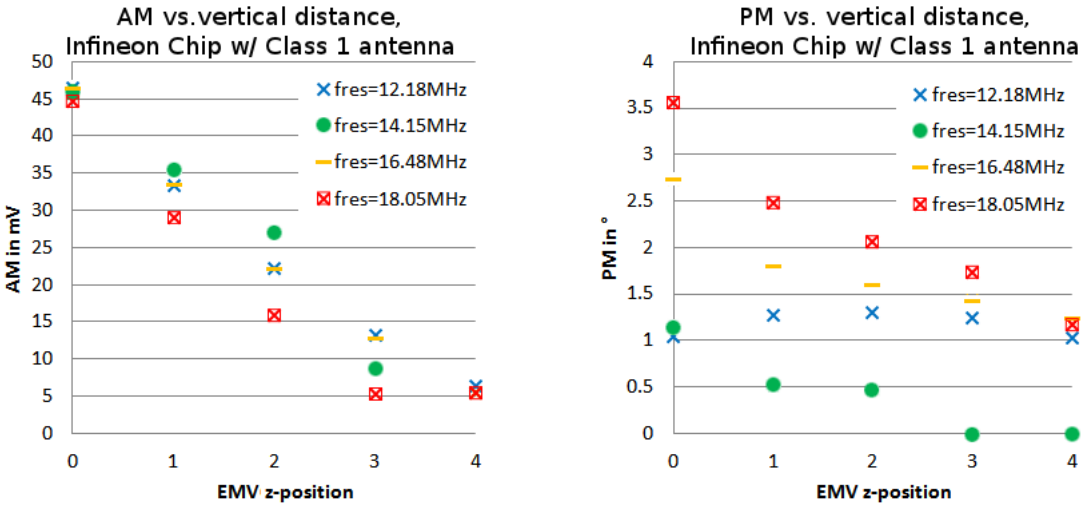

Figure 5.11: AM and PM of an Infineon smartcard IC in combination with a Class 1 antenna at different z-positions of the EMV-TEST PICC

twice as high as the maximum of the upper configuration. AM as well as PM decline monotonically with increasing distance from the PCD-coil.

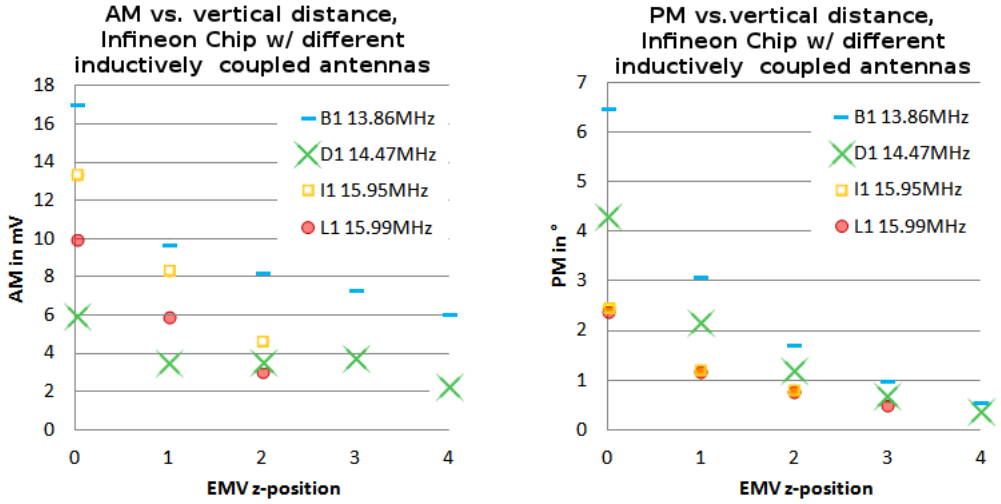

Figure 5.12: AM and PM of an Infineon smartcard IC in combination with various inductively coupled antennas at different z-positions of the EMV-TEST PICC

Figure 5.13 shows how the capability of the EMV-TEST PICC V2.1 to emulate certain chip/antenna-combinations at 0-0-0 can be determined. As examples two results from Figure 5.11 and Figure 5.12 were chosen: an Infineon smartcard IC connected to a Class 1 antenna tuned to 18.05 MHz and another Infineon smartcard IC inductively coupled

to the antenna model B1 with a resonance frequency of 13.86 MHz. The results were obtained the following way:

1. Draw a horizontal line in the AM plot at the AM value of the chip/antenna-combination of interest.
2. Draw a vertical line through the intersect of the AM-limit-curve and the horizontal line. From the intersection with the V_{mod}-axis one knows the voltage range within which such a AM value can be realized.
3. Do the same in the PM plot to find out the voltage range within which the desired PM value can be realized.

In case of the given PICCs this lead to the following results:

- **Infineon smartcard IC with Class1 antenna at** $f_{res} = 18.05\,\mathrm{MHz}$

$$\begin{aligned} AM = 45\,\mathrm{mV} &\rightarrow V_{mod} \geq 2\,\mathrm{V} \\ PM = 3.6\,^{\circ} &\rightarrow V_{mod} \geq 1.67\,\mathrm{V} \\ &\rightarrow \text{emulation possible} \end{aligned}$$

- **Infineon smartcard IC with antenna model B1 at** $f_{res} = 13.86\,\mathrm{MHz}$

$$\begin{aligned} AM = 17mV &\rightarrow V_{mod} \leq 2.2V \\ PM = 6.5\,^{\circ} &\rightarrow V_{mod} \geq 3.38V \\ &\rightarrow \text{emulation not possible} \end{aligned}$$

The results for all measured chip/antenna combinations are summarized in Table 5.2.

Configuration	f_{res}	AM	PM	Emulation at 0-0-0 possible?
-	MHz	mV	∘	-
Chip with Class1 antenna	12.18	46.5	1.1	yes
	14.15	45.8	1.2	yes
	16.48	46.1	2.75	yes
	18.05	44.7	3.6	yes
Chip with antenna model B1	13.86	17	6.5	no
Chip with antenna model D1	14.47	6	4.3	no
Chip with antenna model I1	15.95	13	2.5	yes
Chip with antenna model L1	15.99	10	2.4	yes

Table 5.2: Capability of the EMV-TEST PICC V2.1 to emulate the measured chip/antenna-configurations. By "Chip" a certain Infineon smartcard IC is meant.

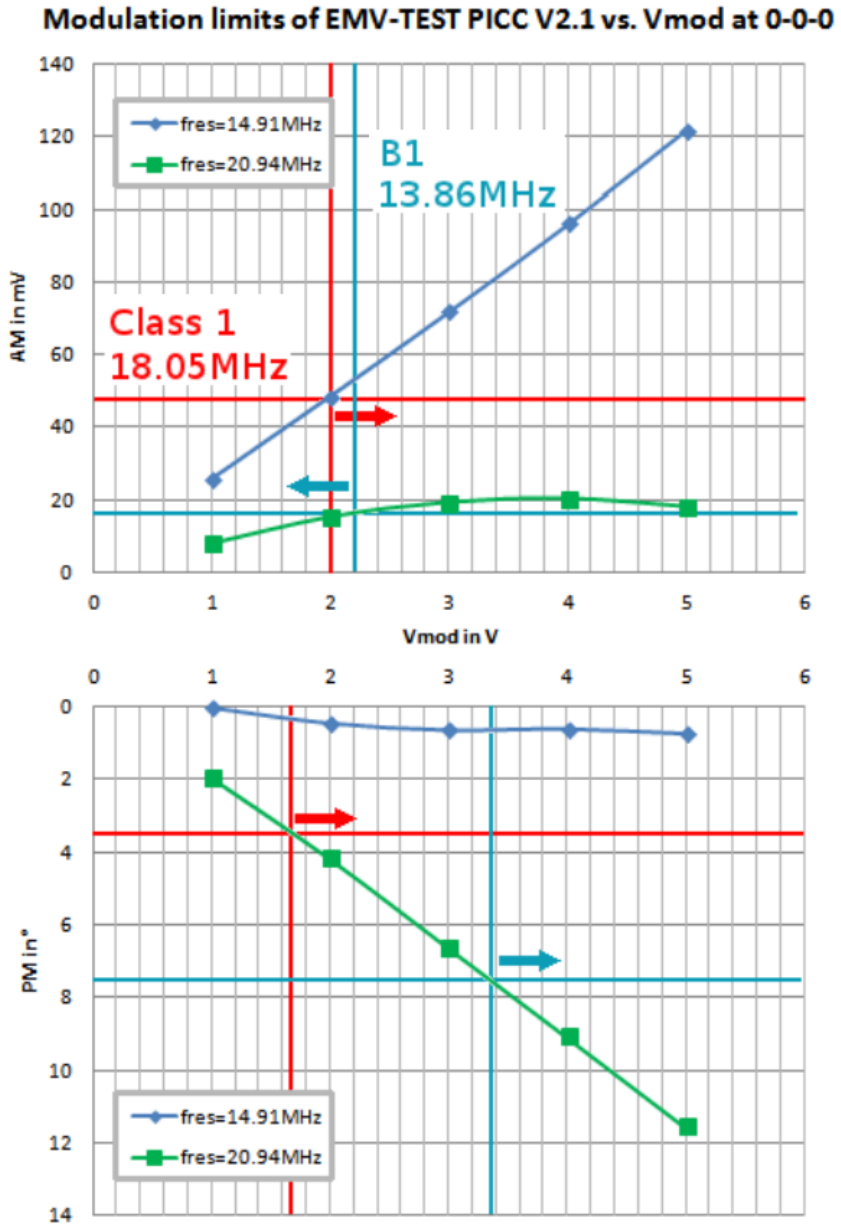

Figure 5.13: Evaluation whether a certain chip/antenna-combination can be emulated with the EMV-TEST PICC V2.1 at 0-0-0. In the plots the range of V_{mod} (indicated by the colored arrows) is determined that allows modulation at the desired AM and PM values.

5.4 Discussion

The analysis above has shown that the current EMV-TEST PICC is not capable of emulating all kinds of chip/antenna-combinations that are currently in the field or at least in development. Finding the right operating point in the f_{res}-V_{mod} plane can also be a very time-consuming process where multiple iterations are necessary. Furthermore the PICCs influence on the field cannot be set independently of AM and PM. Although a lot of different PICCs can be emulated - especially those with conventional galvanically coupled antennas - the demand for a highly flexible reference PICC, which is easy to handle, is not satisfied with the existing device. Therefore, a new reference PICC capable of reaching all operating points in the AM-PM-influence on the field volume needs to be designed.

Chapter 6

Concept of a Future EMV-TEST PICC

6.1 Requirements for a Future EMV-TEST PICC

As shown in the previous chapter, the current EMV-TEST PICC is not capable of properly satisfying the demands of emulating today's PICCs. Therefore the development of a new reference PICC is necessary. But what exactly are the requirements as well as the constraints that have to be considered in the development? The following list mentions and justifies the most important ones:

- **Possibility to easily set AM and PM without affecting the PICC's influence on the field:** This is the core functional requirement. Easily means in this context that the user does not have to go through extensive measuring and tuning procedures before being able to perform any tests.
- **New functions have to be implemented on the basis of the EMV-TEST PICC V2.1:** A proposal of a totally new testing hardware and testing procedures has very little chances to be accepted by EMVCo.
- **Backward compatibility:** It is important that all of the existing tests can still be executed with the proposed future testing hardware while the range of possible tests has been extended. For example, the field strength of the EMV-TEST PCD is set by changing the generator-voltage until the voltage at **J1** of the EMV-TEST PICC V2.1 is 5.53 V. This condition has to remain unchanged by the new PICC (i.e. the influence on the field is kept constant).
- **Realistic representation of real-world PICCs:** The new functionalities shall be implemented in a way that is close to applications in the field. This is especially important for EMV Contactless Level 1 Test Equipment that aims to represent a real-world application environment.

- **Using only standard devices:** The implementation has to be independent of exotic devices that are only available in small number or even in the risk of being discontinued without replacement.

The first requirement leads to the conclusion that some kind of active modulation is necessary in a new reference PICC. The basics of actively modulating PICCs will be explained in the next section.

6.2 Active Modulation of the H-Field

Contrary to the common modulation technique of passive load modulation, where only the load of the PICC is changed, active modulation involves the altering of the H-field with an additional energy source that is energetically independent of the field. In case of the reference PICC, there are two manifest principles of active modulation of the H-field: inductive coupling with an additional antenna or galvanic coupling with an additional current source as shown in figure 6.1. The left picture shows the inductive coupling approach where energy from the active coil is coupled mainly into the PICC's main coil and partially also into the PCD's coil whereas it is decoupled with the Leti coil. Such a coupling configuration can for example be realized with an active coil that is congruent with the main coil of the PICC. The right picture shows the galvanic coupling approach where a current is forced through the PICC by a current source in parallel to the antenna. An ideal current source has an infinitely high internal impedance and hence no influence on the resonance frequency and the Q-factor of the PICC. A theoretical alternative would be a voltage source in series to the antenna though this is much more complicated to realize[1] and will therefore not be touched in the following considerations. All of todays real-world applications that use active modulation work on the basis of galvanic coupling.

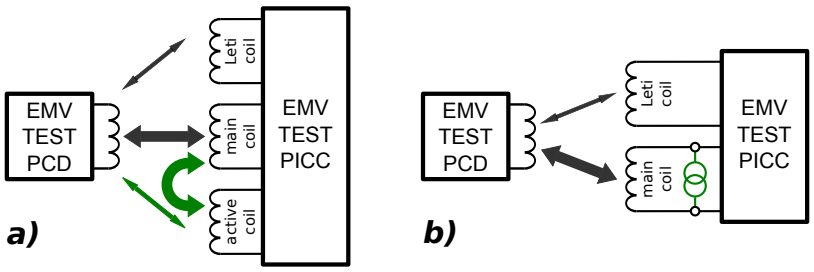

Figure 6.1: Concepts for active modulation of the H-field: a) inductive coupling, b) galvanic coupling.

[1] One has to bear in mind that the local ground of the EMV-TEST PICC V2.1 is on the DC side of the rectifier. A voltage source in series to the antenna is placed on the AC side of the rectifier and has therefore no constant reference potential which makes the implementation very difficult.

As shown in figure 2.7, the transponder can be represented as transformed transponder impedance Z'_T in the PCD. Figure 6.2 shows the equivalent for active modulation: the current $\underline{I}_2$ that flows through the PICC coil L_2 and subsequently effects the current in the PCD coil L_1, can be split up into the parts $\underline{I}_{2,load}$ caused by the loading of the PICC and $\underline{I}_{2,mod}$ caused by some kind of active feeding-in. The effect of $\underline{I}_{2,load}$ on the PCD is represented by $Z'_{T,load}$, indicating that this special part remains unaffected by modulation and is in direct relation to the current $\underline{I}_1$. The independence of $\underline{I}_{2,mod}$ from $\underline{I}_1$ makes a voltage source, $\underline{V}_{mod}$, a more adequate representation of its effect on the PCD than some kind of impedance.

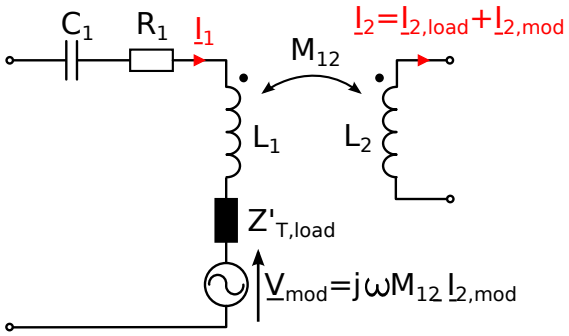

Figure 6.2: Schematic representation of active modulation.

As can be seen in this figure, the amplitude and phase of $\underline{V}_{mod}$ are directly related to amplitude and phase of $\underline{I}_{2,mod}$ which leads to the conclusion that by proper modulation of $\underline{I}_{2,mod}$, amplitude and phase of $\underline{I}_1$ can also be modulated. In the following subsections it will be shown how $\underline{I}_{2,mod}$ can be set.

6.2.1 Setting the Modulation Current Inductively

Figure 6.3 shows a simple equivalent circuit of an actively modulating system on the basis of inductive coupling as depicted in figure 6.1 a). Note that the coupling between the active coil and the PCD's coil is neglected in the equivalent circuit!

As already shown in Figure 2.7 the current through the PCD's antenna $\underline{I}_1$ induces a voltage $\underline{U}_{Q1}$ in the PICC's antenna. This voltage leads to the loading current $\underline{I}_{2,load}$:

$$\underline{I}_{2,load} = \frac{\underline{V}_{Q1}}{R_2 + j\omega L_2 + \underline{Z}_2} \tag{6.1}$$

The current $\underline{I}_{active}$ induces another voltage in the PICC coil. This leads to the second part of $\underline{I}_2$:

$$\underline{I}_{2,mod} = \underline{I}_{active} \frac{j\omega M_{act2}}{R_2 + j\omega L_2 + \underline{Z}_2} \tag{6.2}$$

$\underline{I}_{2,mod}$ is therefore nothing else but $\underline{I}_{active}$ multiplied with a complex scaling factor. This

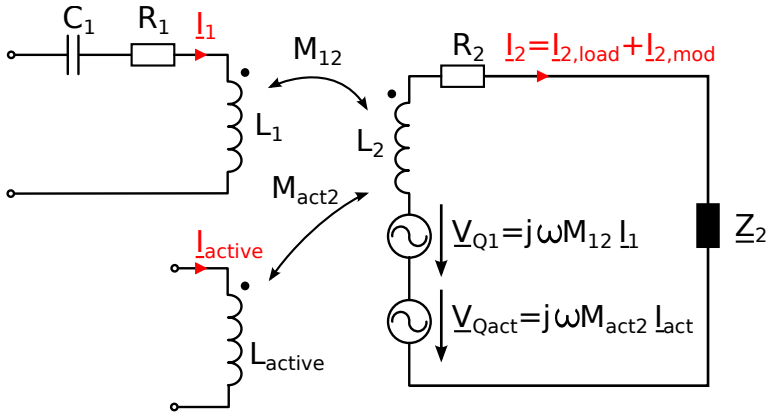

Figure 6.3: Simple equivalent circuit of inductive setting of $\underline{I}_{2,mod}$

simple equivalent circuit involves only linear elements, therefore the single components of $\underline{I}_2$ can simply be added:

$$\underline{I}_2 = \underline{I}_{2,load} + \underline{I}_{2,act} \tag{6.3}$$

6.2.2 Setting the Modulation Current Galvanically

Figure 6.4 shows a simple equivalent circuit of an active modulating system by galvanic feeding-in as depicted in Figure 6.1 b). An ideal current source with infinitely high source impedance is assumed to calculate the currents $\underline{I}_{2,load}$ and $\underline{I}_{2,mod}$. The first is exactly the same as in equation 6.1. $\underline{I}_{2,mod}$ is calculated as follows:

$$\underline{I}_{2,mod} = -\underline{I}_{active}\frac{\underline{Z}_2}{R + j\omega L_2 + \underline{Z}_2} \tag{6.4}$$

This result is very similar to the one obtained in equation 6.2, simply $\underline{I}_{active}$ times a complex scaling factor.

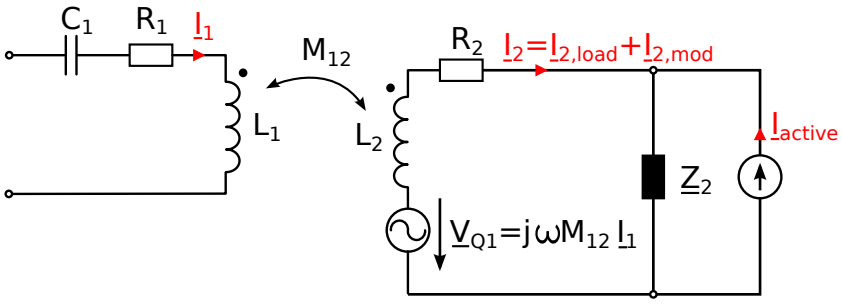

Figure 6.4: Simple equivalent circuit of galvanic manipulation of $\underline{I}_{2,mod}$

6.3 Advantages and Disadvantages of Each Approach

From the theoretical point of view and by making some simplifications, both coupling mechanisms have the same effect. So what are the practical advantages and disadvantages of each approach?

6.3.1 Pros And Cons Of Inductive Coupling

+ Galvanic separation between the EMV-TEST PICC and the modulating source.
+ Simple matching of the signal source to the antenna L_{active}
+ Simple analog front-end because L_{active} can be operated grounded
- Requires extensive modification of the present EMV-TEST PICC because a further antenna must be implemented.
- Very inflexible in reference to different PICC antenna sizes[2] due to strong geometrical dependence.
- Real applications only have one antenna, so the multi-coil concept is a poor representation of reality.
- The coupling between the PCD and the PICC's main coil is changed by the additional antenna.

6.3.2 Pros and Cons of Galvanic Feeding-In

+ Only small modifications of the present EMV-TEST PICC necessary, an SMA-jack at the antenna for connection is already there.
+ Very flexible in reference to different PICC antenna size as independent of geometry.
+ Good representation of real-world applications.
+ The coupling between the PCD and the PICC's main coil remains unchanged.
- No galvanic separation between the EMV-TEST PICC and the modulating source and therefore higher parasitic coupling of signals.
- The analog front-end is more complicated.

[2]One must bear in mind that active modulation is usually utilized in systems with small antennas e.g. in the size of an Mini-SIM card (ISO/IEC 7810:2003, ID-000). Some future reference PICCs may therefore also have small antennas

6.4 Basic Concept of an Active Modulator for the EMV-TEST PICC V2.1

The considerations mentioned before led to the decision for the approach of galvanic feeding-in. The next question was: which parts are necessary to build an extension of the EMV-TEST PICC V2.1 that allows for active modulation? However, when implemented, these functions are absolutely crucial:

- Retrieval of the phase information of the H-field for synchronization to establish a fixed phase relation between $\underline{I}_{2,mod}$ and $\underline{I}_1$.
- Possibility for the user to arbitrarily set the phase between $\underline{I}_{2,mod}$ and $\underline{I}_1$ within reasonable limits.
- Possibility for the user to arbitrarily set the amplitude of $\underline{I}_{2,mod}$ within reasonable limits.
- Appropriate modulator for digital modulation to transmit data.

Two approaches of synchronization are present in state-of-the-art systems that use active modulation: in the two-antenna approach, synchronization and communication are accomplished by two separate coils, one for each purpose. In the one-antenna approach, a phase locked loop is synchronized with the field during the transmission pauses.

The considerations finally led to the concept shown in Figure 6.5. The blocks depicted there have the following functionality:

1. **Leti Coil:** The Leti coil is coupled with the PCD's coil but decoupled with the PICC's coil. The output voltage $L(t)$ is phase related to the H-field that is produced by the PCD's coil.
2. **Input Lowpass Filter:** This filter removes the noise from $L(t)$. The jitter of the zero-crossings is therefore reduced in $L_{filt}(t)$.
3. **Zero-Crossing Detector:** A fast comparator that converts the analog voltage $L_{filt}(t)$ in a digital signal $D(t)$. This step is necessary, because integrated delay lines regularly only shift the flanks of digital signals.
4. **Variable Delay Line:** Enables the user to shift the digital input signal for a certain amount of time. The output signal $D_{delay}(t)$ will have a known amplitude as defined in the data sheet of the delay line (e.g. CMOS, TTL, ECL...). [3]
5. **Bandpass Filter:** Converts the digital input signal into a sinusoidal carrier signal $C(t)$ with fixed amplitude.

[3] **Note:** Every single component in this chain adds delay or phase shift, especially the bandpass filter! So the delay that is set at this position is not an absolute but only a relative value!

6. **Variable Gain Amplifier:** Allows the user to set the amplitude of the carrier signal.
7. **OOK-Modulator:** Provides an interface for digital modulation of the carrier. In this simple approach only on-off-keying is possible.
8. **Controlled RF Current Source:** Converts the modulated signal $S(t)$ in a current that is fed into the PICC.
9. **Main Coil:** Converts the coil current into a magnetic field that acts upon the PCD coil.

In the course of the project it was decided that all further effort should be focused on the controlled current source. The development of this device as well as simulation- and testings-results are topic of the next chapter.

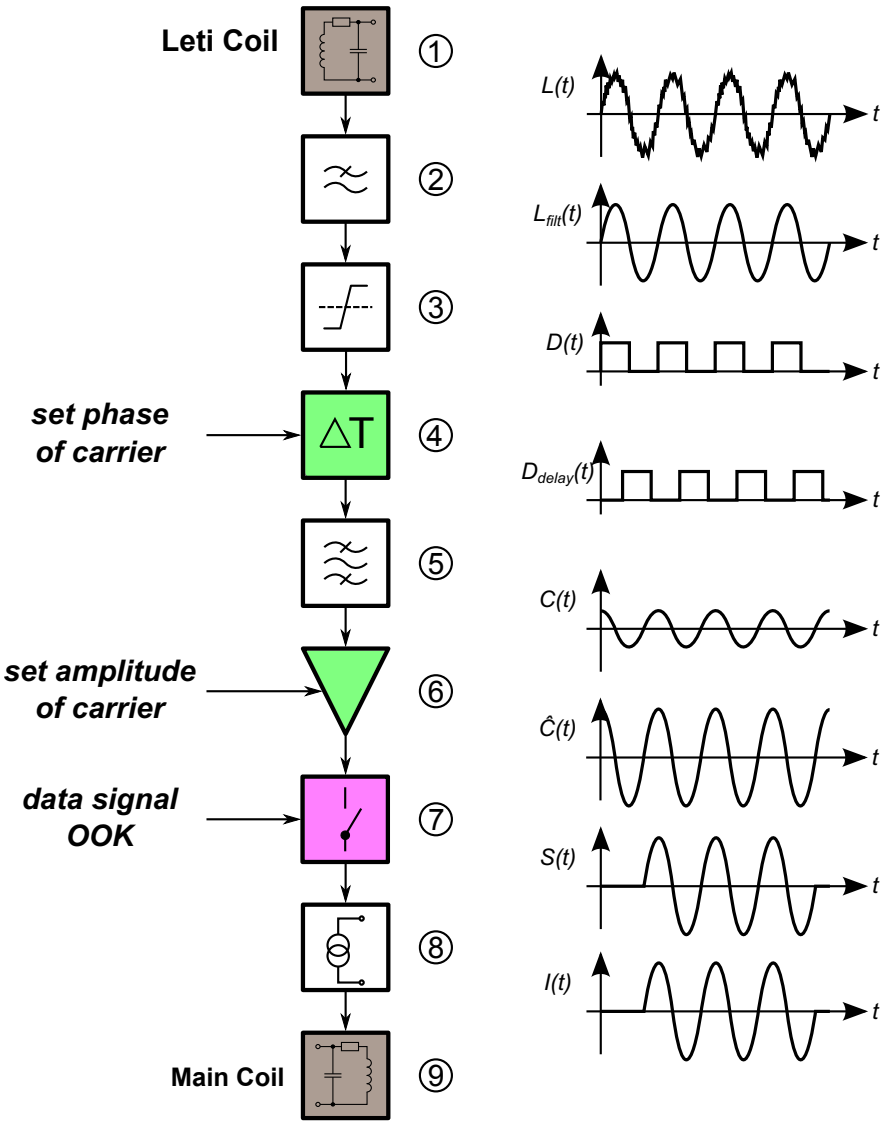

Figure 6.5: Block diagram of a device that adds active modulation capability to the EMV-TEST PICC V2.1. Blocks in grey are already present, blocks in green allow the user to manually modify amplitude and phase of the carrier and the pink block provides an interface for digital modulation. Blocks in white require no user interaction.

Chapter 7

RF Current Source for Active Load Modulation

7.1 Requirements for the RF Current Source

Some of the requirements for a future EMV-TEST PICC apply directly to the RF current source. The demand for little to no tuning effort for the user as well as the avoidance of influencing the present behavior of the EMV-TEST PICC and the use of standard devices is also valid for this explicit part of hardware. Additional to these, following questions also need to be answered before the development can start:

- **Input properties**
  - What kind of input signal will be used, current or voltage?
  - What is the range of the input signal?
  - What is the impedance of the source used for generating the input signal?
- **Output properties**
  - What output currents are necessary to achieve AM and PM values that appear in real-world systems?
  - What voltages can be expected at the antenna of the EMV-TEST PICC?

The questions concerning input properties allow various answers. In this special case it was decided that the signal source should be some kind of waveform generator with a source impedance of $50\,\Omega$. The input voltage range was chosen to be $2\,V_{pp}$, a value that even AWG's with high bandwidths in the GHz-range can deliver into a $50\,\Omega$ load[1] (Tabor Electronics Ltd, Tel Hanan, Israel).

[1] e.g. Agilent's 81180B [2] (Agilent Technologies, Santa Clara, USA) or Tabor's Model WW1281A [20]

The output requirements of the RF current source had to be derived directly from the load, i.e. the EMV-TEST PICC. An analysis of the internal circuitry gives a good estimation for the maximum voltage that appears at the SMA jack **J6** that is connected to the pins of the EMV-TEST PICC antenna. At nominal load setting, this voltage is limited to roughly 20 V by a zener diode with a breakdown voltage of 15 V and five small signal diodes in series to it with a generously estimated forward voltage of 1 V. The maximum negative potential can not be lower than one forward voltage of a rectifier diode below GND, i.e. −1 V.

The necessary output current can be estimated by calculating the current that is drained at the DC side of the rectifier by the modulation circuitry during load modulation. This current is proportional to the voltage applied to **J2** and has a maximum value of around 25 mA when the maximum modulation voltage of 5 V is applied. Under the assumption that this equals the rms value of the active modulation current during feeding-in, it can be concluded that a peak-peak modulation current of around 70 mA is necessary to obtain the same effect. However, such an estimate totally neglects the effects of different phase shifts between the field and the modulation current which has a severe influence on the antenna current. As shown in chapter 5, the EMV-TEST PICC produces an AM of around 120 mV at the maximum modulation voltage of 5 V when tuned to the nominal 16.1 MHz, which is almost three times the AM a modern chip/antenna-combinations can produce. In the end it was therefore decided that a maximum output current swing of 50 mA_{pp} would be sufficient[2].

The input and output properties are summarized in table 7.1:

Input properties	
Input voltage range	2 V_{pp}
Input impedance	50 Ω
Output properties	
Output current swing	50 mA_{pp}
Maximum output potential	20 V
Minimum output potential	−1 V

Table 7.1: Input and output properties of the RF current source

[2]In fact, this decision was made during the setting up of the final prototype. All former estimation approaches were based on wrong assumptions and delivered too high currents.

7.2 Basic Concept

Figure 7.1 shows the basic concept of the RF current source for feeding current into the EMV-TEST PICC. During measurement a GND potential is introduced into the DC side of the PICC's rectifier and therefore no potential at the AC side can be assumed to be constant. This results in the necessity to construct the RF current source with two floating outputs, which is established by the complementary output transistor couple T_3 and T_4. These bipolar junction transistors operate in common base configuration. In this configuration, the transistors work as impedance converters: at the input - the emitter - the impedance is low, at the output - the collector - it is very high. This produces a current amplifier with unity gain.

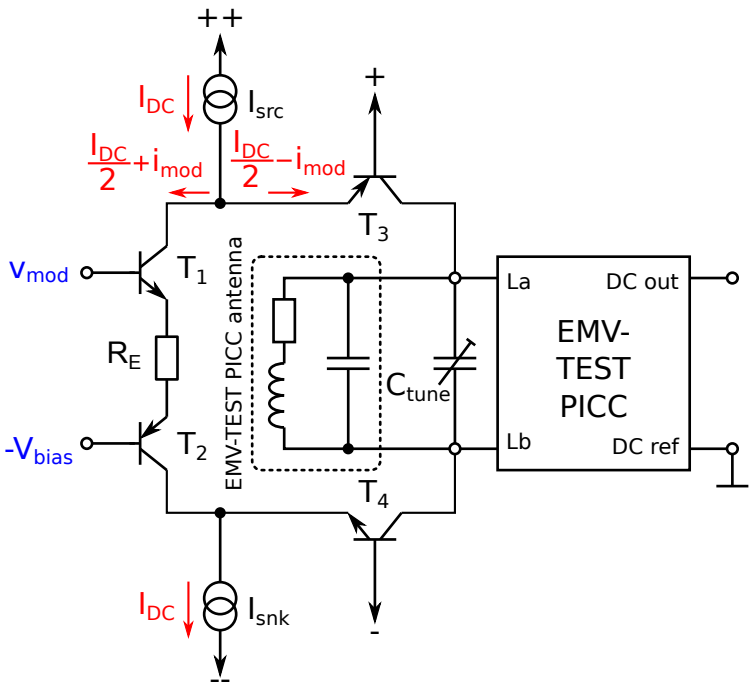

Figure 7.1: Basic concept of the RF current source connected to the EMV-TEST PICC

The input current of the output transistors T_3 and T_4 is created by subtraction of an alternating current i_{mod} from a constant bias current $I_{DC}/2$ which is set by application of a proper base potential $-V_{bias}$ at T_2. Input as well as output stage both rely on a constant bias current for operation. I_{DC} is introduced by the current source I_{src} and extracted from the circuit by the current sink I_{snk}. If an alternating voltage v_{mod} is applied to the input transistor T_1 an alternating current v_{mod}/R_E will be the result. An increase of the input current of i_{mod} leads to a corresponding decrease of the output current. The circuit can be interpreted as inverting transconductance amplifier with a transconductance of $-\frac{1}{R_E}$.

Bipolar junction transistors are the active devices of choice for this approach. In the context of this application, they have the following benefits compared to MOSFETs:

- Smaller output capacitance → higher output impedance.
- Higher transconductance → smaller variation of the emitter potentials due to variation of the collector currents
- Better availability of complementary devices

7.3 Simulation of the Concept

The purpose of a simulation of the concept is to evaluate, if it is possible to create the same modulation behavior with active modulation as the EMV-TEST PICC does with passive load modulation. It was therefore necessary to create reasonable good simulation models of the EMV-TEST PCD and the EMV-TEST PICC as well as the concept of the RF current source. The program chosen for creating and simulating the models was LTspice IV (Linear Technology Corporation, Milpitas, USA). It is a fast and free SPICE simulator, schematic capture and waveform viewer [12]. The software is easy to use and has no limitation concerning the number of nodes or wires placed.

7.3.1 Creating Simulation Models of the EMV-TEST PCD and PICC

Modeling the Antennas

The first step in creating the models was to find the equivalent parameters of the PCD and PICC antennas. The representation chosen was that of an inductor in series with a resistor and a capacitor in parallel. The parameters where measured with the impedance analyzer Agilent 4395A. To measure the parameters of the PCD coil, it had to be attached directly to the impedance analyzer with the connections to all other components cut (e.g. the shunt resistor or the matching network). The measurement at the reference PICC was executed at the device as a whole, tuned to the nominal resonance frequency of 16.1 MHz as described in the specification [7].

As all transient simulations of the models would be executed at a carrier frequency of 13.56 MHz, the sweeping range of the impedance analyzer needs to be set closely around 13.56 MHz. The equivalent parameters can be directly calculated by the 4395A. The measurement results were as follows: The comparatively large C_p of the EMV-TEST

Device	L_s	R_s	C_p
-	nH	Ω	pF
EMV-TEST PCD V1.2	628	0.766	35.9
EMV-TEST PICC V2.1	2281	1.78	42.4

PICC comprises a parallel tuning capacitor with a value of 27 pF as well as the variable capacitor VC1 with a value somewhere between $1 - 10$ pF.

Modeling the EMV-TEST PCD

Additionally to the coil as well as the known shunt and damping resistors, the EMV-TEST PCD comprises a matching network of two capacitors to match the signal source with an internal impedance of 50 Ω to the antenna. The values of these capacitors can be calculated analytically as done by Hoelzl [8]. Figure 7.2 shows the resulting model of the EMV-TEST PCD V1.2 for LTspice IV including the signal source.

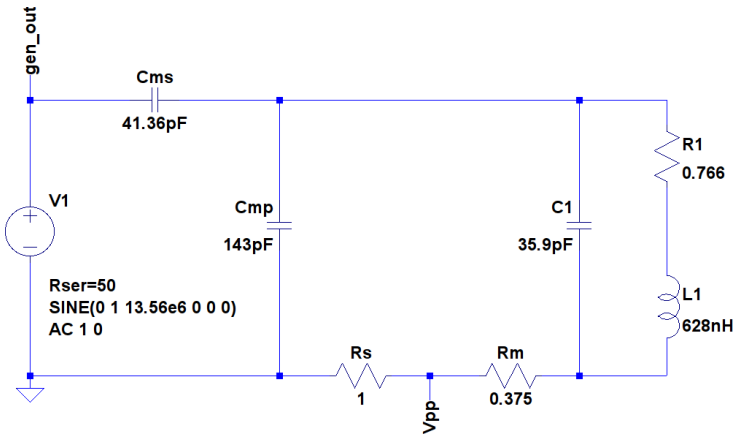

Figure 7.2: Model of the EMV-TEST PCD V1.2 for LTspice IV.

Modelling the EMV-TEST PICC

The internal circuitry of the EMV-TEST PICC is not available to the public, yet Infineon - as a technical associate of EMVCo - has access to documents that show the detailed construction of the EMV-TEST hardware. Figure 7.3 shows the LTspice-model of the EMV-TEST PICC V2.1 with all internal devices packed into a subcircuit. The ports **LA** and **LB** represent the pins of the coil. In the EMV-TEST PICC V2.1 these two are connected to *J6* which is shown in Figure 4.1. The physical equivalent of **MOD_IN** is the connector *J2*, for **DC_OUT** it is *J1*. The port **DC_REF** is necessary to introduce a local ground into the model of the EMV-TEST PICC. In reality this potential will be

set to GND as soon as a generator is attached to *J2* with a coaxial cable, or the voltage at *J1* is measured with a passive probe.

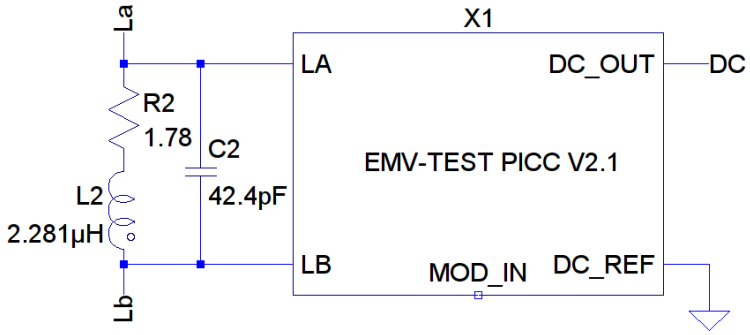

Figure 7.3: Model of the EMV-TEST PICC V2.1 for LTspice IV. The internal circuitry is packed into the subcircuit X1.

Modeling The Coupled System

After the models of the single devices have been constructed it had to be evaluated how large the generator voltage at the input of the PCD as well as the coupling factors between PCD-coil and PICC-coil are for different positions. To retrieve representative values a number of voltages was measured at the EMV Contactless Level 1 Test Equipment, as shown in Figure 7.4. At the connector *J2* of the EMV-TEST PICC a rectangular modulation burst with four pulses, a frequency of 847.5 kHz and voltage levels of 0 V and 5 V respectively were applied. The transient behavior of the single voltages was recorded at the positions 0-0-0 and 0-0-2 within the operation volume as explained in section 4.2. The power of the H-field had been set to the nominal value beforehand. The voltage at the pins of the antenna was measured with a 100:1 differential high impedance probe, shielded with aluminium foil, all other voltages where measured with passive 10:1 high impedance probes.

After the measurement, the amplitude of the generator voltage and the coupling factor between the coil in the simulation model were varied until a reasonable good equivalence between measurement values and model had been established.

Figure 7.5 shows the values that were used to compare the simulation model to the real system.

Figure 7.6 shows the final simulation model of the coupled EMV-TEST system. The coupling factor is set to 0.15 for simulation of the PICC placed at the position 0-0-0 in the operation volume and 0.06 for simulation of the PICC placed at the position 0-0-2 in the operation volume. A generator source voltage amplitude of 16.7V delivers reasonable good results as can be seen in table 7.2. Although some of the simulated values differ

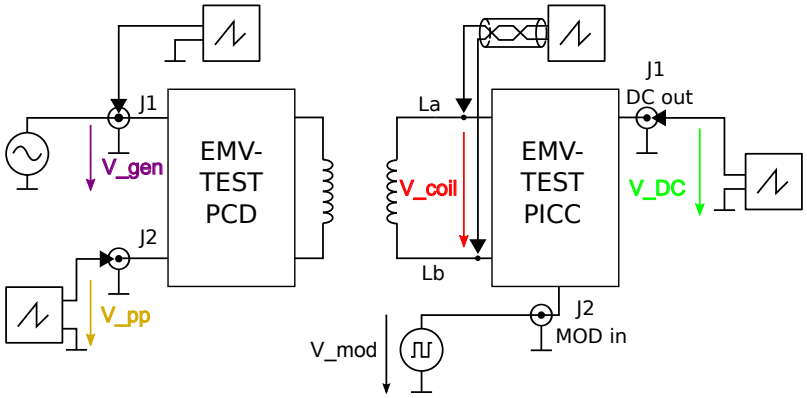

Figure 7.4: Setup for the measurement of important voltages of the coupled system.

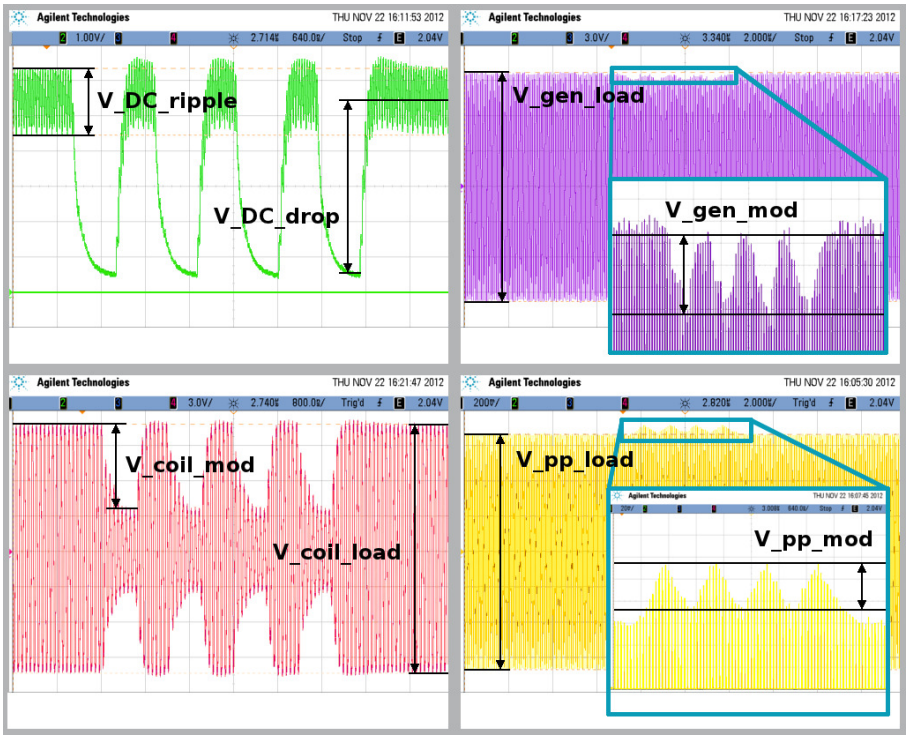

Figure 7.5: Transient behavior of the measured voltages under applied load modulation including the naming of certain parameters.

significantly from the measured ones, the simulation model offers sufficient ground for rough estimations of the real behavior.

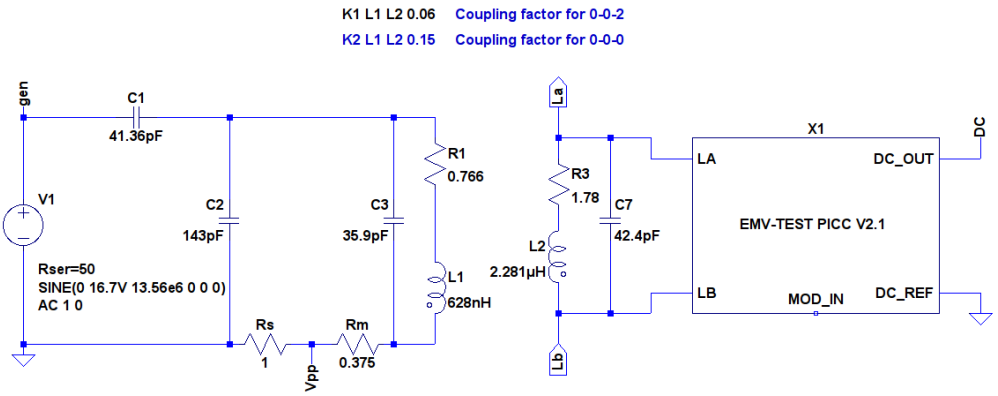

Figure 7.6: Final simulation model of the coupled EMV-TEST system.

Position	Quantity	Unit	measured	simulated
0-0-0	V_DC_ripple	V	3.3	1.8
	V_DC_drop	V	4.3	4.9
	V_gen_load	V	23.8	23.4
	V_gen_mod	mV	715	795
	V_coil_load	V	29	28.4
	V_coil_mod	V	4.9	5.8
	V_pp_load	mV	821	880
	V_pp_mod	mV	92	76
0-0-2	V_DC_ripple	V	1.9	1.0
	V_DC_drop	V	5.1	4.8
	V_gen_load	V	19.5	18.7
	V_gen_mod	mV	415	460
	V_coil_load	V	21.2	20.9
	V_coil_mod	V	7.3	7.6
	V_pp_load	V	1.33	1.34
	V_pp_mod	mV	43	35

Table 7.2: Comparison of the measured vs. the simulated values of the coupled system.

7.3.2 Simulation Model of the Concept of the RF Current Source

In the first approach the RF current source was modeled with ideal parts only. It is shown in figure 7.7. Contrary to the concept depicted in figure 7.1, the bias points of the bipolar transistors are already set with resistors and capacitors, which is already a step towards the real implementation. Furthermore the supply voltages were defined as +24 V, +19 V, +5 V and −5 V. The constant currents I_1 and I_2 were set to 60 mA. The complete schematic obviously includes the coupled system shown in figure 7.6. The resonance frequency of the EMV-TEST PICC is not changed by the attachment of the

RF current source.

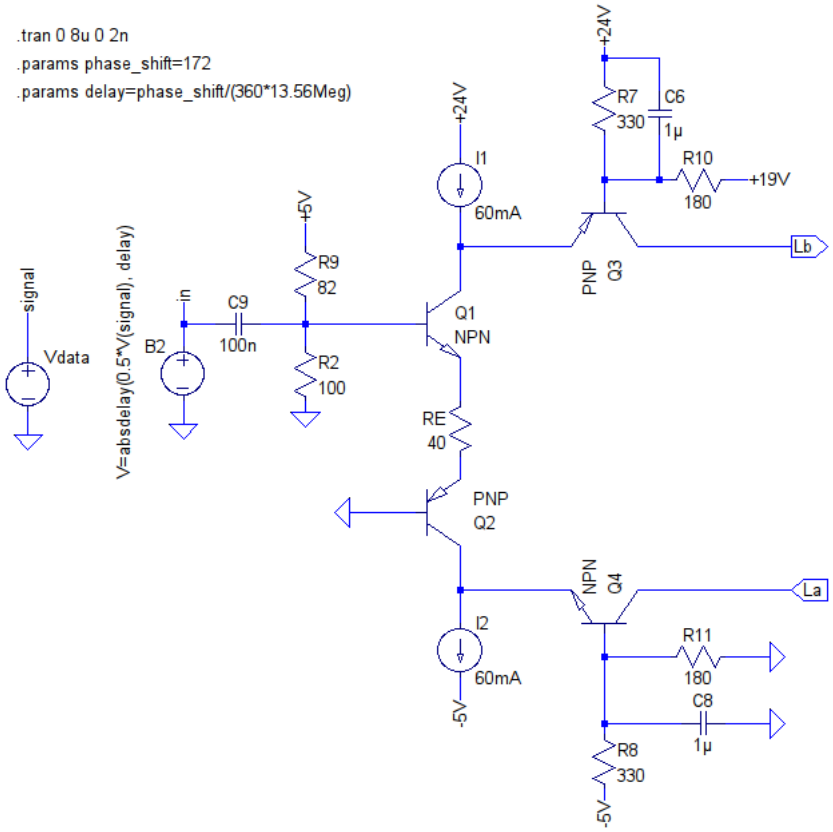

Figure 7.7: LTspice model of the concept of the RF current source.

7.3.3 Simulation Settings

The simulations of the load modulation as well as the active modulation system were executed with the default parameters derived in section 7.3.1 for nominal power at position 0-0-2 in the operation volume.

In the simulation of the passive load modulation system, a rectangular voltage burst with four pulses, a frequency of 847.5 kHz and on-voltage levels of 2.5 V and 5 V respectively, were applied to the **MOD_IN** port of the model of the EMV-TEST PICC. The off-voltage level was 0 V in both cases.

Figure 7.8 shows the input signal used for active modulation. It is a pulsed sine wave with a carrier frequency of 13.56 MHz, a pulse frequency of 847.5 kHz and total number of four pulses. The generic phase is 0° or in other words, with no phase shift added, the pulses of the input signal of the RF current source *V(in)* (see fig. 7.7) would be congruent

with *V(gen)* (see fig. 7.6), the input voltage of the EMV-TEST PCD. A phase shift of 172° was deliberately introduced between these two signals in figure 7.6.

In the course of this thesis, the input signal will be expressed in the form $r\angle\varphi$, were r stands for the peak-peak value of the input voltage and φ stands for the phase difference between the input voltage of the EMV-TEST PCD and the carrier of the input signal of the RF current source, e.g. $1\,\mathrm{V}\angle 172°$ for the signal in figure 7.8.

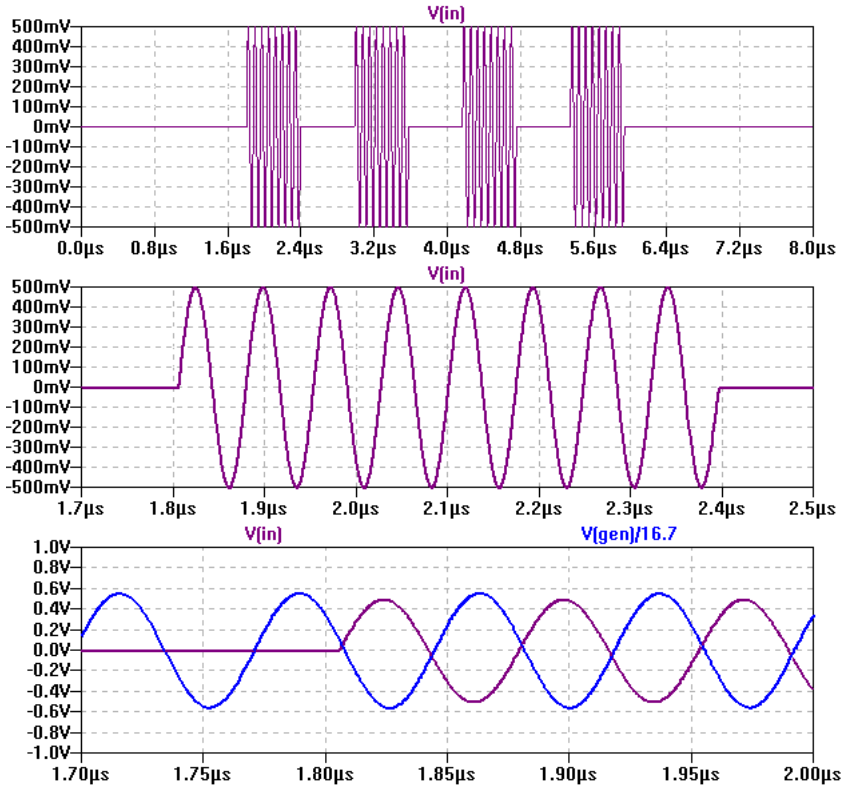

Figure 7.8: Input signal used for active modulation. The plot at the top shows the signal in the total time range, the medium plot shows a single pulse of the input burst and the plot at the bottom shows the phase shift between the input signal of the EMV-TEST PCD and the input signal of the RF current source.

7.3.4 Results

Figure 7.9 shows the simulated amplitude and phase modulation of the voltage *V(Vpp)* during load modulation with a modulation voltage of 2.5 V applied to the port **MOD_IN** of the model of the EMV-TEST PICC. AM is around 10 mV while PM is around 1°.

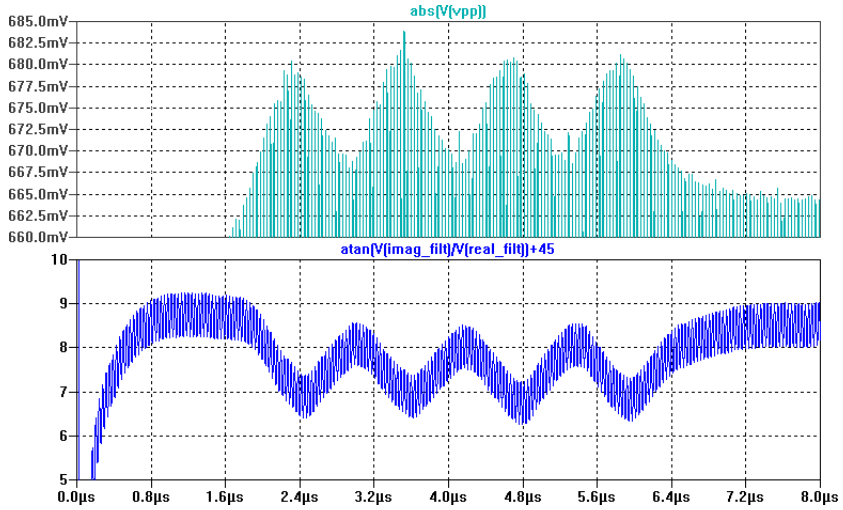

Figure 7.9: Simulation results of amplitude (upper plot) and phase modulation (lower plot) of the shunt voltage *V(Vpp)* of the EMV-TEST PCD obtained with passive load modulation. A modulation voltage of 2.5 V was applied to **MOD_IN** of the EMV-TEST PICC.

Figure 7.10 shows the same voltages but this time active modulation was applied. The current fed into the EMV-TEST PICC by the RF current source has a peak-peak value of 25 mA and a phase shift of 172° relative to the input voltage of the EMV-TEST PCD. The 25 mA are half of the maximum output current swing. This time, AM is found to be around 15 mV while the PM is slightly below 1°.

If a load modulation voltage with an amplitude of 5 V is applied to the port **MOD_IN** of the model of the EMV-TEST PICC, the modulation shown in figure 7.11 is the result. AM is about 35 mV in this case, PM about 1.3°.

Finally, active modulation with the full-scale modulation current of 50 mA_{pp} and a relative phase shift of 172° between the input voltages of the RF current source and the EMV-TEST PCD leads to the results shown in figure 7.12. AM is around 30 mV, PM is around 1.3°. The waveshape of the amplitude is considerably different compared to all other amplidute plots in the figures of this section: after a sharp rise for about 0.3 μs the envelope of the curve bends to a much smaller value, prohibiting an amplitude modulation above a certain level. This phenomenon can be observed at different phase shifts when modulation currents in this range are fed into the EMV-TEST PICC. However, in this specific configuration the characteristic is pronounced very strongly.

7.3.5 Discussion

The motivation behind these simulations was to evaluate, if it is possible to emulate the passive load modulation system with the active modulation approach. As the results

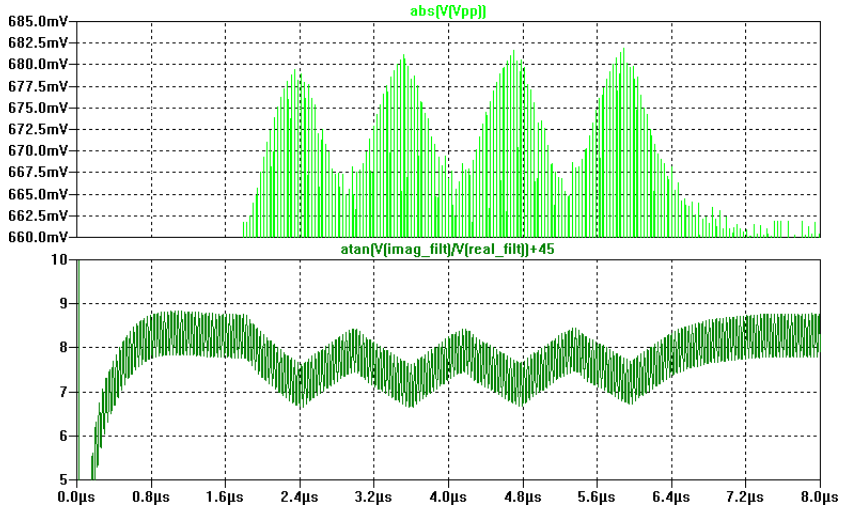

Figure 7.10: Simulation results of amplitude (upper plot) and phase modulation (lower plot) of the shunt voltage *V(Vpp)* of the EMV-TEST PCD obtained with active modulation at the input signal $1\,\mathrm{V}\angle 172°$.

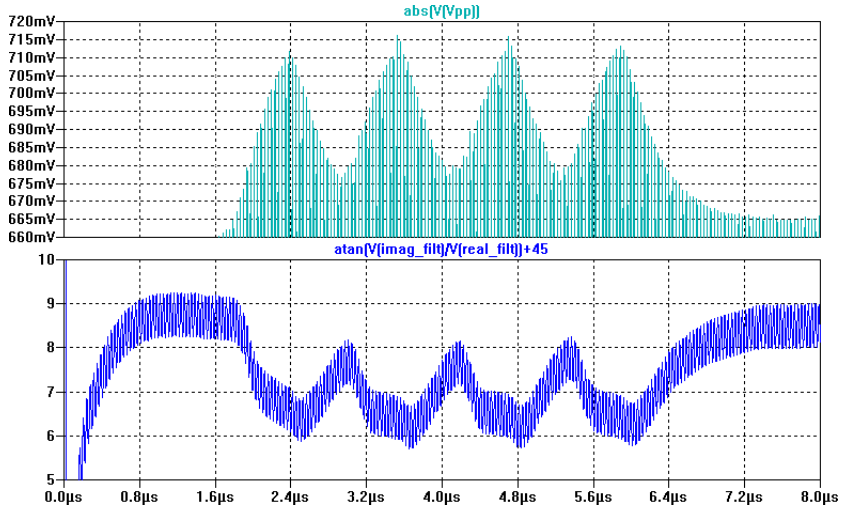

Figure 7.11: Simulation results of amplitude (upper plot) and phase modulation (lower plot) of the shunt voltage *V(Vpp)* of the EMV-TEST PCD obtained with passive load modulation. A modulation voltage of 5 V was applied to**MOD_IN** of the EMV-TEST PICC.

show, this is no problem with smaller modulation signals. However, the simulation with higher modulation current suggests that there is a certain limit of AM that can not be passed by simply increasing the amplitude of the input signal of the RF current source. This seems to be the result of the dynamic phase shift of the antenna current due to feeding-in. In other words: the phase shift between the antenna currents $\underline{I}_{2,load}$

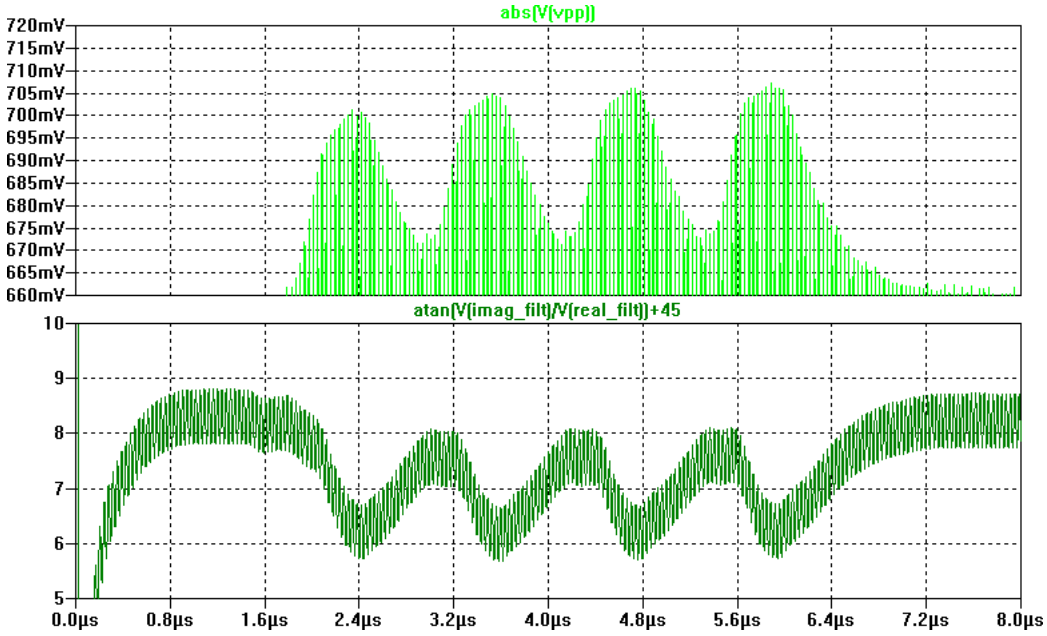

Figure 7.12: Simulation results of amplitude (upper plot) and phase modulation (lower plot) of the shunt voltage *V(Vpp)* of the EMV-TEST PCD obtained with active modulationat the input signal $2\,\mathrm{V}\angle 172°$.

and $\underline{I}_{2,mod}$ according to figure 6.2 is not static during a modulation pulse but varies depending on amplitude and relative phase of the modulation current pulse. It is an open question if this behavior is reduced or enhanced under realistic conditions: One has to bear in mind that the carrier of the modulation current is derived from the field in the final configuration and is therefore subjected to phase modulation too.

All in all the simulation proved the ability of the concept to fulfill the requirements.

7.4 Implementing the Subcircuits

The next step in the development of the RF current source was the implementation of the so far ideal components with real devices. To simplify this process, the circuit was split into three subcircuits:

- **RF Current Deflector:** The complete RF part of the device, comprising the input and output transistors T_1 - T_4 as well as the resistor R_E depicted in figure 7.1.
- **Matched Constant Current Source/Sink:** I_{src} and I_{snk} of figure 7.1.
- **Power Supply:** The sum of the externally applied and internally generated supply voltages.

7.4.1 RF Current Deflector

Figure 7.13 shows the final implementation of the RF current deflector. At the points **I_SRC** and **I_SNK** it is connected to the matched current source/sink, a DC current of roughly 60 mA flows between these points from the top to the bottom. As a result of the minimum and maximum potentials that have to be expected at the output pins, the base potentials of **T8** and **T9** were set to roughly 21 V and -2 V respectively. Assuming a base-emitter voltage of 0.7 V, the voltage between **I_SRC** and **I_SNK** is around 24.4 V, which leads to a total power dissipation of around 1.5 W inside the RF current deflector. When no modulation signal is applied this power is shared in equal parts between the input branch - comprising **D5**, **T6**, **T7**, **R_E1** and **R_E2** - and the output branch comprising **T8** and **T9**.

The output transistors were the most critical parts to choose. To keep distortions of the circuit at a minimum and the output impedance at a maximum, small parasitic collector-base capacitances were required. As a simulation showed, the collector potentials of the output transistors change with more than 1000 V/μs due to the voltage induced in the EMV-TEST PICC Antenna leading to roughly 1 mA of erroneous base current for every picofarad of collector-base capacitance. This led to a demand of transistors with C_{obo} well below 10 pF, the smaller the better. It was finally decided to use the complementary transistor couple *PZT3904* and *PZT3906* that have at a collector-base voltage of 5 V_{DC} a maximum C_{obo} of 4 pF and 4.5 pF respectively. They withstand collector-emitter voltages up to 40 V and continuous collector currents up to 200 mA. At an ambient temperature of 25°, each of these BJTs (bipolar junction transistor) can dissipate as much as 1 W. Both transistors have an SOT-223 case and are widely available. **T8** dissipates generally more power than its NPN counterpart **T9**. For this reason its collector is connected to the GND pins of the SMA connector **X2**. This provides a large thermal mass for **T8** and extracts heat efficiently.

The base potentials of **T8** and **T9** were simply set with resistor dividers and stabilized with ceramic capacitors. Special attention was payed to providing a low-impedance

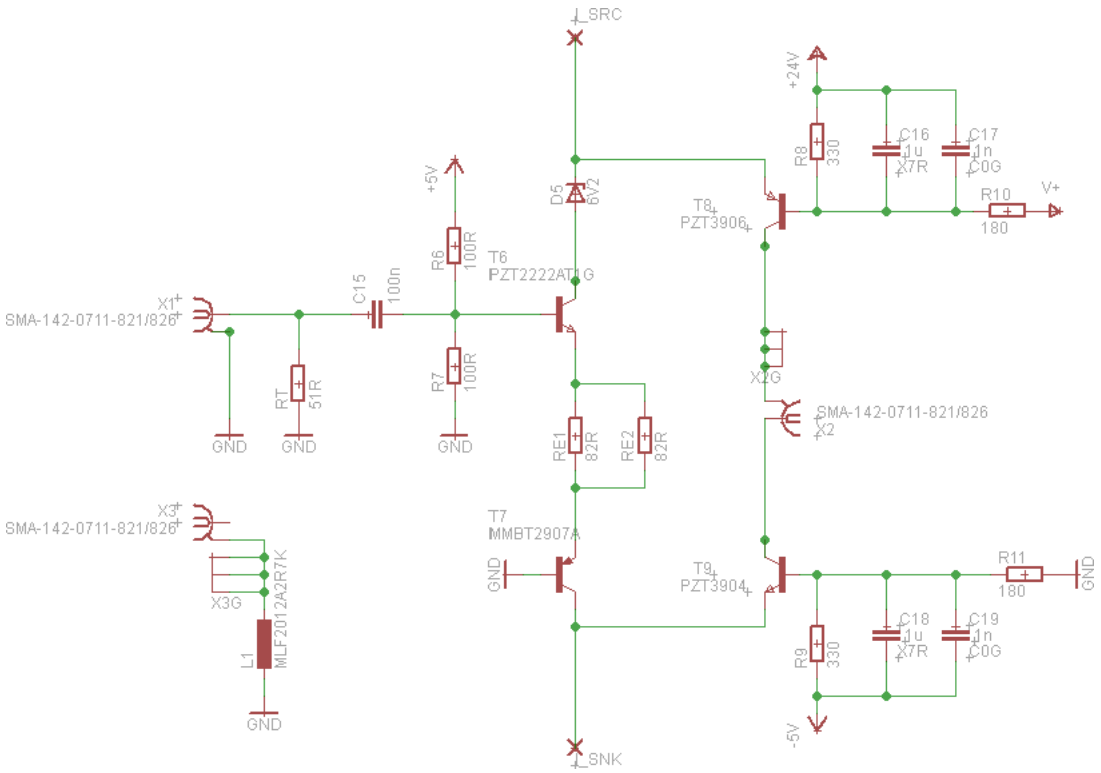

Figure 7.13: Schematic of the RF current deflector

path to GND for the base currents generated by transients on the collectors. Capacitors with the dielectric C0G have an exceptionally low equivalent series resistance at high frequencies and are therefore predestined for this purpose.

The input branch is less critical in terms of output capacitance. To relieve the input transistor **T6**, a zener diode with a breakdown voltage of 6.2 V is connect in between **I_SRC** and its collector. The base potential of the input transistor is set to 2.5 V, which leads to a voltage of around 1.1 V - 1.3 V across the resistors **R_E1** and **R_E2**, depending on temperature. This results in a bias current of 27 mA up to 32 mA respectively. For **T6** the transistor type *PZT2222A* was chosen. It is widely available, comes in an SOT-223 package and has a maximum total power dissipation of 1.5 W. At its bias point, **T6** has a collector-emitter voltage of around 12 V leading to an average power dissipation of about 400 mW. The PNP transistor complementary to the *PZT2222A* is the *PZT2907A*. Due to the small average power dissipation of only about 100 mW at the transistor **T7** it was decided to take the same type in a smaller SOT-23 package and so an *MMBT2907A* was used instead.

To introduce a DC reference into the EMV-TEST PICC, another SMA jack was placed in the circuit. **X3** is connected to local GND via a filter inductance to prevent the coupling of high-frequency distortions between the circuits.

7.4.2 Matched Constant Current Source/Sink

It is obvious from the concept shown in figure 7.14 that a difference between the currents of **I_SRC** and **I_SNK** also leads to different collector currents of the output transistors. Due to the fact that charge cannot be created or destroyed, the difference between the output currents has to be compensated by another current. This current flows via the

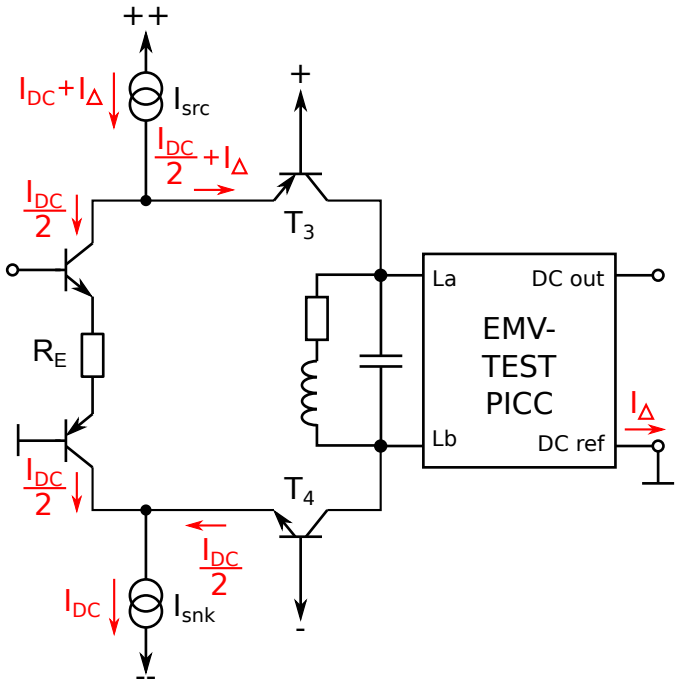

Figure 7.14: Different output currents lead to a compensation current I_Δ via the local GND connection DC ref.

local GND connection into or out of the EMV-TEST PICC and leads to additional voltage drops at the internal circuitry. As a result, the voltage at the connector **J1** is changed, which is very undesirable, because - as described in section 4.1 - the PCD field strength is measured at this point. Any variation of this voltage leads therefore directly to erroneous measurement results.

As a simulation showed, a difference between the output currents of 1 mA changes the voltage at **J1** of the EMV-TEST PICC for up to 200 mV, a value that is by no way acceptable.

The logical consequence was that the current source and sink need to be matched properly. A maximum difference between source and sink current of 200 μA was found to be easily approachable as well as acceptable.

Up to now it has been completely neglected that the base currents of the transistors will also change the currents in the input and output branch. To keep this influence at a

minimum only complementary transistor couples are used. Nevertheless, different DC current gains due to device tolerances and different junction temperatures will indeed add different base currents and hence, different output currents will be the result. It is hard to give a precise estimate of this error current but its maximum value will be in the order of a few hundred μA.

In theory it would be possible to directly measure the output currents of the transistors **T8** and **T9** with a shunt resistor. Several reasons make this a difficult task:

- Any additional load in form of shunt resistors degenerates the performance of the output transistors.
- Different RF common mode voltages decrease the measurement precision.
- The RF voltages at the antenna of the EMV-TEST PICC will decrease the measurement precision due to coupling with the measurement circuit.

Figure 7.15 shows the concept of the matched constant current source/sink. Under the assumption of ideal devices, the operational amplifiers will set their output voltages in a way that the difference between their input voltages becomes zero. The reference current

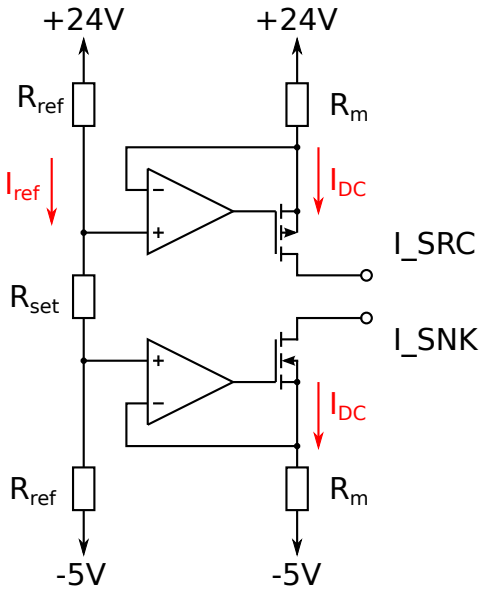

Figure 7.15: Concept of the matched current source/sink

I_{ref} is a function of the supply voltages and the resistors in the reference branch and is simply calculated the following way:

$$I_{ref} = \frac{24\,\mathrm{V} + 5\,\mathrm{V}}{2R_{ref} + R_{set}} \tag{7.1}$$

Equation 7.2 shows how the source/sink currents are calculated:

$$I_{DC} = I_{ref} \frac{R_{ref}}{R_m} \tag{7.2}$$

It is obvious that the matching accuracy between the currents of **I_SRC** and **I_SNK** is directly related to resistance tolerances, temperature dependencies and parasitics of the operational amplifiers. Figure 7.16 shows the final implementation that was found to keep the influence of these quantities at an acceptable value.

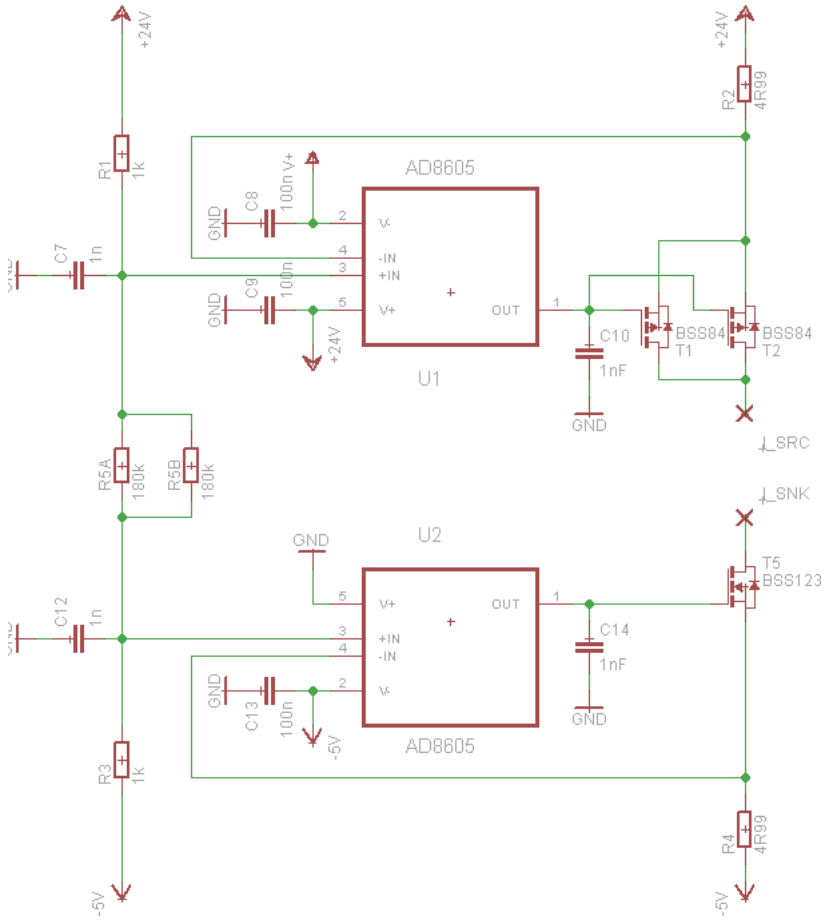

Figure 7.16: Schematic of the matched current source/sink

Following considerations led to the devices in the output branch as it is:

- The MOSFETs shall have small output capacitances on the one hand and yet a high output impedance in the operating point on the other hand.
- To minimize heating, the power dissipated by **R2** and **R4** should be kept at a minimum

To properly function as voltage controlled current sources that have a high output impedance, the MOSFETs need to operate in their saturation regionthat means, enough V_{DS} has to be supplied. As shown in section 7.4.1, the potentials at **I_SRC** and **I_SNK** are about 21.7 V and −2.7 V respectively, leaving a total voltage of only 2.3 V for the measurement resistors **R2** and **R4** and the MOSFETs.

The N-channel MOSFET of choice was the *BSS123*. It can deliver the requested drain current of around 60 mA while operating in saturation mode at a V_{DS} of down to 1 V. The output capacitance is somewhere between 15 pF and 30 pF in this operating point.

It is always more difficult to find an appropriate P-channel MOSFET. Two *BSS84* in parallel were found to be an adequate solution. A single device would have to operate very close to the border between the linear region and the saturation region, if a V_{DS} of about 2 V is assumed, as figure 7.17 suggests. With two devices in parallel it can be assumed that both will operate in their saturation region.

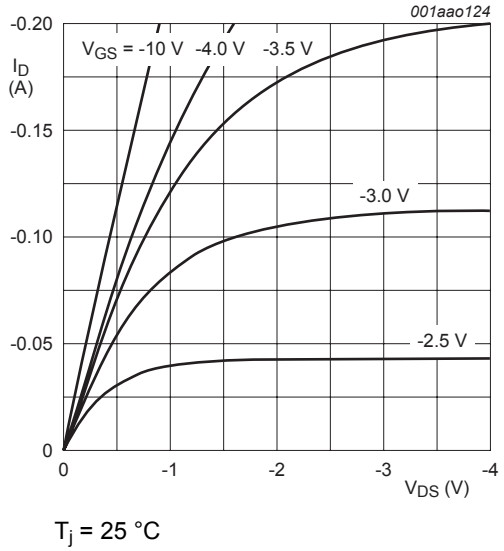

Figure 7.17: Output characteristics, drain current as a function of drain-source voltage; typical values [15]

The resistor type chosen for measuring the drain currents of the MOSFETs was the *RP73D2A4R99BTG* by TE Connectivity (TE Connectivity Ltd., Berwyn, USA). Its nominal value is 4.99 Ω with a resistance tolerance of ±0.1% and a temperature coefficient of ±15 ppm/°C, the case type is 0805. An intended output current of 60 mA leads to a voltage drop of only 300 mV. This leaves a drain-source voltage of around 2.4 V for each of the MOSFETs. Note that the nominal resistance varies only for ±4.99 mΩ. It is a challenge to make a layout that does not degenerate this value significantly.

The *AD8605* was the operational amplifier finally chosen. It is a precision amplifier with the following key parameters at a supply voltage of 5 V:

- **Offset Voltage:** typ. 80 μV
- **Input Bias Current:** max. 1 pA
- **Output Voltage High:** min. 4.96 V at a load current of 1 mA
- **Output Voltage Low:** max. 40 mV at a load current of 1 mA
- **Single-Supply Operation:** 2.7 V - 5.5 V

To keep the influence of the input bias currents negligible and yet the power dissipation in the reference branch as small as possible, the reference current was defined to be in the range of a few hundreds of microamperes. According to equation 7.1 a reference current of 299 μA is the result of the device values shown in figure 7.16 which leads to the desired 299 mV of voltage drop across the reference resistors with a nominal value of 1 kΩ, resistance tolerance of $\pm 0.01\%$ and a temperature coefficient of ± 25 ppm/°C.

According to the nomenclature used in figure 7.15, the maximum mismatch between the source/sink current can be calculated as follows:

$$\Delta I_{DC,max} = \frac{I_{ref} R_{ref,max} + V_{OS}}{R_{m,min}} - \frac{I_{ref} R_{ref,min} - V_{OS}}{R_{m,max}} \tag{7.3}$$

Under the assumption of zero temperature differences and the admissible neglect of the input bias currents of the operational amplifiers, the value of $\Delta I_{DC,max}$ is 164.3 μA.

7.4.3 Power Supply

Due to the fact that the RF current source will only be used in a laboratory environment the availability of a power supply unit was assumed. In the simulation model described in section 7.3.2 the values +24 V, +19 V, +5 V and −5 V were already introduced. Most of the current in the circuit flows from +24 V to −5 V so it was reasonable to take these voltages from the power supply unit. The +19 V are necessary to supply one of the operational amplifiers and to bias the PNP bipolar transistor at the output of the RF current source. Only a relatively small current of around 10 mA will flow into this supply and can thus be created by a linear voltage regulator from the +24 V supply without dissipating too much power. The same applies for the +5 V supply. Figure 7.18 shows the final implementation of the power supply circuitry. **D1** and **D2** are for inverse-polarity protection, **D3** prevents over-voltage between the supply pins of one of the operational amplifiers.

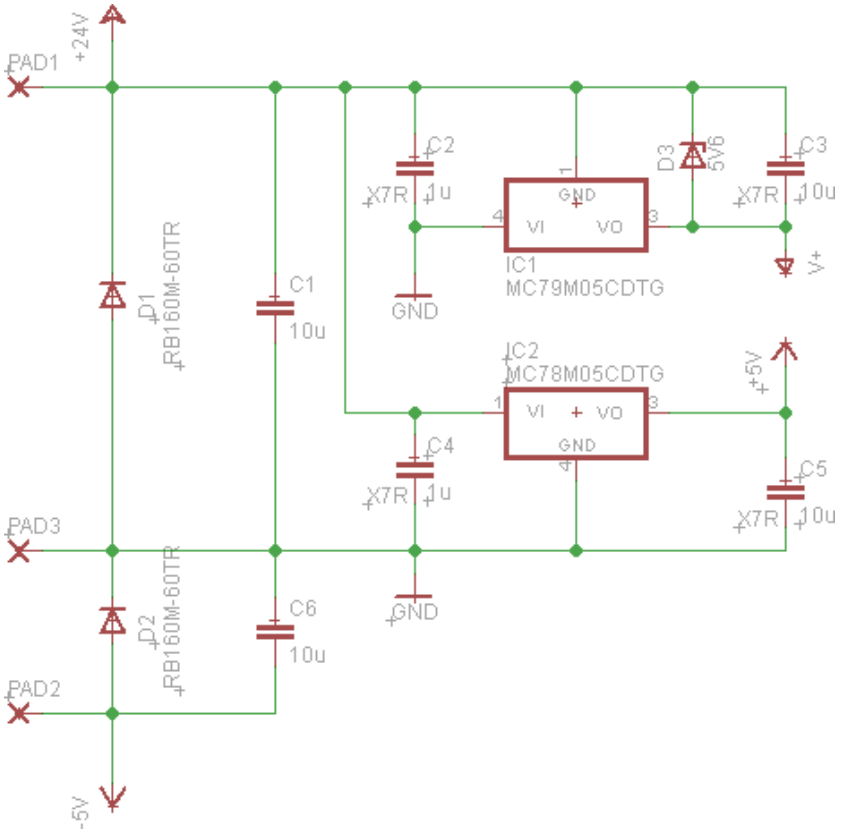

Figure 7.18: Final implementation of the power supply circuitry.

7.5 Simulating the Subcircuits

In this section the schematics of the RF current deflectors as well as the matched constant current source/sink were simulated separately with the proper device models. LTspice doesn't offer the functionality to simulate full layouts but for estimation purposes a schematic simulation was found to be sufficient.

Device Models

Realistic device models were only used for the active devices but not for the passive ones. In the frequency domain of the signals used, this is an acceptable simplification. The output transistors were expected to be the main source of distortion so the focus was placed on finding decent subcircuits for these devices, including the parasitics of the package.

Not every model was available in form of such a subcircuit, some had to be combined manually. Table 7.3 shows, where the models or their single components have been downloaded from.

Subcircuit	**Component**	**Source**
PZT2222A	complete	www.nxp.com [16]
MMBT2907A	transistor parameters of SMBT2907A	www.infineon.com [9]
	package parasitics of subcircuit BC327C	www.infineon.com [9]
PZT3904	transistor parameters of PZT3904	www.infineon.com [9]
	package parasitics of subcircuit PZT2222A	www.nxp.com [16]
PZT3906	transistor parameters of PZT3906	www.infineon.com [9]
	package parasitics of subcircuit PZT2222A	www.nxp.com [16]
BSS84	complete	www.nxp.com [14]
BSS123	complete	www.nxp.com [13]
AD8605	complete	www.analog.com [3]

Table 7.3: Device models and their reference sources

7.5.1 RF Current Deflector

Figure 7.19 shows the final LTspice model of the RF current deflector. It is exactly the circuit depicted in figure 7.1, except for the device models and the additional zener diode in the input branch.

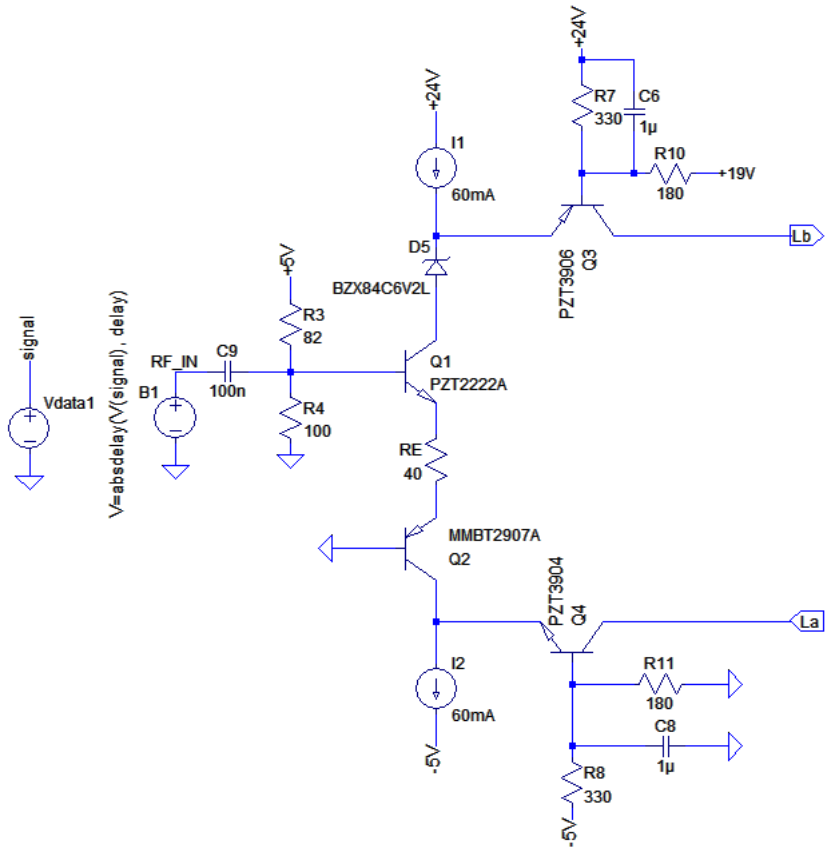

Figure 7.19: LTspice model of the RF current deflector

AC Simulation to Tune the Resonance Frequency

According to the EMV specifications, the nominal resonance frequency of the EMV-TEST PICC is 16.1 MHz [7]. The spice models of ideal BJTs take no parasitic capacitances into account and therefore the resonance frequency of the EMV-TEST PICC remained constant after connection to the concept of the RF current source. However, real transistors will detune the resonant circuit considerably, which makes it necessary to change the tuning capacitance denoted in section 7.3.1.

To correctly measure the resonance frequency of the combination RF current deflector/EMV-TEST PICC it was necessary to change the measurement procedure. According to the EMV specification, the resonance frequency is measured contact based at the Calibration Connector **J6**. With the extended reference PICC this is no longer possible due to two reasons:

1. **J6** is already used to connect the RF current source.

2. The RF current source itself introduces a GND on the DC side of the rectifier. A further GND introduced on the AC side by the impedance analyzer completely changes the behavior of the device and therefore also the resonance frequency.

For these reasons, the resonance frequency of the combined circuits can only be measured contactlessly. Figure 7.20 shows the simulation model used for this purpose. As explained in section 2.3.2, the transformed transponder impedance behaves like a parallel resonant circuit that has the same resonance frequency as the PICC. The inductor **L1** itself has an impedance of $j230.74\,\Omega$ at 16.1 MHz which is much smaller than the expected resonant impedance of $\underline{Z}'_T$. So in a first approach it can be neglected and the resonance frequency of the serial connection of **L1** and $\underline{Z}'_T$ simply can be assumed to be the resonance frequency of $\underline{Z}'_T$. However, real impedance analyzers usually offer a function for fixture compensation to correct this error.

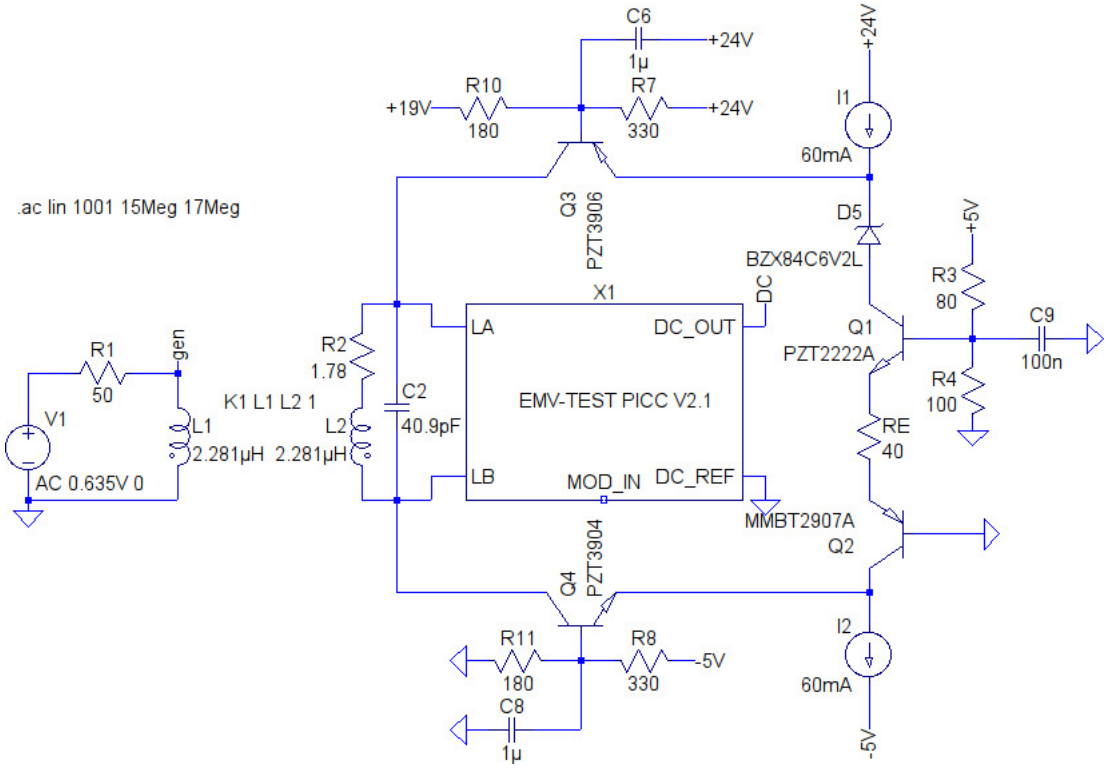

Figure 7.20: Simulation model to tune the resonance frequency.

To find the correct value for the tuning capacitor **C2**, the simulation is repeated with different values until the source sees the peak load at 16.1 MHz. The result of the final simulation is shown in figure 6.2. To obtain this result, the value of **C2** had to be changed to 40.9 pF. Remember that the initial value was 42.4 pF. The small change of only 1.5 pF was very satisfying.

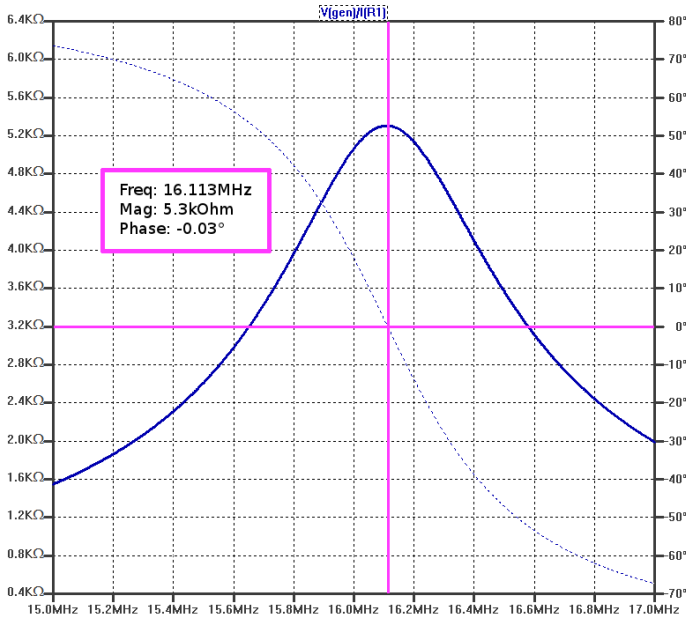

Figure 7.21: Load curve as seen by the generator during contactless measurement of the PICC's resonance frequency.

Transient Analysis

The transient analysis of the RF current deflector aims to answer two questions:

- How strong is the output current degenerated compared to the conceptional analysis?
- What is the relation between the modulation of the PCD antenna current and the input signal properties?

To answer the first question, a number of simulations with the parameters and the input signal specified in section 7.3.3 were executed.

Figure 7.22 shows the degeneration of the signal along the signal chain (input voltage - input branch current - output current - current through inductance) at an input voltage burst of $0.2\,\mathrm{V}\angle 172°$. In the top plot of the figure, the input signal voltage of the RF current source is depicted.

The spikes of the current through the resistor **RE** (see figure 7.19) are generated by the fast transients of the output transistors emitter potentials. These transients are in the final analysis caused by the fast voltage transitions at the output transistors collectors that induce a current through the collector-base capacitance. In other words, the spikes on all signals are not a result of the input signal, but of the heavy voltage variation at the output.

It is obvious from the third plot in figure 7.22 - which depicts the collector current of the PNP at the output - that this erroneous current will have a measurable influence on the system. But, as already said, this current is for the most part caused by the voltage induced in the EMV-TEST PICC Antenna and therefore independent of the modulation current. This means in terms of the schematic representation shown in figure 6.2 that it affects only $\underline{Z}'_{T,load}$ while AM and PM remain unchanged.

The plot at the bottom finally shows the current through the inductor of the equivalent circuit of the EMV-TEST PICC Antenna. During the modulation pulse the amplitude is slightly reduced.

Figure 7.23 shows the results of the same simulation, the only difference is the larger peak-peak value of the input signal of 0.5 V which leads to an output current of 25 $\mathrm{mA_{pp}}$. As expected, the signal to noise ratio has observably improved. The amplitude of the current through L2 drops again during the modulation current pulse just to return to the initial value afterwards.

Figure 7.24 finally shows the results at modulation with the full-scale input signal. Instead of the desired output current swing of 50 mA, a value of only 45 mA is achieved. This is the result of the finite transconductance of the input transistors. Compared to the previous figures, the current I(L2) behaves very different and undergoes heavy modulation of amplitude as well as phase.

Figure 7.25 shows the effect of the input signal burst $2\,\mathrm{V}\angle 172°$ on the current through the antenna of the EMV-TEST PCD in terms of AM and PM[3]. Note that this is the same input signal as in the figure above, only the plots of the currents are arranged differently. As can be seen in the top plot, the phase difference between the output current and I(L2) changes significantly during the modulation pulse: at around 4.3 μs, both currents are almost in phase, while they are in phase opposition only 100 ns later.

The medium plot shows the transient behavior of the absolute value of V_{pp}, the voltage at **J2** of the EMV-TEST PCD. The dotted line represents the envelope of the curve, the difference between its max- and min-value is a measure for the AM. Its shape obviously differs from the exponential loading shape that results from passive load modulation as shown in figure 7.11.

Exactly the same applies for the transient behavior of the phase modulation, as depicted in the plot at the bottom of figure 7.25.

Figure 7.26 shows the results of the simulation with the input signal burst $2\,\mathrm{V}\angle 227°$. Note that compared to the previous simulation, only the phase of the input signal carrier was changed. This time, the current amplitude through L2 monotonically falls to a certain level as the modulation pulse is applied and returns to the initial value after the end of the modulation pulse. Amplitude as well as phase of the shunt voltage have almost the

[3]Exactly the same as the fourth simulation in section 7.3.4, the only differences are the device models.

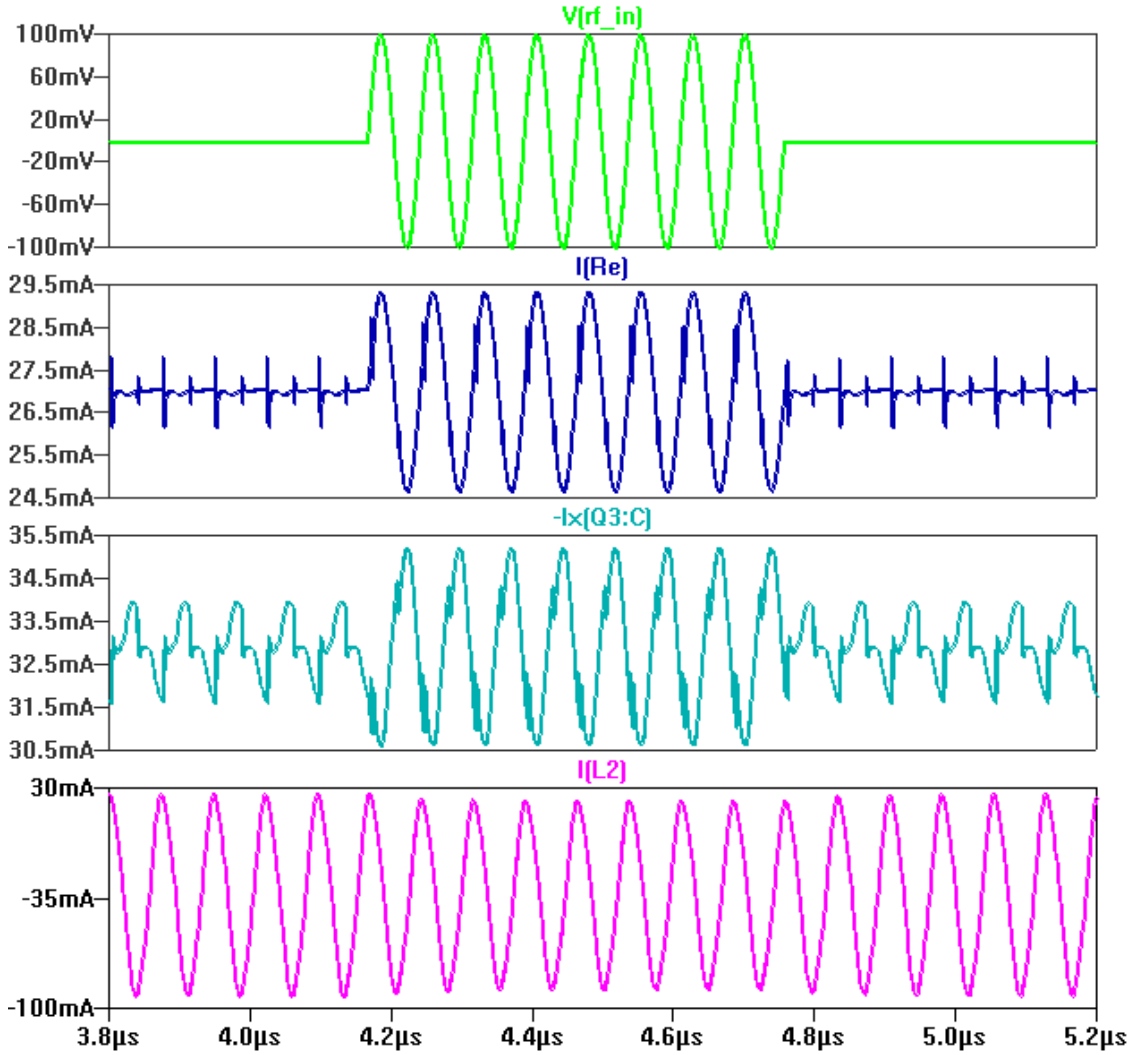

Figure 7.22: Signal degeneration along the chain at the input voltage burst $0.2\,\mathrm{V}\angle 172°$ and a coupling factor of 0.06. From top to bottom: input voltage - current through R_E - collector current of PNP at output - current through inductance of EMV-TEST PICC Antenna

classical exponential loading curve envelope.

The simulations show that amplitude and phase of the modulation signal pulses not only affect AM and PM of the PCD antenna current, but also its shape. This has nothing to do with the output transistors of the RF current source but is a simple matter of physics: the magnetic energy of an inductance which is directly related to its current can not be changed infinitely fast because this would require infinite power. So for certain amplitude/phase combinations of the modulation current, the larger part

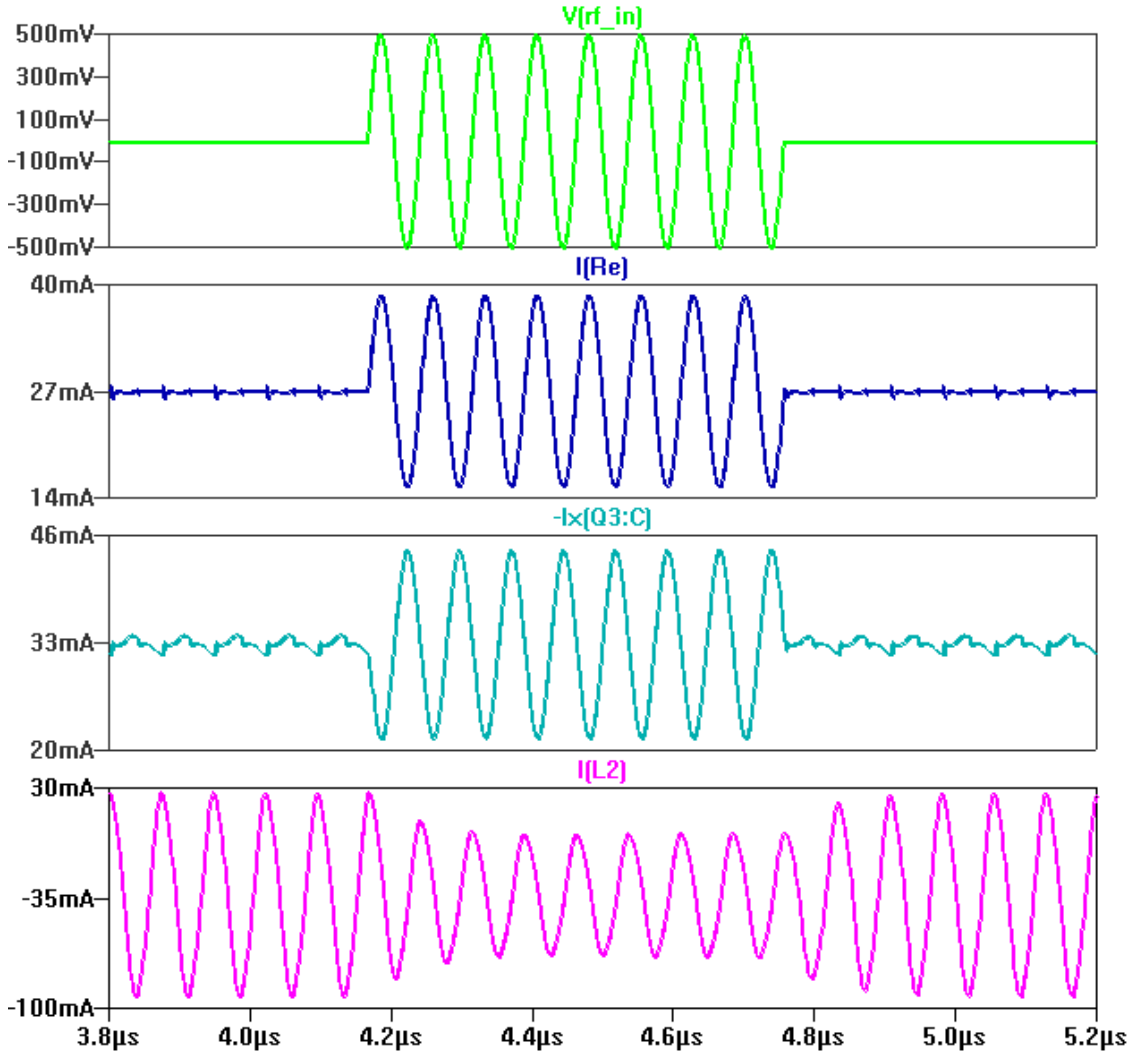

Figure 7.23: Signal degeneration along the chain at the input voltage burst $1\,\mathrm{V}\angle 172°$ and a coupling factor of 0.06. From top to bottom: input voltage - current through R_E - collector current of PNP at output - current through inductance of EMV-TEST PICC Antenna

will flow through the capacitance parallel to the antenna and increase its energy. This additional energy will subsequently commute between inductance and capacitance of the antenna which influences amplitude as well as field and therefore also the coupling conditions considering the modulation voltage.

As further simulations revealed, the effect shown in figure 7.25 is less pronounced the larger the amplitude of the unmodulated current through L2 is. This suggests that the field strength of the PCD dictates the maximum amplitude of the RF current sources

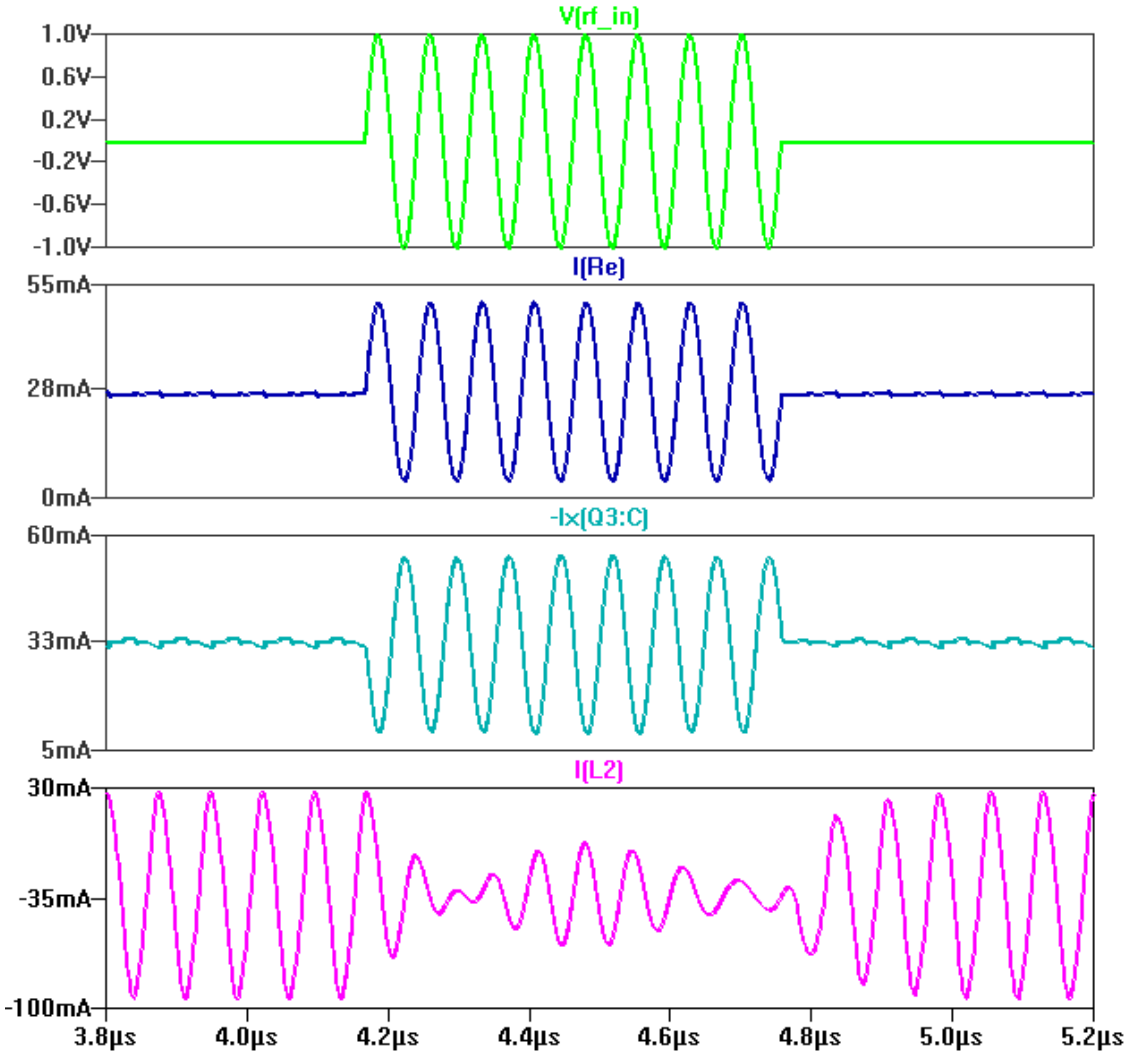

Figure 7.24: Signal degeneration along the chain at the input voltage burst $2\,\mathrm{V}\angle 172°$ and a coupling factor of 0.06. From top to bottom: input voltage - current through R_E - collector current of PNP at output - current through inductance of EMV-TEST PICC Antenna

input signal that leads to the typical modulation shapes.

The final transient analysis aimed at finding the AM and PM values that result from a certain phase of the input voltage pulses carrier. For this reason, a parametric analysis was executed where this phase was shifted from 0° to 340° in steps of 20°. The peak-peak value of the input signal was 2 V, in other words, a full scale modulation signal was applied. To prevent the distortion of the shapes, k was set to 0.15, which represents a measurement at the position 0-0-0 in the operation volume. The results are shown in

figure 7.27.

The values of AM and PM were obtained by visual estimations from the LTspice waveforms and are therefore of low precision. This applies especially to the values around the zero crossings, where it is hard to say whether the modulation is positive or negative. Nevertheless, the plot allows the observation of certain characteristics:

- The AM curve has a $-\cos(\varphi)$-like shape.
- The PM curve has a distorted $-\sin(\varphi)$-like shape
- Both curves are asymmetric:
  - max. positive AM: 80 mV
  - max. negative AM: −65 mV
  - max. positive PM: 9°
  - max. negative PM: −12°

The asymmetric behavior of the modulation is a result of the modulation dependent matching of the generator to the antenna of the EMV-TEST PCD: the modulation not only changes the current through the EMV-TEST PCDs antenna, it also changes its impedance and therefore the power that is transferred from the generator to the antenna. Again, this is not due to any nonlinearity of the RF current source but a result of the inductive coupling between PCD and PICC.

Conclusion

All of the simulation results created confidence in the concept. The use of realistic device models does not degenerate the performance in a way that meaningful operation is no longer possible. Furthermore it was found that different amplitude/phase combinations of the modulation pulses lead to different modulation shapes of the PCDs antenna current.

7.5.2 Simulating the Matched Constant Current Source/Sink

Figure 7.28 shows the LTspice simulation model of the matched constant current source/sink. The simulation executed was a simple transient simulation with a stop time of 8 μs, which the same stop time as of all of the previous transient simulations.

One must bear in mind that the matched constant current source/sink is not connected to the RF current deflector at points of constant potential. Figure 7.29 shows a typical variation of the connection points - which are the base potentials of the output transistors - during a modulation process. To simulate the behavior of the matched current

source/sink under real conditions, the drains of the MOSFETs were connected to voltage sources that applied the voltages shown in figure 7.29 to them. These voltages were exported from a previous simulation of the RF current deflector and imported into this simulation. Even though the output transistors are complementary types, the base potential of the PNP transistor V(src) varies only about 0.18 V whereas the base potential variations of the NPN transistor V(snk) have a peak-peak value of up to 0.5 V. This can be explained by the fact that the output capacitance of a BJT is inversely proportional to the voltage V_{CB}. As already mentioned in section 7.4.1, the output PNP has usually a larger V_{CB} than its NPN counterpart. Therefore, the spikes of the voltage-induced base current are lower, which leads subsequently to reduced variations of the base potential. However, although the voltages in figure 7.29 can be considered as representative for the majority of cases, there may also be operating points, in which the variation of V(src) is larger than the variation of V(snk).

Figure 7.30 shows the result of the transient simulation. Note that the device tolerances of the resistors were omitted. The voltage spikes at the MOSFETs drains will induce an erroneous base current which leads in the final analysis to spikes in the drain current. Concerning the depicted input current of the sink, the peak-peak value of the spikes is 22 mA which is about 35% of the DC value. Even the plot of the difference between the source and sink current shows spikes of $+15\,\mathrm{mA}/-11\,\mathrm{mA}$. However, the average difference in the interval shown is only $36.14\,\mu\mathrm{A}$. This corresponds quite well with the mismatch that is expected due to the input offset voltages of the operational amplifier.

Conclusion

Even though massive spikes are superposed to the source and sink current, the matching of the DC values is as expected from theoretical considerations and therefore suitable for the application.

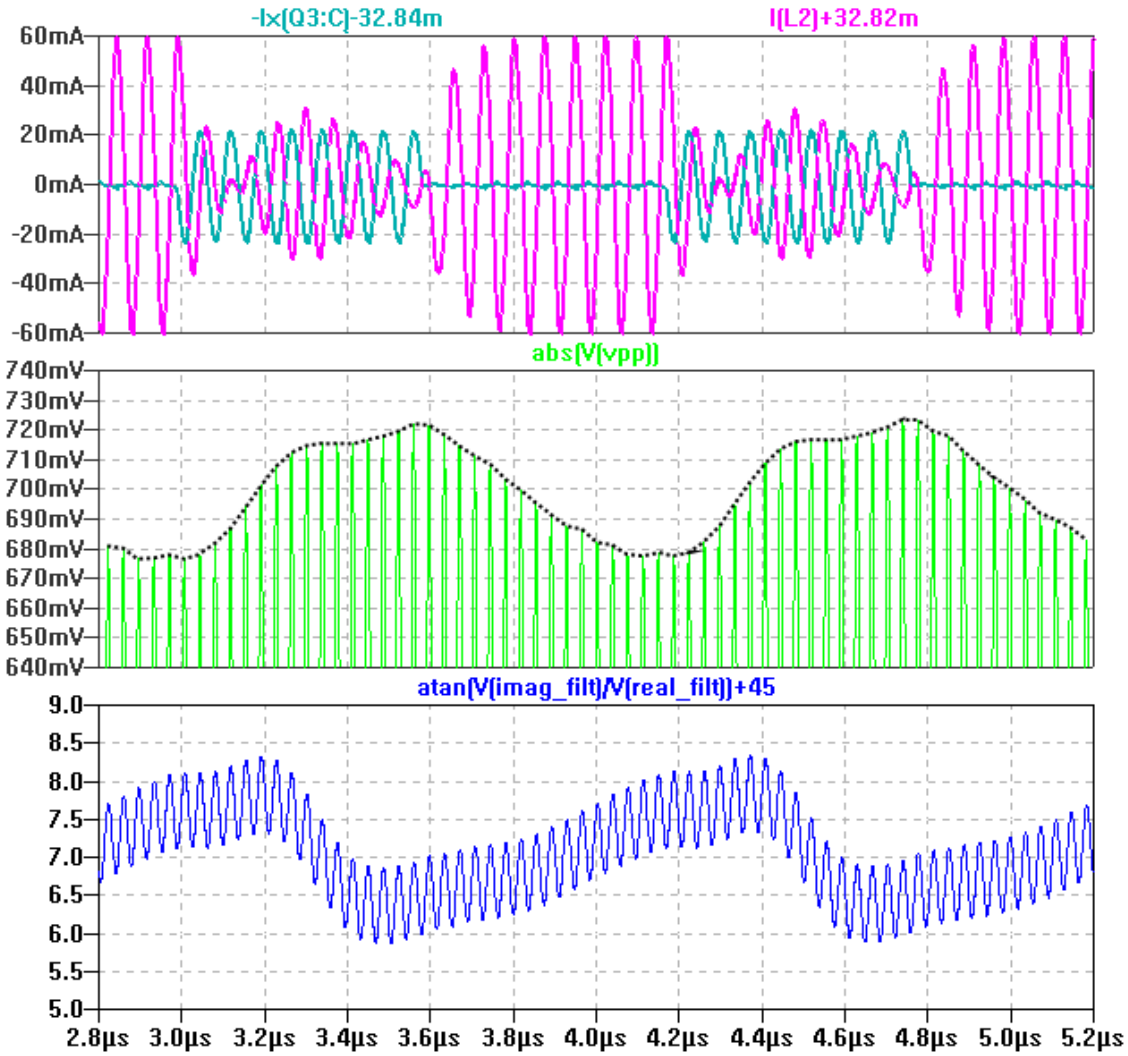

Figure 7.25: Transient behavior of the output current (-Ix(Q3:C)), the current through L2 (I(L2))and AM as well as PM at an input burst $2\,\mathrm{V}\angle 172°$ and a coupling factor of 0.06.

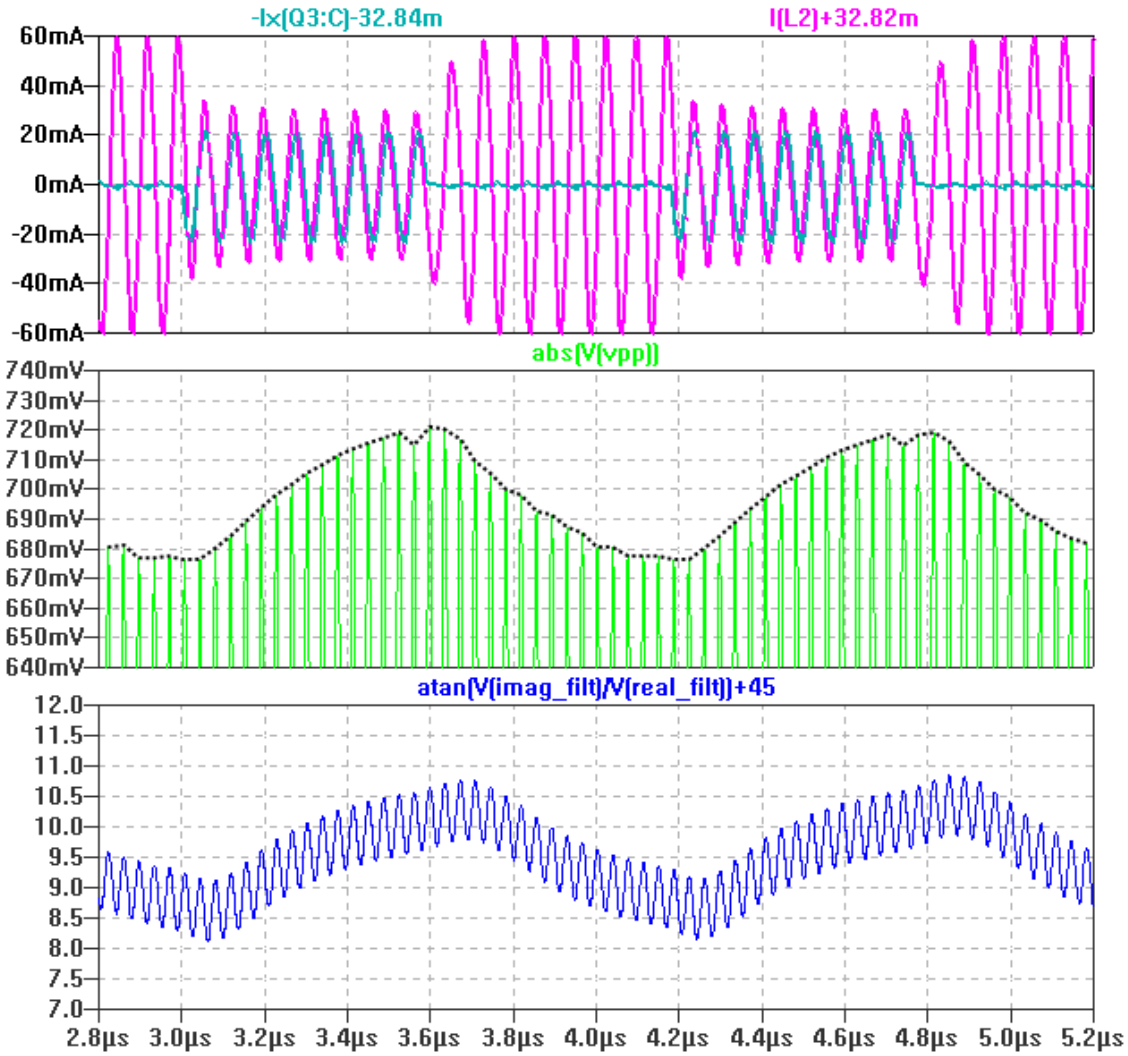

Figure 7.26: Transient behavior of the output current (-Ix(Q3:C)), the current through L2 (I(L2))and AM as well as PM at an input burst $2\,\mathrm{V}\angle 227°$ and a coupling factor of 0.06.

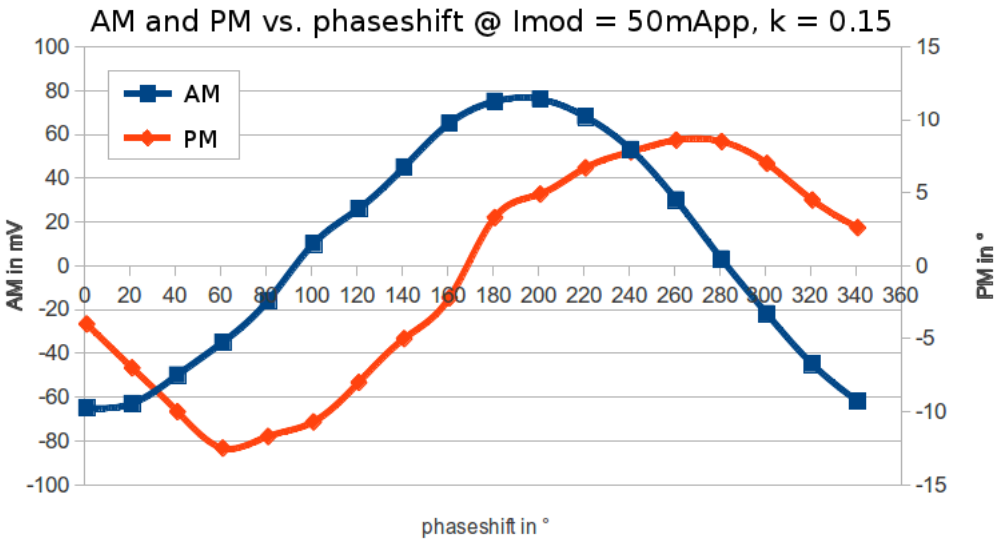

Figure 7.27: AM and PM of the shunt voltage vs. relative phase of the input signal.

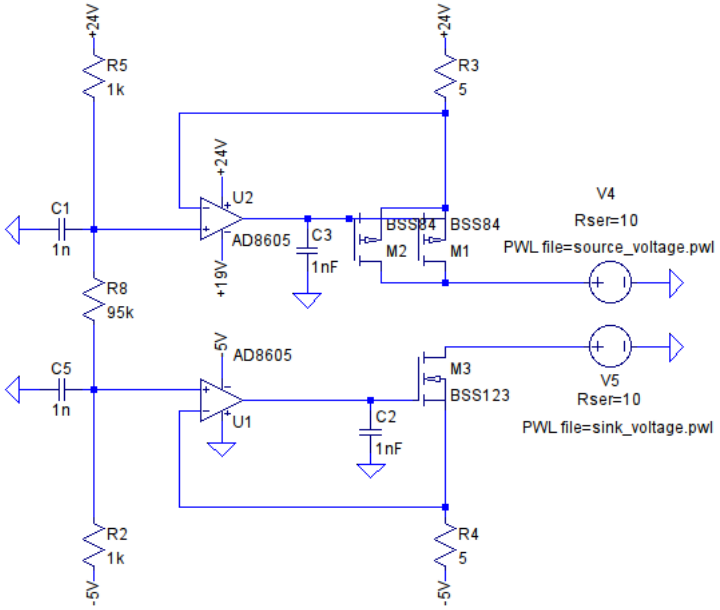

Figure 7.28: LTspice simulation model of the matched constant current source/sink.

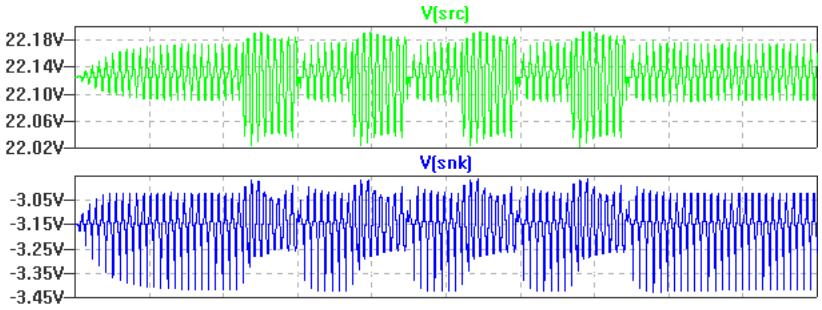

Figure 7.29: Voltage variations at the connection points of the RF current deflector and the matched current source/sink

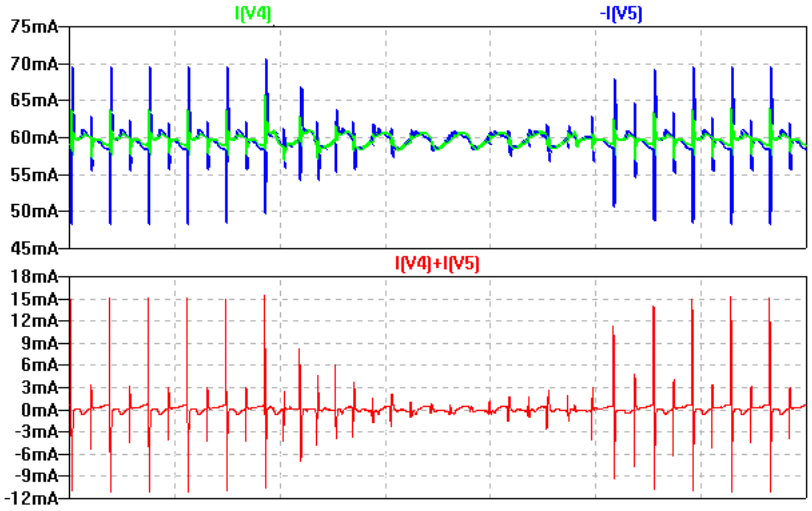

Figure 7.30: Top: Output current of the current source I(V4) and input current of the current sink I(V5). Bottom: Difference between these currents.

7.6 Assembling the Device

After all subcircuits had been simulated successfully, a layout of the circuit was made and a PCB (printed circuit board) was manufactured. To keep the influence of the PCD's magnetic field on the RF current source as small as possible, it was decided to place it in parallel to the flux lines in the operation volume, i.e. perpendicular to the EMV-TEST PICC's surface. Figure 7.31 shows the final configuration of the active modulating reference PICC. Special care was taken that the RF path doesn't take any

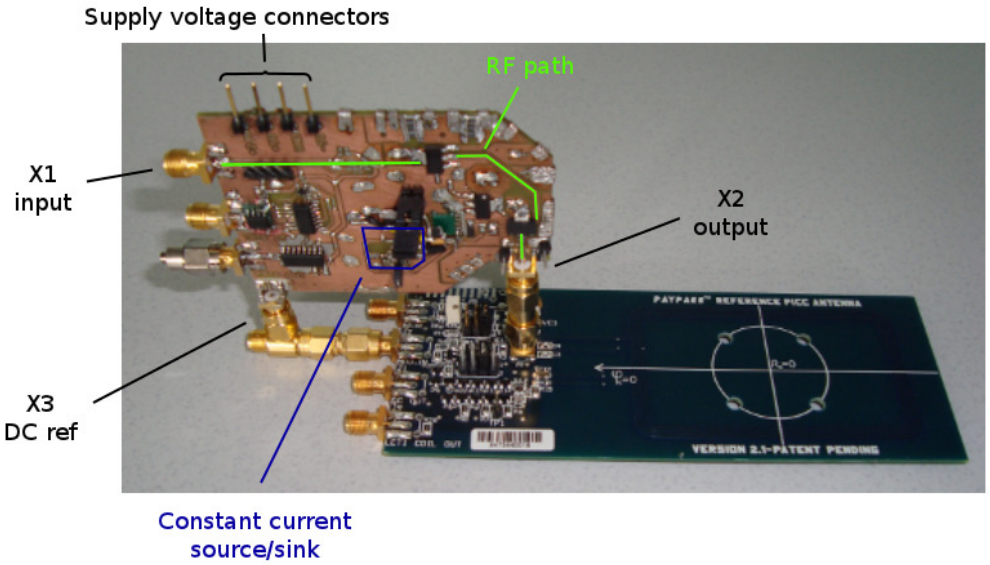

Figure 7.31: Fully assembled active modulating reference PICC

sharp curves and that the matched constant current source/sink is built up as symmetric as possible and far away from heat sources like the output transistors. To effectively extract the heat from these devices, they were supplied with large collector pads.

The heedful reader will notice that the PCB in figure 7.31 comprises a total number of five SMA jacks - instead of the three that are mentioned - as well as a number of integrated circuits, all placed in the south-west of the RF current source. These parts implemented a function that was removed in the final version of the device and is therefore not included in the schematics shown in the previous sections. Due to a lack of time, it was not possible to create a layout and a PCB of the final version of the RF current source.

7.7 Testing the RF Current Source with the EMV-TEST PICC, Version 2.1

In this section, the measurements performed with the extended EMV-TEST PICC will be described and their result will be discussed.

7.7.1 Resonance Frequency and Influence on the Field

Before the capability of active modulation could be tested, the resonance frequency of the EMV-TEST PICC in combination with the RF current source had to be tuned to the nominal value of 16.1 MHz. In the course of this procedure it should also be verified that influence on the field is not changed significantly with the new configuration. For this reason, the field strength of the EMV-TEST PCD was measured two times with the EMV-TEST PICC placed in the operation volume:

1. Measurement with the simple EMV-TEST PICC V2.1 tuned to 16.1 MHz
2. Measurement with the EMV-TEST PICC V2.1 in combination with the RF current source, again tuned to 16.1 MHz

As already pointed out, the voltage at **J1** of the EMV-TEST PICC is a measure for the PCD field strength. To ensure that the magnetic field strength of the EMV-TEST PCD was the same at both measurements, it was measured and set with a second EMV-TEST PICC, denoted as REFERENCE PICC in the rest of this section. The resonance frequency of the REFERENCE PICC was also tuned to 16.1 MHz prior to the measurement. The results of the test were satisfying, if the voltages measured at **J1** of the EMV-TEST PICC were the same, whether the RF current source was connected to it or not. As input signal to the EMV-TEST PCD, a continuous sinusoidal voltage with a frequency of 13.56 MHz was used.

The procedure was executed as follows:

1. Place the REFERENCE PICC at the position 0-0-2 in the operation volume of the EMV-TEST PCD.
2. Change the field strength until the voltage at **J1** of the REFERENCE PICC equals 5.53 V
3. Tune the EMV-TEST PICC to a f_{res} of 16.1 MHz as described in [7].
4. Place the EMV-TEST PICC at the position 0-0-2 in the operation volume of the EMV-TEST PCD.
5. Measure the voltage $V_{OV,simple}$ at **J1** of EMV-TEST PICC.
6. Connect the RF current source to the EMV-TEST PICC.

7. Tune the resonance frequency of the EMV-TEST PICC in connection with the RF current source - from now on denoted as EXTENDED PICC - contactless to 16.1 MHz
   (a) Connect antenna for contactless measurement of f_{res} to the impedance analyzer
   (b) Set fixture compensation to "short"
   (c) Ensure that the RF current source is supplied with power
   (d) Place the EXTENDED PICC upon the measurement antenna
   (e) Change the capacitance in parallel to the antenna of the EXTENDED PICC until it's resonance frequency equals 16.1 MHz
8. Place the REFERENCE PICC at the position 0-0-2 in the operation volume of the EMV-TEST PCD.
9. Change the field strength until the voltage at **J1** of the REFERENCE PICC equals 5.53 V
10. Place the EXTENDED PICC at the position 0-0-2 in the operation volume of the EMV-TEST PCD.
11. Measure the voltage $V_{OV,extended}$ at **J1** of EXTENDED PICC.

The results that were obtained during this measurement are shown in table 7.7.1. It shows that the influence on the field remains virtually the same after connecting the RF current source to the EMV-TEST PICC, when both configurations are tuned to the same resonance frequency.

$V_{OV,simple}$	$V_{OV,extended}$
5.33 V	5.32 V

Table 7.4: Voltages at **J1** of the EMV-TEST PICC when the RF current source is detached or attached.

According to the simulation in section 7.5.1, the tuning capacitance in parallel to the PICC's antenna only has to be reduced for about 1.5 pF in order to tune the EXTENDED PICC to 16.1 MHz. It was expected that this value would be larger for some pF due to parasitics on the PCB as well as the capacitance of the connection between the RF current source and the EMV-TEST PICC. In the end, the fixed tuning capacitor of 27 pF was replaced by two capacitors in parallel with values of 15 pF and 4.7 pF respectively.

7.7.2 Active Modulation Test

Finally, the active modulation capability of the EXTENDED PICC was tested. Thereby it should be verified that an AM and PM of the current through the antenna of the EMV-TEST PCD can be arbitrarily set within a certain range, by changing amplitude and phase shift of the input modulation pulses.

Measurement Setup

Figure 7.32 shows the measurement setup that was used to acquire the data. It is very similar to the one shown in figure 5.1, where the effects of passive load modulation were measured. One important difference between the setups for active and passive

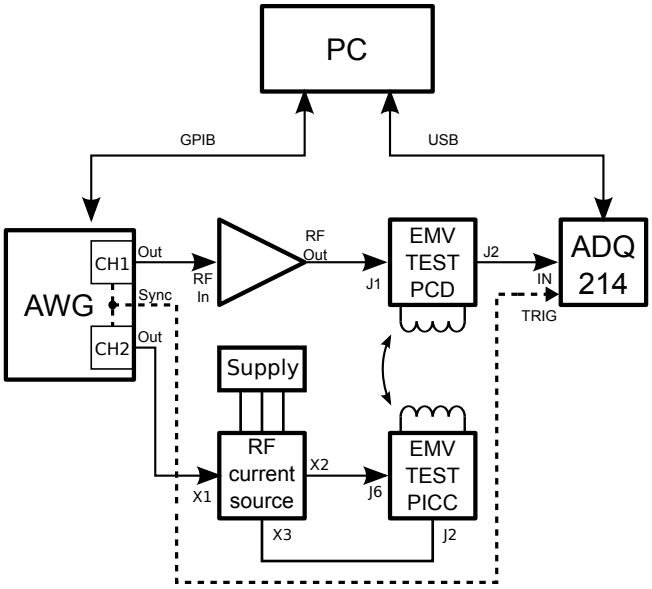

Figure 7.32: Measurement setup for testing the active modulation capability.

modulation are the signal sources. In case of the active modulation measurement, the phase shift between the input PCD's input voltage and the carrier of the modulation pulses is a key parameter and has to be set precisely. For this reason, an AWG with two synchronized output channels was used. The first channel supplied the PCD with a sinusoidal continuous wave with a frequency of 13.56 MHz, whereas the second channel sent the modulation signal to the RF current source. Figure 7.33 shows a schematic representation of the pattern of channel 1 and 2.

The field strength of the EMV-TEST PCD was set to the nominal value as described in section 7.7.1. Subsequently a number of shots were acquired with the EXTENDED PICC placed at the positions 0-0-0 and 0-0-2 in the operation volume. In every position

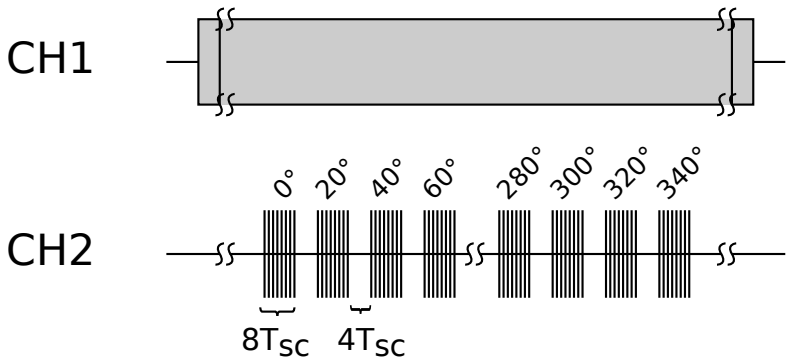

Figure 7.33: Schematic representation of the pattern of channel 1 and 2. Every burst contains eight subcarrier cycles of the OOK-modulated (On-Off Keying) carrier signal. The relative phase shift between the modulation carrier and the signal of channel 1 is increased by 20° from one burst to the next.

the measurement was executed with a number of different amplitudes of the modulation bursts.

To obtain the AM and PM values of the PCD's antenna current, the acquired data was analyzed with the MATLAB program already described in section 5.2.3.

Results

Figure 7.34 shows an exemplary set of sampled data. A first glance already shows that the single bursts have a different influence on the amplitude of the acquired signal.

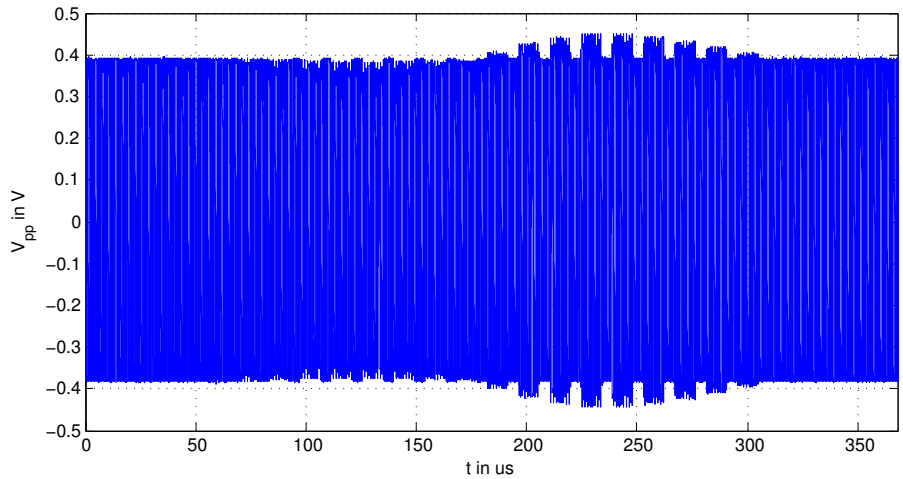

Figure 7.34: Shunt voltage vs. time while the active modulation pattern is applied to the EXTENDED PICC.

The MATLAB program used for the extraction of the AM and PM values prints the plots of magnitude and phase over time, see figure 7.35 and figure 7.36.

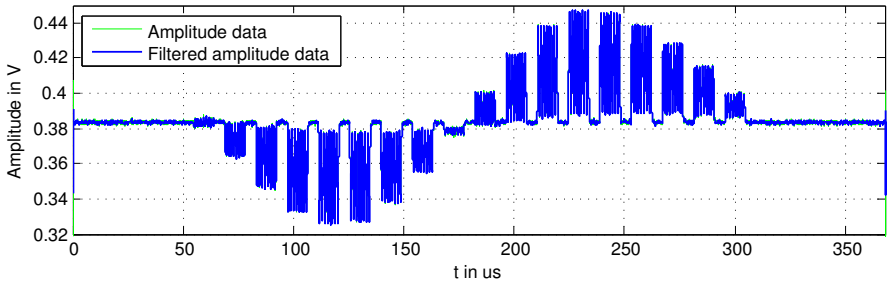

Figure 7.35: Magnitude of the Hilbert transform of the sampled signal.

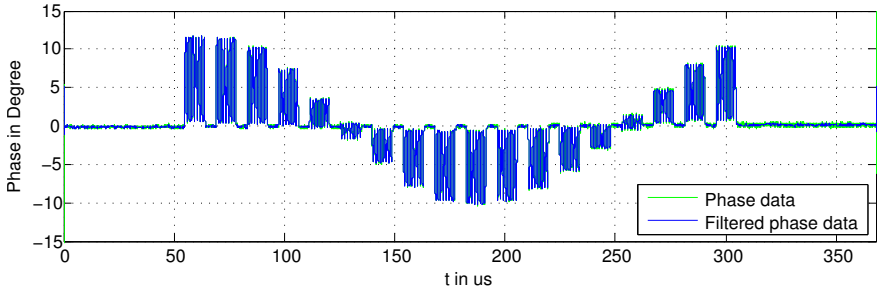

Figure 7.36: Phase of the Hilbert transform of the sampled signal.

Figure 7.37 shows the AM versus the relative phase shift between the signal of channel 1 and the carrier signal of the temporally corresponding modulation burst of channel 2 of the AWG, measured at 0-0-0. As expected from the simulation, the $AM(\Delta\varphi)$ curves express a sinusoidal development that is asymmetric, i.e. the maximum positive AM happens to be 60 mV, while the maximum negative AM is −50 mV. The values themselves are a little lower than in the simulation, where the maximum positive AM was 80 mV and the maximum negative AM was −65 mV for an input voltage swing of $2\,V_{pp}$. Furthermore, the maximum AM the passive load modulation system could create was 120 mV and is therefore twice as much as the EXTENDED PICC is capable of. However, real-world combinations of a modern smartcard IC and a class 1 antenna only create an AM of around 45 mV as shown in section 5.3.2. These values lie well within the range of the EXTENDED PICC. When looking at the $AM(\Delta\varphi)$ plot in figure 7.27 obtained by simulation, one will notice a phase shift of the plots of about 90°. This can be explained by the fact that the output voltage of the AWG is phase shifted by the connected RF amplifier. This must be taken into consideration, when the setting of a certain AM/PM-combination is desired.

The corresponding $PM(\Delta\varphi)$-plot is shown in figure 7.38. A maximum positive PM of around 12° can be obtained with this configuration, the maximum negative PM is −9°. The first of these values is about the maximum PM that could be achieved with passive

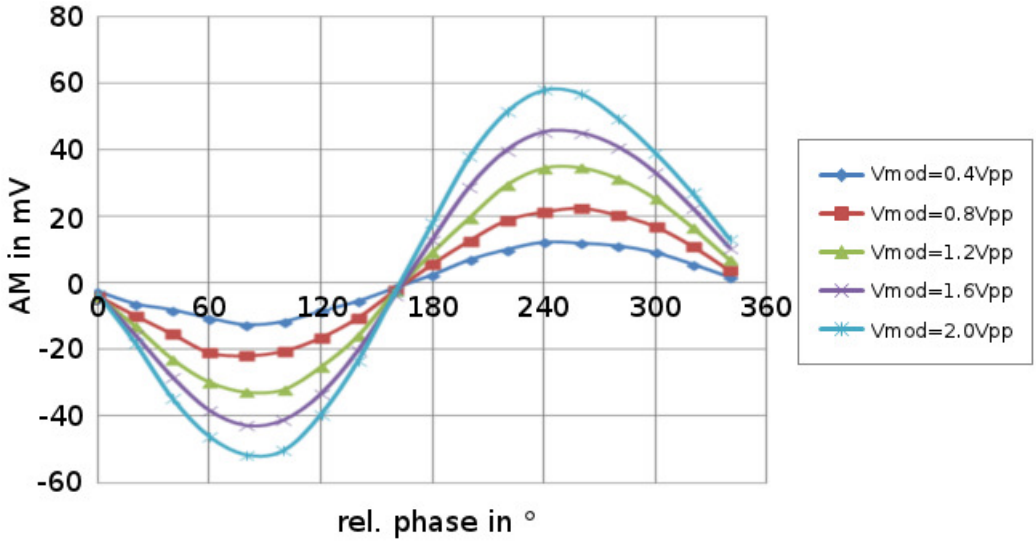

Figure 7.37: AM of the shunt voltage over the relative phase shift, measured at the position 0-0-0 in the operating volume.

load modulation. It has again a sinusoidal shape with the maximum values at the phase shifts, where the AM is almost zero. An important finding is the fact that the AM and PM curves are in fact not shifted for exactly 90° as one might expect. The maximum negative PM for example was measured at a relative phase shift of 180°, the zero crossing of the AM curve, however, is a little above 160°. This phenomenon already occurred in the simulation but has not been described there. It is assumed that the reason for this behavior is again the variation of the matching of the antenna to the generator and not any nonlinearity of the circuit.

Figure 7.39 shows the AM of the shunt voltage versus the relative phase shift, this time measured at the position 0-0-2. This time the asymmetry is much more pronounced than at the position 0-0-0. The maximum positive AM is around 45 mV, the maximum negative AM is only −25 mV. Remembering the deformed envelope of the shunt voltage that was simulated with an input signal burst of $(2V\angle 172°)$ and is shown in figure 7.25, the question arose, if the real shunt voltage behaves in a similar way. A first examination of the magnitude of the Hilbert transform of the sampled signal showed that this question can be answered with no. All of the signals had the typical exponential loading-curve-like shape. The reason for this discrepancy is not known yet.

Figure 7.40 shows the PM of the shunt voltage versus the relative phase shift, measured at the position 0-0-2 in the operating volume. Contrary to the AM curve, the PM curve shows only minor deformation. PM values between −3° and 4° can be obtained with this configuration.

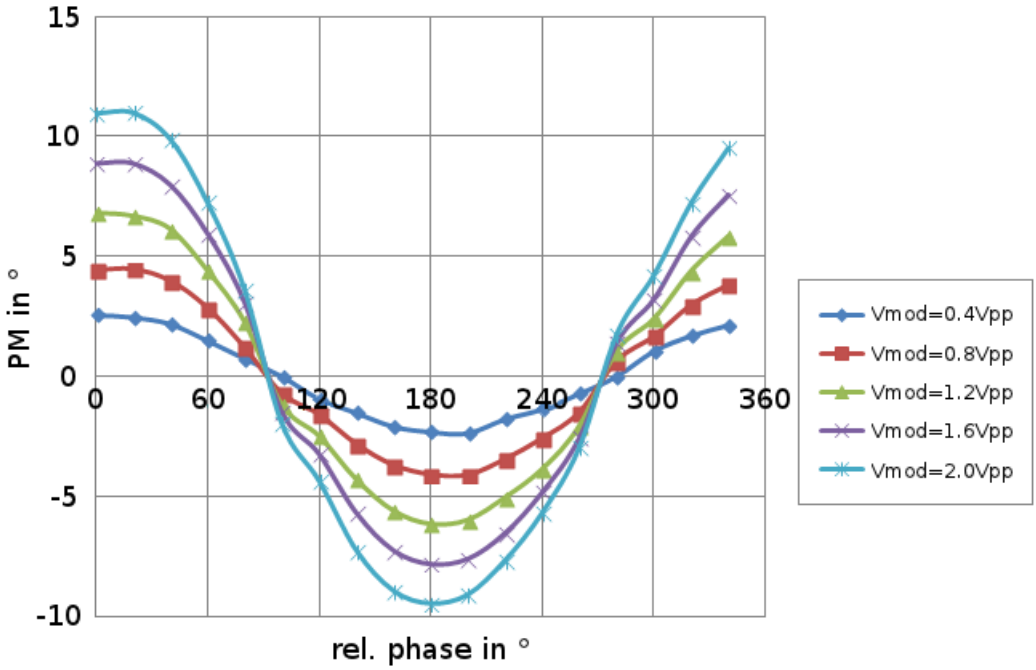

Figure 7.38: PM of the shunt voltage over the relative phase shift, measured at the position 0-0-0 in the operating volume.

Summary

The measurement results show that the basic functionality of an active modulating PICC on the basis of the EMV-TEST PICC could be realized. AM as well as PM show an asymmetric behavior, i.e. positive modulation yields in general larger values than negative modulation. The asymmetry is stronger pronounced in the AM curves and is inversely proportional to the field strength at which the EXTENDED PICC works. These findings could stimulate further investigations to find operation points where active modulation is highly efficient.

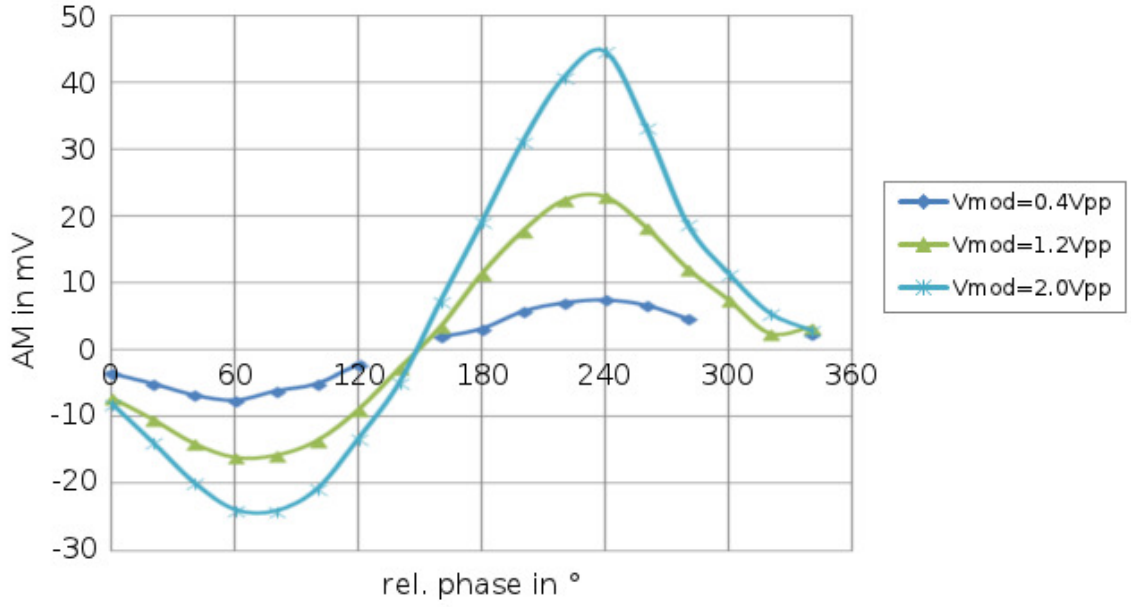

Figure 7.39: AM of the shunt voltage over the relative phase shift, measured at the position 0-0-2 in the operating volume.

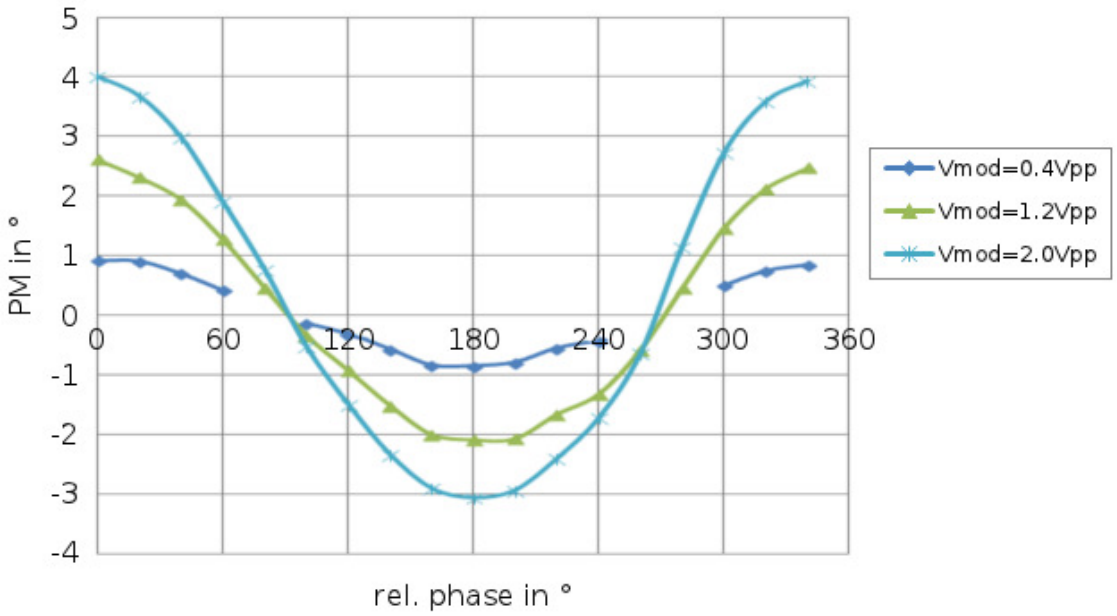

Figure 7.40: PM of the shunt voltage over the relative phase shift, measured at the position 0-0-2 in the operating volume.

Chapter 8

Conclusion

One of the numerous RFID markets that is predicted to grow strongly in the coming years is contactless payment. For the standardization of the interaction of contactless payment cards and their readers, members of the EMVCo have developed the EMV™ Contactless Specification for Payment Systems. This specification includes the definition of the EMV Contactless Level 1 Test Equipment which is used to perform the tests. Although this hardware was initially designed with the focus on a realistic representation of real-world systems it was suspected to fail this requirement today.

One component of the EMV Contactless Level 1 Test Equipment is the EMV-TEST CMR Circuit Board. It plays a key role in calculating the value of the amplitude modulation but is incapable to support the calculation of the phase modulation. For this reason, a MATLAB program was created that calculates AM, PM and the influence on the EMV-TEST PCD's field.

In the course of this thesis a PICC with the ability to actively modulate a reader device's magnetic field on the basis of the present EMV-TEST PICC was developed and measured. Prior to the development of the new reference PICC, a number of measurements was performed with the EMV-TEST PICC to find out its limitations concerning the amount of AM, PM and the influence on the EMV-TEST PCD's field. For this reason the EMV-TEST PICC's resonance frequency was varied a suitable range. Furthermore, a number of real-world PICCs was measured with the intention to emulate their behavior with the EMV-TEST PICC. It turned out that certain configurations can not be emulated with the present EMV-TEST PICC.

The results that were obtained until then, showed that for guaranteeing full interoperability the demand for a reference PICC with the ability to set the load modulation's amount of AM, PM and the influence on the field arbitrarily within a certain range, because nowadays' and future real-world systems indicate that readers also should be tested against load modulation with certain amount of AM and PM. Furthermore, the influence on the field of this reference PICC should be independent from the modulation

parameters. It was decided that an actively modulating reference PICC on the basis of the present EMV-TEST PICC would suit the requirements best. In the further course the possible coupling mechanisms for realizing an active modulation were discussed. It turned out that the approach of galvanically feeding a modulation current into the EMV-TEST PICC is a better representation of real-world PICCs than the active modulation of the field with a second antenna. For this purpose an RF current source that delivers a modulation current proportional to an input voltage of the EMV-TEST PICC has been developed.

To gain the ability of simulating the RF current source prior to its construction, simulation models of the present EMV-TEST PCD and EMV-TEST PICC were created in LTspice. A conceptual simulation showed that the actively modulating PICC is capable of emulating the behavior of passive load modulation within the range that is relevant for PCD tests. On the basis of this verified simulation model, the actual RF current source was developed. The key subcircuits - the RF current deflector and the matched constant current source/sink - were simulated with appropriate device models. All of the simulations delivered promising results.

In the further process, the RF current source was built up on a two sided PCB and connected to the EMV-TEST PICC. A number of measurements was performed to test the capabilities of the new reference PICC. As a first measurement showed, the influences on the field of the unmodified EMV-TEST PICC and the one in combination with the RF current source are the same, when both are tuned to the nominal resonance frequency. Thereby, one of the key requirements was fulfilled.

Finally, the active modulation functionality was tested. For this purpose, modulation pulses with different amplitudes and phase shifts relative to the field were applied to the RF current source connected to the EMV-TEST PICC. The new reference PICC was placed at different positions in the operating volume of the EMV-TEST PCD and the signal used for evaluating the load modulation's parameters was acquired using a suitable sampling device. The analysis of the data with the developed MATLAB software showed that in order to profoundly understand the relation between the load modulation's amount of AM and PM and the relative shift of the modulation signal's parameters regarding the field further measurements and investigations will be essential. However, with the software usable for analyzing load modulation parameters and the improved reference PICC capable of load-modulating a reader's magnetic field actively, both developed in course of this thesis, the tools needed for these tasks are available.

Bibliography

[1] AVISIAN Publishing: *Frost & Sullivan: Mobile, contactless big in 2013*. Web: 4. Mar. 2013 (27. Dec. 2012)
http://www.nfcnews.com/2012/12/27/frost-sullivan-mobile-contactless-big-in-2013

[2] Agilent Technologies *81180B - 4.6 GSa/s Arbitrary Waveform Generator*. Web: 27. Feb. 2013.
http://www.home.agilent.com/en/pd-1809255-pn-81180B/
46-gsa-s-arbitrary-waveform-generator?nid=-536902257.930158&cc=AT&lc=ger

[3] Analog Devices, Inc.: *AD8605 SPICE Macro-model*. Web: 8. Mar. 2013. (8. Oct. 2012) http://www.analog.com/en/all-operational-amplifiers-op-amps/operational-amplifiers-op-amps/ad8605/products/mod-spice-models/resources.html

[4] EMVCo: *About EMVCo*. Web: 26. Sep. 2012
http://www.emvco.com/about_emvco.aspx

[5] EMVCo: *A Guide to EMV - Version 1.0*. Web: 27. Sep. 2012
http://www.emvco.com/best_practices.aspx?id=217

[6] EMVCo: *EMV Contactless Specifications for Payment Systems - Book D: EMV Contactless Communication Protocol Specification Version 2.1*

[7] EMVCo: *EMVCo Type Approval Contactless Terminal Level 1: PCD Analogue Test Bench and Test Case Requirements Version 2.1a*

[8] Hoelzl J: *Extended Card Modulation - Test Methods*. Master's Thesis (2011)

[9] Infineon Technologies AG: *Infineon Technologies - Discrete & RF Semiconductors - SPICE Library Version 5.4*. Web: 8. Mar. 2013 (18. Apr. 2005)
http://www.infineon.com/dgdl/S_AFBJT.LIB?folderId=
db3a304314dca389011545f4eb561884&fileId=db3a3043156fd5730115a3f6c81509a8

[10] International Electrotechnical Commission: *About the IEC - Welcome to the IEC*. Web: 26. Sep. 2012.
http://www.iec.ch/about/

[11] International Organization for Standardization: *About ISO*. Web: 26. Sep. 2012. http://www.iso.org/iso/home/about.htm

[12] Linear Technology Corporation: *LTSPICE IV*. Web: 27. Feb. 2013. http://www.linear.com/designtools/software/#LTspice

[13] NXP Semiconductors: *BSS123 SPICE model*. Web: 8. Mar. 2013. http://www.nxp.com/documents/spice_model/BSS123.prm

[14] NXP Semiconductors: *BSS84 SPICE model*. Web: 8. Mar. 2013. http://www.nxp.com/documents/spice_model/BSS84.prm

[15] NXP Semiconductors: *BSS84AK - Product data sheet*. Web: 8. Mar. 2013. (23. May 2011) http://www.nxp.com/documents/data_sheet/BSS84AK.pdf

[16] NXP Semiconductors: *PZT2222A SPICE model*. Web: 8. Mar. 2013 (Feb. 2009) http://www.nxp.com/documents/spice_model/PZT2222A.prm

[17] The UK Cards Association: *Key Facts and Stats*. Web: 26. Sep. 2012. (25. Jun. 2012) http://www.contactless.info/Facts-and-Stats.asp

[18] Finkenzeller K: *RFID Handbuch - 6. Auflage*. Munich, Carl Hanser Verlag (2012)

[19] Raggam P: ISO/IEC - Proximity coupling Chipkarten. In: Finkenzeller K (Ed.): *RFID Handbuch - 6. Auflage*. Munich, Carl Hanser Verlag: 312 - 344 (2012)

[20] Tabor Electronics Ltd: *Model WW1281A - 1.2GS/s Single-Channel Arbitrary Waveform Generator*. Web: 27. Feb. 2013 http://www.taborelec.com/products_home.asp?prod=arbitrary_waveform_function_generator&model=WW1281A&over=products&prod3=single_channel_arbitrary_waveform_generators

[21] Etherington D: *Forrester: U.S. Mobile Payments Market Predicted To Reach $90B By 2017, Up From $12.8B In 2012*. Web: 4. Mar. 2013 (16. Jan. 2013) http://techcrunch.com/2013/01/16/forrester-u-s-mobile-payments-market-predicted-to-reach-90b-by-#